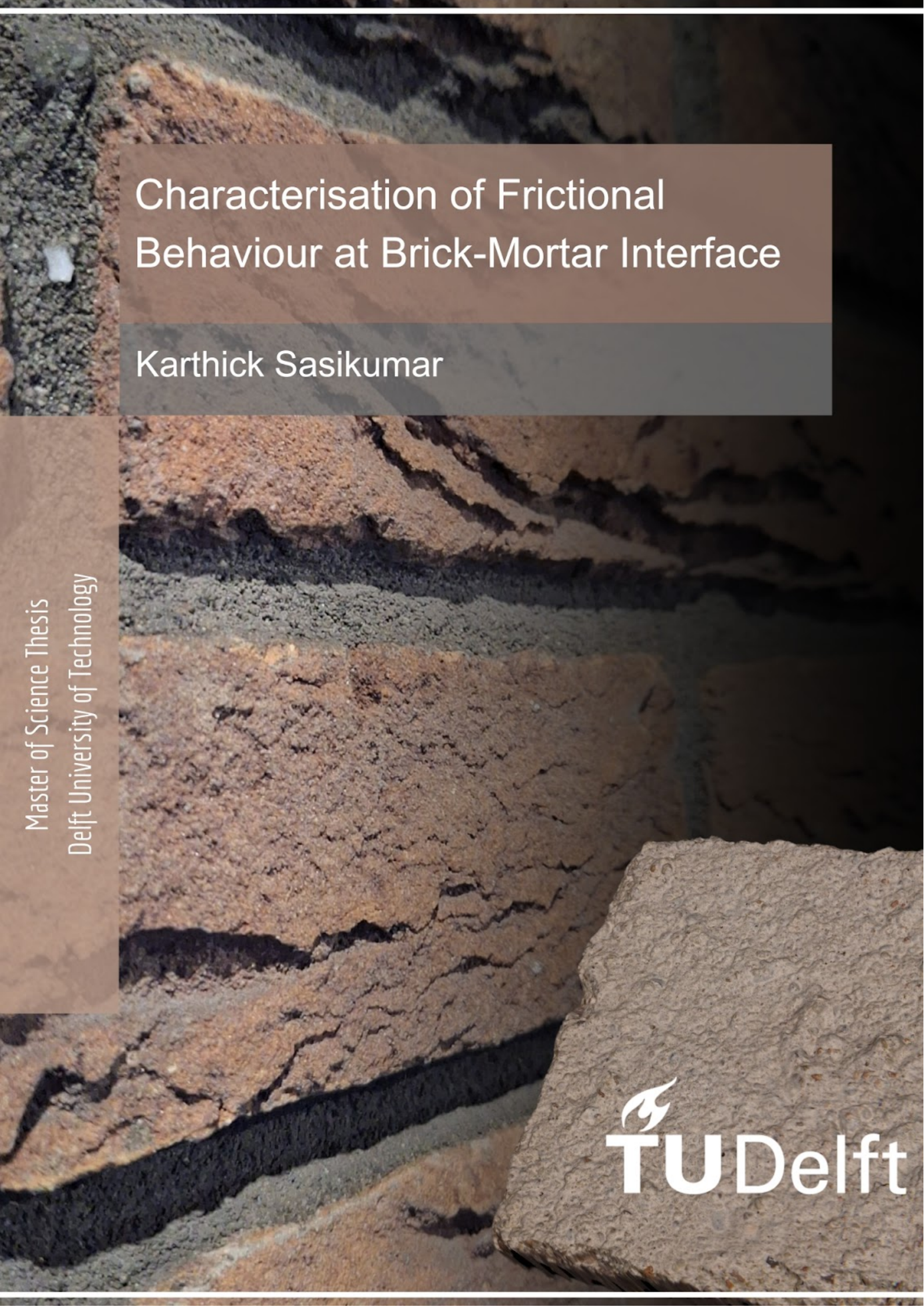

Characterisation of Frictional Behaviour at Brick-Mortar Interface

Karthick Sasikumar

Master of Science Thesis
Delft University of Technology

TU Delft

CHARACTERISATION OF FRICTIONAL BEHAVIOUR AT BRICK-MORTAR INTERFACE

by

KARTHICK SASIKUMAR

January 23, 2024

In the partial fulfilment of the requirement for the degree of

Master of Science

in Civil Engineering

Track: Structural Engineering

at the Delft University of Technology

Faculty of Civil Engineering and Geosciences

Thesis Committee:	Dr. R. Esposito	Applied Mechanics
	Dr. A. Cabboi	Mechanics and Physics of Structures
	Dr.ir. A.A.M.Dieudonné	Geo-Engineering

Student number: 5494974

An electronic version of this thesis is available at https://repository.tudelft.nl/

TU Delft

TABLE OF CONTENT

ACKNOWLEDGEMENTS

This thesis is the culmination of my Master’s in Structural Engineering at TU Delft where I investigate, through experimental analysis, the behaviour of friction between brick and mortar at the joint interface.

I extend my heartfelt gratitude to my supervising committee, consisting of Dr. Rita Esposito, Dr. Alessandro Cabboi, and Dr. Anne Catherine Dieudonné. I am immensely grateful to Dr. Rita and Dr. Alessandro for introducing me to this engaging and insightful research topic, which has been a source of passion and dedication for me over the past few months. Your inspiration, motivation, and the invaluable skills you imparted have greatly enriched my master's journey.

Special thanks to Dr. Alessandro for generously sharing his extensive knowledge, offering unwavering support, and providing crucial insights into the practical aspects of the research. Collaborating with him has instilled in me a deep interest in practical research, curiosity, and a distinctive mode of thinking that I aspire to maintain in the future. I express my profound gratitude for your explanations, time, and enthusiasm for meaningful discussions.

I would like to express my sincere appreciation to Dr. Rita Esposito for her role in guiding me through the intricate world of masonry. Her expertise and unwavering support have not only broadened my understanding of the subject but also fostered a deep appreciation for the nuances within this field. Dr. Rita's patience, insightful advice, and critical perspectives have been indispensable in shaping the trajectory of my research and academic growth.

I extend my heartfelt thanks to Dr. Anne Catherine Dieudonné for her consistent and valuable feedback. Her prompt responses and apt insights have been instrumental in refining the quality of my work. Dr. Anne Catherine's dedication to providing constructive criticism and guidance has significantly contributed to the development and enhancement of my research endeavours.

I am grateful to my friends, Jayesh Balaji Kottiswaran, Sridharan Kandasamy, Daan Smolders, Vivek Kurup, Swarnangshu Ghosh, my family away from home: Board 8 and the rest of U-BASE. In you people, I found support, love and motivation. Thank you for sharing this exciting journey with me.

To my dad, whose sweat and blood ensured my happiness. To my mom who taught me to dream and chase my dreams. To Kavya for making me what I am. Without your love, support and encouragement this wouldn’t have been possible.

Thank you.

Karthick Sasikumar

Den Haag, January 2024

ABSTRACT

Unreinforced Masonry, a popular construction material with a rich historical legacy, has been resilient through centuries, despite its susceptibility to failure through various loading conditions such as seismic forces. Understanding the mechanical behaviour of masonry, particularly the cohesion and frictional mechanisms at interfaces between bricks and mortar, is crucial for assessing its structural reliability .

This thesis presents an experimental study characterising masonry frictional interfaces using a tribometer test, a novel approach in masonry research. The study aims to investigate the frictional behaviour of brick-mortar interfaces under varying precompression levels and test frequencies (3 Hz and 0.2 Hz). A novel sampling method was implemented, wherein the required specimens were extracted from a bonded masonry couplet specimen. The couplets were bond wrenched and then subjected to a mechanical extraction. Bond wrenching, through tension, separates the couplets, thereby isolating frictional response from the influence of cohesion by decoupling cohesion between the unit and joint. A tribometer was chosen for the investigation of frictional parameters, tribometers are typically employed with metal surfaces and rarely applied to masonry. Consequently, experiments were conducted using a reciprocating tribometer, featuring a novel specimen extraction procedure and a modified setup. The novel extraction involved mechanically altering a parent brick couplet to extract compatible specimens. Customised holders were procured and used to accommodate the prepared specimen. The obtained specimens were then, fastened into the appropriate sample holders. Tests were performed on the specimen with displacement, tangential force, normal force and time being recorded. Three key parameters, the mean Coefficient of Friction (CoF), the Energy Coefficient of Friction (ECoF), and tangential contact stiffness were analysed from the collected data. The above mentioned parameters were evaluated through two approaches, (i) Mean Curve approach and (ii) Cycle approach. A mean curve is the averaged curve of the measured hysteresis loop, which encompasses the overall behaviour exhibited by the hysteresis loop.

The experimental results revealed a dependency between the coefficient of friction and the applied pre-compression level, showing a non-Coulomb behaviour; this is in contradiction with assumptions of several models used for the analyses of masonry structures. Initially, experiments were conducted at a higher frequency (3 Hz) and followed by experiments at a lower frequency (0.2 Hz), and the results in both cases revealed a non-Coulomb friction behaviour characterised by a nonlinear connecting trend between kinetic and static friction region. The connecting trend between the kinetic and static region demonstrated a reduction in the degree of non-linearityan enhanced symmetry in the hysteresis profile as the precompression levels increased. The mean curve and the cycle approach yielded identical estimates for the coefficients of friction (CoF) and effective coefficients of friction (ECoF).

The evolution of Coefficient of friction (CoF), did not exhibit any clear systematic time dependency, while Energy Coefficient of friction (ECoF) showed a systematic decrease over time. The ECoF related the energy dissipated by friction across each cycle to a hypothetical Coulomb energy dissipation. Therefore the ECoF captures the energy dissipation due to friction during one cycle, while the CoF captured the static friction region. The energy

dissipation across different precompression levels were also studied and it was observed that the energy dissipation increased for increasing precompression levels.

Tangential Contact stiffness refers to the tangential force required to effect a unit displacement in the tangential direction. The contact stiffness was calculated from the slope of the region of the hysteresis loop associated with displacement reversal. Contact stiffness was observed to increase with increasing precompression levels. This observation was also validated by the theoretical model which illustrates a proportionality between the applied normal load (precompression) and tangential contact stiffness.

Additionally, the study highlights the impact of frequency on the observed frictional behaviour, noting more prominent static and kinematic components at lower frequencies due to reduced inertial forces. A preliminary study using the LuGre model was used to plot the analytically derived frictional force-velocity relationship, to briefly study the impact of sliding velocity on frictional force. It was deduced that the velocity had an influence over the frictional force at the interface.

In conclusion, the findings provide valuable insights into the frictional characteristics of masonry interfaces under varying loading conditions. The results also shed light on the practical aspects of testing methods and offer considerations for further research in the field of masonry engineering.

SYMBOLS AND ABBREVIATIONS

Parameter Name	**Symbol**	**Unit**
Length/Width/Height	*L/W/H*	mm
Diameter	*D*	mm
Sliding distance	*d*	mm
Time	*t*	s
Area	*A*	mm^2
Compression Strength	f_c	N/mm^2
Tensile Strength	f_t	N/mm^2
Shear Stress	τ	N/mm^2
Shear Stress (cohesion)	τ_c	N/mm^2
Shear Stress (friction)	τ_f	N/mm^2
Poisson's ratio	ν	-
Fracture Energy	G_f	J/m^2
Compressive fracture energy	G_c	J/m^2
Tangential force	*Q*	N
Normal force	*P*	N
Cohesion	c	N/mm^2
Friction Coefficient (CoF)	μ	-
Energy Coefficient of Friction (ECoF)	μ_e	-
Internal friction angle	φ	Degrees
Velocity	v	mm/s
Contact Stiffness	$k_{b,j}$	N/mm
Spring stiffness	k_i	N/mm
Frequency	freq	Hz

1 INTRODUCTION

1.1 General Background

Unreinforced masonry (URM) is a composite construction material utilising a brick unit usually made from clay or concrete bonded together on a bed of mortar, often made of cement and sand [1]. In this study, the term "masonry" refers to unreinforced solid clay brick masonry. Renowned for its compressive strength and finding application since historical times, masonry has caught the attention of a strong group of engineers for its construction simplicity and complicated mechanics. Proper bonding between the unit and mortar at unit joints is necessary for the masonry to achieve efficient performance in terms of structural behaviour, serviceability and durability. This is achieved through a combination of chemical and mechanical mechanisms at the unit joints [2,3]. Masonry is susceptible to failure through cracking mechanisms at unit or mortar or unit joints or a combination of such mechanisms due to different load cases such as seismic activity, in-plane, and out-of-plane loading etc [4,5]. The failure at the unit-joint interface is often governed by the shear behaviour associated with the unit-joint interface.

For masonry, the behaviour and capacity depend on the bond strength between the mortar and units. Based on the Mohr-Coulomb criterion, the bond strength depends on the initial shear strength (cohesion), friction coefficient, and normal stress level [6,14]. A few independent tests have been performed on masonry most of them varying by their sampling method and test setups. Tests like Bauschinger's couplet shear test [9] and Van der Pluijm's Dutch masonry couplet test [10] aimed at comprehending the contribution of Cohesion and friction to shear strength at the unit-joint interfaces of masonry based on Mohr-Coulomb criterion. These test setups and similar tests on masonry where compared by Mahdi [7] based on the parameters postulated by Riddington [8], to identify the most optimal test to determine the shear strength at the unit-joint interface. Riddington [11] identified a series of five parameters that each test setup must fulfil to determine the quality of a shear test experiment. These are: (i) a uniform normal and shear stress across the joint, (ii) most of the joint should be near failure during the initiation of failure at one point (iii) tensile stresses are to be avoided along the joint, (iv) failure should be initiated away from the joint edge, and (v) the test setup should be kept as simple as possible. Segura [11] indicates as per Popal and Lissel [13] that most of the current test setups fail to achieve all five parameters of Riddington [12].

In today's scenario, the shear test on masonry has been standardised into the European standards with the EN 1052-3 proposing a triplet test as the standard test to estimate the shear strength of masonry joints. The principle behind the test is based on the slippage between bricks which will occur when the shear stress at the interfaces reach a critical value given by Eq(1),

$$\tau_{max} = c_0 + tan\varphi_0, \tag{1}$$

where c_0 is the cohesive strength and φ_0 is the friction angle. After reaching the critical value τ_{max}, the shear strength is purely due to friction due to the loss of cohesion with the cracking at interfaces [14]. It is essential to note that, almost all the methodology adopted so far estimates the shear strength of a joint as a combined mechanism of cohesion and friction.

Van der Pluijm [10] studied the shear behaviour of masonry joints based on the Coulomb failure criterion. Van der Pluijm indicates that the shear strength was analysed as a function of normal stress based on Coulomb's friction failure criterion. Considering Coulomb's criterion to hold true, cohesion is determined through linear regression of failure points of tests at different precompressions. This is the concept used in the triplet test mentioned in section 1.3. The study concludes that the mode II fracture energy of the joint interface is linearly dependent on the normal stress level as shown in Fig.1. The maximum values of shear stress obtained across different normal loads are used to form a linear regression. The frictional angle is calculated from the slope of this linear regression. The frictional coefficient calculated from the processing of the triplet test is asserted to apply to a brick-mortar interface independent of the normal load.

As discussed earlier, although different methods have been developed to determine the bond strength or cohesion, namely shear bond strength test, tensile bond strength test etc [16], the currently adopted triplet test (discussed in 1.2) fails to fulfil the tensile quality criteria postulated by Riddington [12]. Limited tests were conducted to identify the underlying friction parameter. This emphasises the importance of understanding the contribution of friction through a standalone test, to break down the interpretation by existing method and simultaneously predict the friction mechanism.

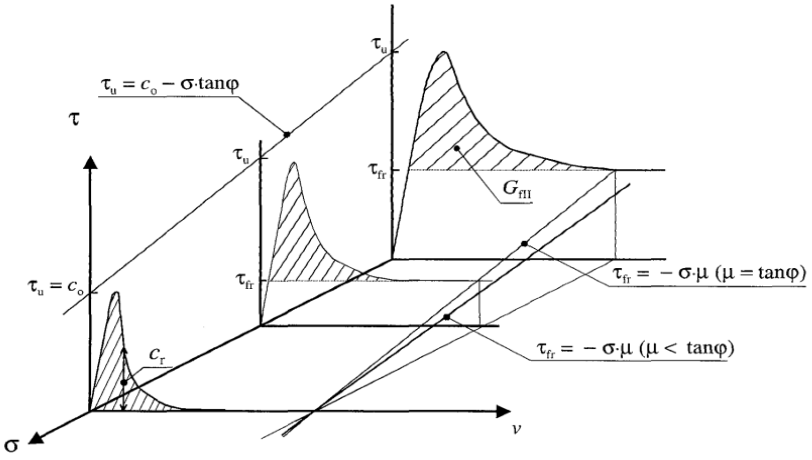

Figure 1: Schematic of deformation-controlled shear tests under 3 different constant normal compression stress levels [10], here τ_u is the peak shear strength, τ_{fr} is the residual friction component of shear stress, σ is the normal load, μ is the coefficient of friction and φ is the internal friction angle.

1.2 State of the art

As mentioned earlier, the Triplet test is the standard test laid down by the Eurocodes to determine the shear strength of horizontal bed joints. This test is also used to determine the cohesion and friction values of the horizontal bed joints. EN 1052-3:2002 [15] elaborates on the experimental determination of the in-plane initial shear strength of horizontal bed joints. The initial shear strength of masonry is derived from the strength of small masonry specimens tested to destruction under a four-point load with precompression perpendicular to the bed joints (Fig 2a). The triplet test being a four loading test, results in the development of concentration of stresses and additional bending [7], this implies that the test setup experiences a tensile stress in the joints, therefore the setup fails to meet the tensile stress

criteria mentioned by Riddington [12] and the shear concentrations becomes a source of inaccuracy for the test (Fig. 2b).

The test is performed at different pre-compression levels lower than 1.0 MPa and the shear strength is plotted against the normal stress. The initial shear strength is defined by the linear regression curve to zero normal stress (Fig.1) and the internal friction angle is determined by the slope of the regression curve [15]. It is notable here that friction is indirectly measured through the said method. The shear strength of the bed joint which is a combined effect of cohesion and friction is evaluated experimentally and the contribution of friction and cohesion are evaluated analytically from the results based on theoretical models.

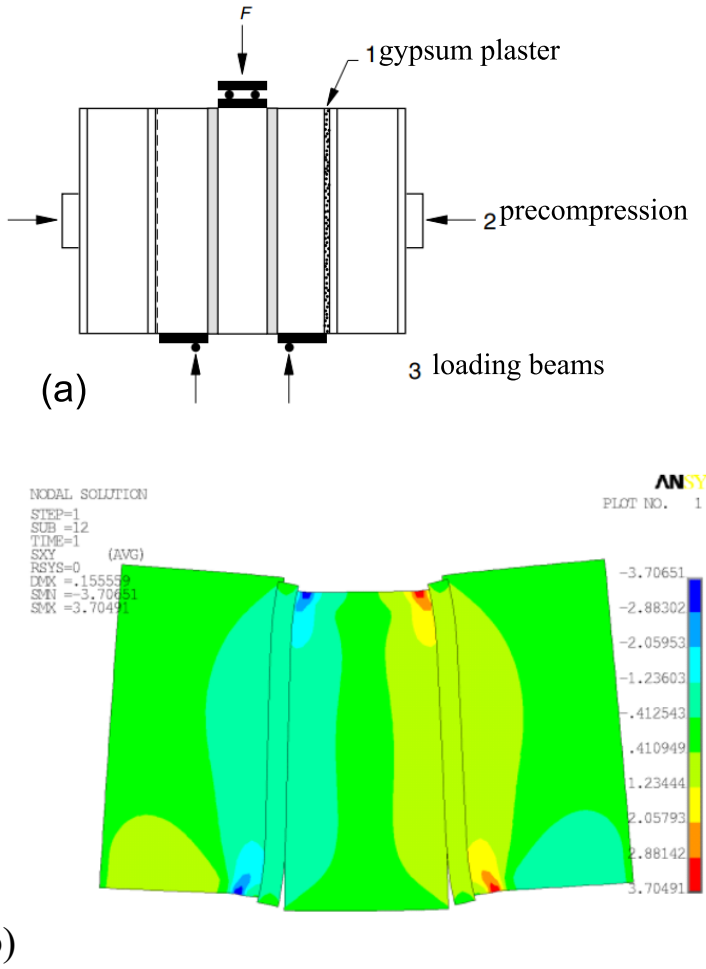

Figure 2(a-b): (a)Test assembly of standard triplet test (Source: EN 1052-3:2002), F corresponds to the shear load (EN 1052-3:2000). (b) Shear concentration in the specimens observed during numerical simulation of EN 1052-3:2000 testing (source: Mahdi et al 2014)

Advancing beyond the conventional shear test methods, this study aims at utilising a reciprocating tribometer to study the frictional behaviour at the unit-joint interfaces. A reciprocating tribometer makes use of a sliding contact to measure the resistance in motion caused by friction (Fig. 3a). This also means that a novel sampling method has to be adopted to set-up the experiments (discussed in section 1.4). In comparison to the EN method, tensile stresses are avoided through this setup.

The data obtained from a reciprocating tribometer includes (i) the relative displacement d, (ii) tangential force Q, (iii) normal force P and (iv) time t. The plot between tangential force Q

and relative displacement yields a hysteresis loop termed “tangential hysteresis loop” [18]. The area under the tangential hysteresis loop of each cycle equates to the energy dissipated by friction in that cycle [19]. If the Amonton-Coulomb behaviour holds true, the plot would resemble a rectangle. In contrast, the plot of the measured data resembles a hysteresis loop and demonstrates a deviation from the expected Amonton-Coulomb behaviour [18].The plot of the ratio between tangential force Q and normal force P against the relative displacement yields a hysteresis loop called “Q/P hysteresis” (Fig.3b). The test is performed across multiple cycles at a prescribed frequency resulting in fretting, i.e. the removal or dislodgement of material due to the sliding interaction [20]. In the case of a brick-mortar specimen being subjected to the tribometer test, fretting would be a significant mechanism due to the brittle nature of the material (discussed in section 2.3).

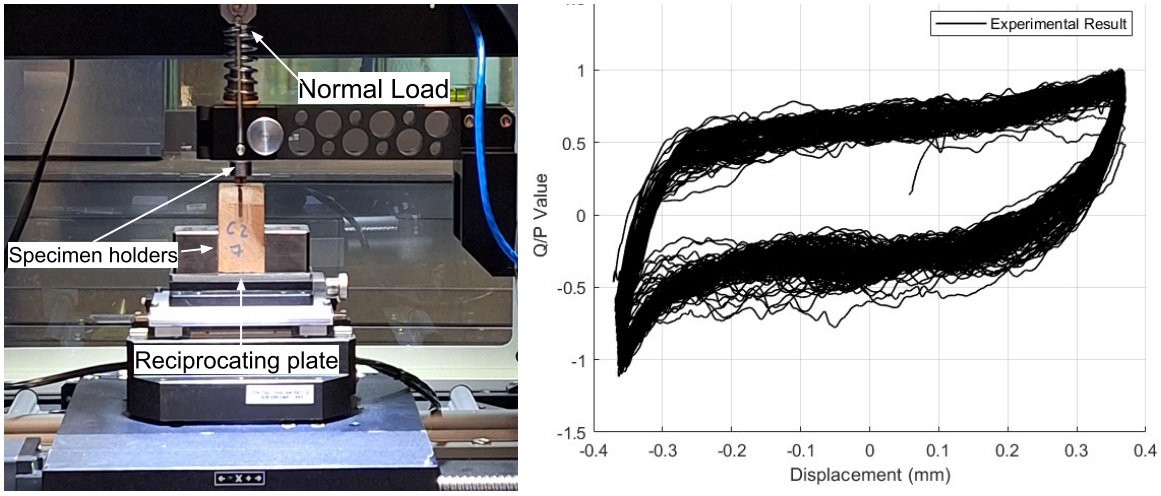

Figure 3(a-b): (a) Reciprocating tribometer setup,(b)A measured Q/P hysteresis (a plot of Tangential force ‘Q’/Normal load ‘P’ against the relative displacement) performed across 180 cycles.

1.3 Research objectives and research questions

The study aims to investigate the contribution of dry friction to the shear strength of masonry through a standalone test, in order to study the frictional mechanism and analyse the compliance of these mechanisms to the derived results from existing methods, namely the EN method. The research aims to explore the reciprocating tribometer to directly evaluate and study the frictional behaviour of brick-mortar interface under different normal compressive load levels (precompression levels). Through the experiments, the researcher focuses on answering the following research question and sub-questions:

What are the key parameters that mostly affect the frictional behaviour at a cracked unit-joint interface?

- How can tests be conducted using a tribometer on a cracked unit-joint interface?
- How does the pre-compression level and test frequency influence the coefficient of friction CoF?
- How does frequency or precompression affect the energy dissipation through friction?

1.4 Research Methodology

This study follows a novel testing approach using an RTEC MFT 5000 reciprocating tribometer along with a novel sample preparation method to analyse the behaviour of dry friction between unit-joint interfaces. The novel testing approach is based on the idea of two interfaces under reciprocating sliding with interfaces under complete "contact". The contact area refers to the apparent contact area which is the gross area of the smaller specimen which undergoes sliding. We use the term apparent contact, since the specimen on a macro and micro level could have a lower contact area than the overall geometry. Unlike the more prominent shear test methods which uses a complete couplet or triplet assembly and require complex loading mechanisms, the tribometer setup is relatively simpler and straightforward. The tribometer test utilises specimens mechanically extracted from bond wrenched masonry couplets, which are devoid of cohesion. The samples are therefore smaller than the traditionally used samples (couplets and triplets).

The tribometer is slightly modified to accommodate the couplet specimen, which consists of a water sawn cylindrical bore sample of 9 mm diameter for the top holder and a water sawn cuboid extract of the dimension 30 x 30 x 50 mm for the bottom holder of the tribometer, both extracted from near proximity. Throughout the study, the cylindrical sample contained the brick interface, while the bottom cuboidal sample contained the mortar interface. Three masonry couplets were chosen for the experiment and samples were prepared from each of these parent samples.

An experiment matrix is setup to identify and restrict key parameters of the experiment such as sliding distance, frequency, number of cycles, time period and normal force. The data obtained from the tests include, tangential force, relative displacement, normal force and time history. These data are analysed by first building a:

- Tangential force Hysteresis (Tangential force Q against relative displacement)
- Q/P Hysteresis (Q/P ratio against relative displacement)

The loops are then averaged over time at each unique position, to obtain a mean curve for each measured hysteresis. This mean curve is then used to determine the coefficient of friction, energy coefficient of friction and contact stiffness as laid down by Llavori [21]. The analysis is repeated across each adopted precompression levels and the observed trends are analysed for interpretations.

1.5 Outline of Thesis

The thesis consists of three sections. Chapter 1 presents a comprehensive introduction to the study followed by Chapter 2 which concisely describes the study, its procedure, experiments and results. Chapter 3 discusses and elaborates the results and draws a conclusion to the study.

2 PAPER

Characterisation of frictional behaviour at brick-mortar interface.

Abstract: Unreinforced brick masonry, a popular construction material with a rich historical legacy, has been resilient through centuries, despite its susceptibility to failure through various loading conditions such as seismic forces. Understanding the mechanical behaviour of masonry, particularly the cohesion and frictional mechanisms at interfaces between bricks and mortar, is crucial for assessing its structural performance. This paper presents an experimental study characterising masonry frictional interfaces using a tribometer test, a novel approach in masonry research.

The study investigates the frictional behaviour of cracked unit-mortar interface under varying pre-compression levels and sliding frequency. The frictional behaviour was characterised by means of the mean coefficient of friction (CoF), the energy coefficient of friction (ECoF), the tangential contact stiffness, and the dissipated energy. Experiments were conducted using a reciprocating tribometer, and in order to accommodate the specimens in the tribometer, a novel specimen extraction procedure was developed with an ad-hoc holding setup. Tests were performed on clay brick masonry with lime-cement mortar.

In the field of masonry, the Coulomb friction is frequently used as the primary criterion for analysing the behaviour of masonry at brick-mortar interface. The experimental results revealed a non-Coulomb behaviour in the coefficient of friction (CoF) and its dependence on precompression levels, contradicting assumptions in masonry structure analysis models. Higher frequency (3 Hz) and lower frequency (0.2 Hz) experiments showed a non-Coulomb behaviour with a non-linear trend between kinetic and static friction, becoming relatively linear with increased precompression levels. CoF showed no systematic time dependency, while Energy Coefficient of Friction (ECoF) exhibited a systematic decrease over time, relating energy dissipation across cycles. Energy dissipation increased with higher precompression levels. Tangential contact stiffness, the force required for unit displacement in the tangential direction, increased with precompression in accordance with existing mathematical models. Influence of frequency on frictional behaviour, was briefly studied using a preliminary constitutive modelling approach using the LuGre model. Analysis indicated velocity's influence on frictional force at the interface.

The findings provide general insights into the frictional characteristics of cracked brick-mortar interfaces under varying loading conditions. The observed decrease in both the frictional coefficients with increase in precompression level, sheds light on the practical aspects of testing methods and offer considerations for further research in the field of masonry engineering.

Keywords: Coefficient of Friction, Energy Coefficient Friction, Contact Stiffness, Energy Dissipation, Tribometer Tests.

2.1 INTRODUCTION

Unreinforced masonry (URM) is a composite construction material utilising a brick unit usually made from clay or concrete bonded together on a bed of mortar, usually made of cement and sand [1]. Masonry becomes functional through the bond between units and mortar, these bonds are achieved through mechanical and chemical mechanisms at the interface[2,3]. The shear strength of unit-joints of unreinforced masonry plays a vital role in masonry structures by providing adequate resistance against structural failure when subjected to various loads, including seismic activity, strong winds, unexpected impacts etc[4,5,23]. These structures are often valuable assets, such as historical heritage sites that reflect our cultural legacy, and residential dwellings.

The shear resistance of masonry is often related to the behaviour at the unit-mortar interface, as this is the weakest link in the system[14,23]. The combined contribution between the strength and cohesion of the individual masonry units and the mortar that binds them together along with the presence of vertical and horizontal joints influences the overall strength including the shear resistance [17]. Therefore, understanding the shear behaviour at unit-mortar interface is a key focus in masonry design and construction[22].

Researchers have earlier conducted tests on the shear sliding behaviour of unit-joints, these experimental studies were essential to gain insights into the behaviour and performance of masonry under different loads and load combinations, allowing for the identification and assessment of parameters like cohesion and internal frictional angle. Previous studies agree that the increase in the applied precompression was accompanied by an increase in the shear strength of the unit-joint and the level of this increase varied between different types of masonry [23]. It was found that the mortar used also contributed to the shear strength of the joints, a stronger mortar meant that the shear strength and cohesion were stronger, but the coefficient of friction was deduced to be independent of the mortar strength [24]. Previous studies on bonded masonry specimens evaluated the shear properties at the unit-mortar interface in masonry, typically on couplets or triplets [7]. The shear test is one of the major types of tests performed on a couplet or triplet and such a test would give insights into the shear capacity of the unit-mortar interface. A key aspect of processing results of the shear test involves calculating the cohesion and frictional forces at the unit-mortar interface, which is achieved through the application of a Coulomb friction failure criterion, an important framework in mechanics for modelling the behaviour of friction [15]. The criterion assumes Amonton-Coulomb's law: for which the friction force is directly proportional to the normal load and governed by a coefficient of static or kinetic friction.

In the past years different shear tests have been performed on masonry units, each unique through the geometry of the specimen and loading method. Riddington [12] postulates five quality criteria for shear tests, yet most of the current methods fail to achieve all five quality parameters [11]. The European standards (EN 1052-3) have standardised the triplet test to estimate the shear strength of bed joints. The code [15] elaborates on the specimen preparation, loading arrangement and processing of results for a standard triplet test. The triplet test requires a few laboratory-prepared triplet specimens, and each test is loaded with different axial pre-compression levels [15]. The central brick is subjected to a shear load which slides out the central brick at a slow rate of displacement. The peak shear strength τ is plotted against the compressive stress σ, the results were processed to obtain the Coulomb friction failure criteria:$\tau = c_0 + tan\varphi_0$, where c_0 is the initial shear strength obtained by the

y-intercept of the interpolated linear regression of the results to 0 pre-compression levels and φ_0 is the internal friction angle obtained from the slope of the linear regression [25].

The contribution of cohesion (c_0) and friction component of shear stress(τ_{fr}) to the shear stress is described in Figure 2a. The residual friction part of shear stress is the resistance in the surface after the residual cohesion c_{rs} ceases. The residual friction is the constant tail observed after the peak shear stress. The frictional coefficient is calculated from the internal friction angle obtained from the slope of the linear regression of peak measurements taken across independent tests at different precompression stress levels (in the linear region, i.e. < 1.0 MPa, [23]). A possible pitfall of the followed approach is the assumption that the coefficient of friction is a constant paramter, independent of the precompression. We can see that except for the case of: $\sigma = 0$, the peak shear stress (τ_u) has an active indistinguishable contribution from both the cohesion component of shear stress and the frictional component of shear stress (Fig.4). When a body is loaded, the surface subjected to fracture undergoes displacements that can be categorised as Mode I-tensile opening, Mode II-sliding shear and Mode III-tearing shear. The crack propagation in mode II fracture operates such that the fracture surfaces slide past each other in the opposite direction [26]. Mode II fracture energy represents a material's inherent resistance to crack propagation in a mode II fracture mode [17]. It is important to note that during mode II fracture, cohesion and friction contribute to the fracture energy.

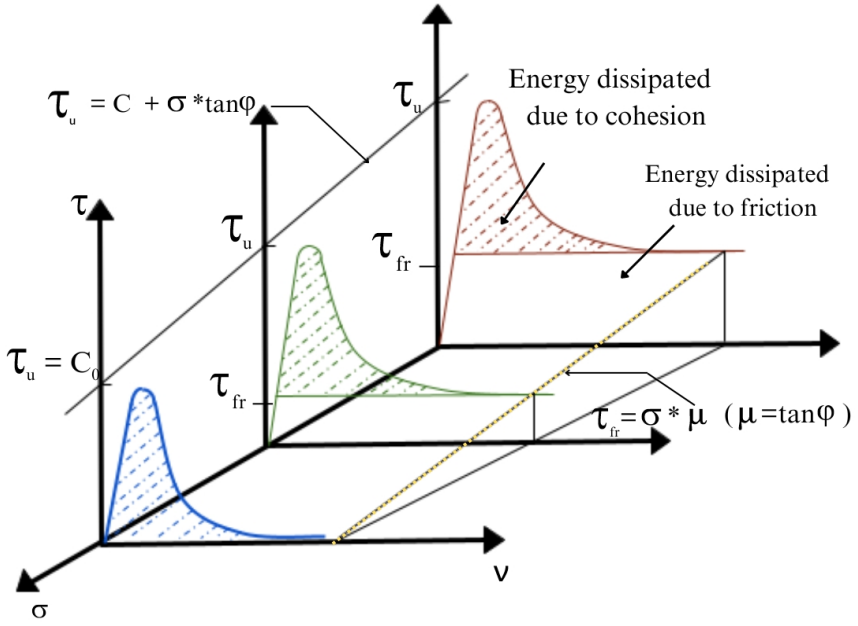

Figure 4: Schematic diagram of deformation-controlled shear tests under 3 different constant normal compression stress levels (as depicted by Van der Pluijm [17]), here τ_u is the peak shear strength, τ_{fr} is the residual friction stress, σ is the normal load, μ is the coefficient of friction and φ is the internal friction angle.

The presence of this dependency complicates the predictability and reliability of masonry structures, as it introduces uncertainty in the behaviour of the material under different conditions. Consequently, it introduces the need for continued research and refinement in our understanding of shear resistance and energy dissipated in the shear failure of masonry.

In the pursuit of a comprehensive understanding of the frictional response within the unit-mortar interface of masonry materials, a novel investigative technique was introduced

and implemented: the utilisation of a tribometer test. This specific test aims to introduce an innovative specimen extraction method, explicitly eliminating the influence of cohesion at the interface. The primary focus is on a thorough investigation of the interface's frictional behaviour while deliberately excluding the impact of cohesion. This novel approach is designed to explore the isolated contribution of pure friction and assess how it varies with applied parameters. The objective is to facilitate a cross-validation of existing data by emphasising the exclusive examination of friction-related aspects: the mean CoF, the Energy Coefficient of Friction (ECoF), and tangential contact. Study of friction using a tribometer also depends on parameters such a temperature, moisture level and surface roughness. The dependency on temperature and moisture level could not be investigated due to the limitation of the available tribometer modules. Study on the dependency of surface roughness on coefficient of friction by Rabinowicz [36], indicates that the coefficient of friction is independent of surface rough to a certain region based on the material in contact. Since masonry is a rough material (Appendix B), and the lack of classification of the roughness region where coefficient of friction is independent of surface roughness, surface roughness is not included in the scope of the current study.

2.2 Material and Method

2.2.1 Tribometer Setup

The tribometer used in the study is an RTEC MFT-5000 reciprocating tribometer (Fig.5), the upper horizontal arm holds a vertical specimen and imparts normal force via a spring contact. The instrument also uses a movable lower plate onto which a mounted sample can be moved in reciprocation at a frequency setting. The tribometer has an operating range between 0.1 Hz and 80 Hz enabling the possibility of both high frequency and quasi static tests .The sample units (discussed in section 2.2.3) are extracted and mounted onto the setup through a modified holder (discussed in section 2.2.2),

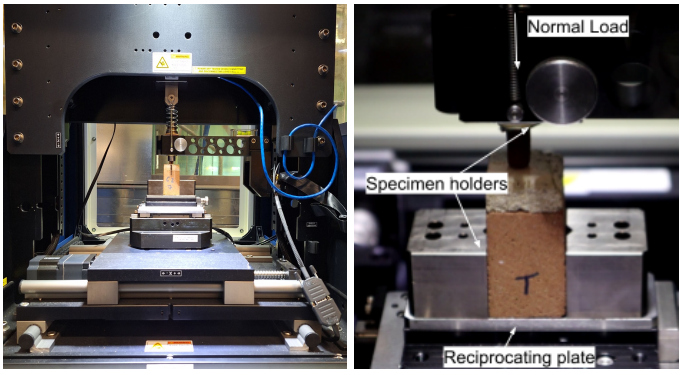

Figure 5: Experimental assembly of RTEC MFT 5000 Multi-function Tribometer used for the experiments

The regular reciprocating tribometer utilises a pin-on-plate setup, this arrangement is infeasible in the case of masonry. Therefore, the setup was modified to accommodate a suitable sample model (Fig.6). For this, a steel casing with an external diameter of 19 mm was used. The drill of 10 mm diameter with a depth of 45 mm was made into the steel casing to accommodate a cylindrical brick sample. This would provide enough confinement against bending in the brick specimen.

The reciprocating plate was replaced, with a 30 x 30 mm cut of the couplet half with a layer of mortar bed as the bottom specimen. This would restrain the maximum imposed amplitude

of the sliding displacement 0.8 mm (+0.4 mm and -0.4 mm) to be 10.1mm from the edges of the bottom specimen. This constraint is applied to ensure that at no point in the experiment, the samples are in partial contact.

The normal load applied to each experiment is derived from the predetermined precompression stress levels. The precompression levels across the study were performed on the levels of 0.6 MPa, 0.4 MPa, 0.2 MPa and in some cases with an additional cases of 0.1 MPa and 0.05 MPa. Therefore the normal load in each case was obtained from the chosen stress level and apparent area of contact. The term apparent is used to highlight the assumption that the actual surface of the specimen was overlooked at a meso level to not consider elastic and plastic deformation, as well as the change in interface contact due to material removal or wear.

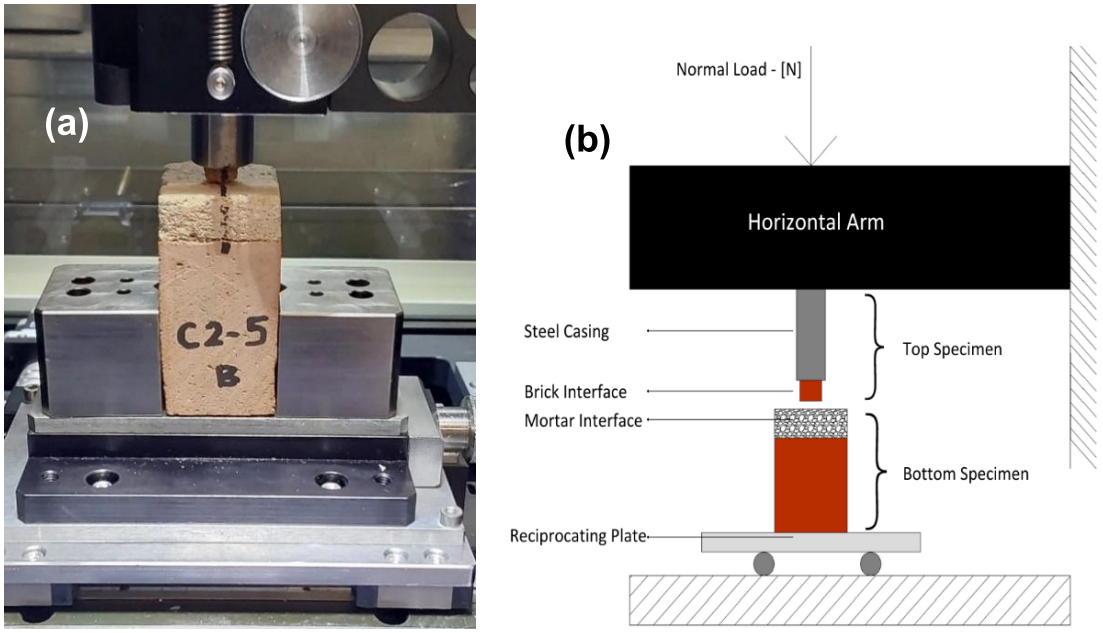

Figure 6(a-b): (a)Modified tribometer setup to accommodate brick-mortar extract specimens. (b) Schematic representation of modified tribometer setup

2.2.2 Sample Preparation

Three solid clay brick couplets were chosen to be processed and prepared for this experimental study using a reciprocating tribometer. The couplets were marked for identification, bond wrenched and sawn to the required size. The masonry couplet investigated in this research is an unreinforced clay brick masonry with the following properties given by table 2.1,table 2.2 and table 2.3,[23]:

Type	Flow (mm)	Mortar Proportion (C:L: Sa)*	Mortar Flexural strength f_{mb}MPa	C.o.V	Mortar Compressive strength f_{m}MPa	C.o.V
Cement Mortar	188	1:2:9	1.40	0.12	3.81	0.09

Table 2.1 : Mortar properties (MAT-3, S.Jafari,2021[23])

Type	Size [mm]	Normalised Compressive Strength f_b [MPa]	C.o.V
Clay-Solid	210x50x100	28.31	0.10

Table 2.2: Material properties of the unit (MAT-3, S.Jafari,2021[23])

Type	Compressive Strength (MPa)	C.o.V	Youngs Modulus E2 (MPa)	C.oV
Masonry	14.02	0.04	4640	0.25

Table 2.3 : Properties of the masonry from vertical compression test (MAT-3, S.Jafari,2021[23])

In addition to the properties mentioned in table 2.1, table 2.2 and table 2.3, the bond strength (f_w) determined from the bond wrench test on this masonry was 0.14 MPa with a coefficient of variation of 0.46 [23]. The experiments focus only on the frictional behaviour of the unit-mortar interface therefore the prepared samples should be devoid of any cohesion. This is achieved using a bond wrench assembly. A couplet is pulled open using a machine-controlled or manual bond wrench. This would break the cohesive bond of the interface and the path can be retraced to put the couplet back to its initial position. The top specimen is a slender cylindrical bore extract from the top half of a bond-wrenched couplet. The slender cylinder is then carefully placed into a metal cylinder with a drill hole matching the extracted specimen's dimension range. This offers the slender brick cylinder continuous bracing against buckling. Meanwhile, the bottom specimen is obtained by sawing the bottom half of the couplet in a rotary saw, along the marked grid lines (Fig.7).

The bottom specimen can be mounted onto one of the manufacturer's add-on holders. The holder unit consists of two blocks between which an extracted brick sample (3x3 cm) with the other interface of significance can be mounted and tightened. The holder grips the sample during the reciprocating motion, restraining any unwanted movement of the sample in the direction of reciprocation.

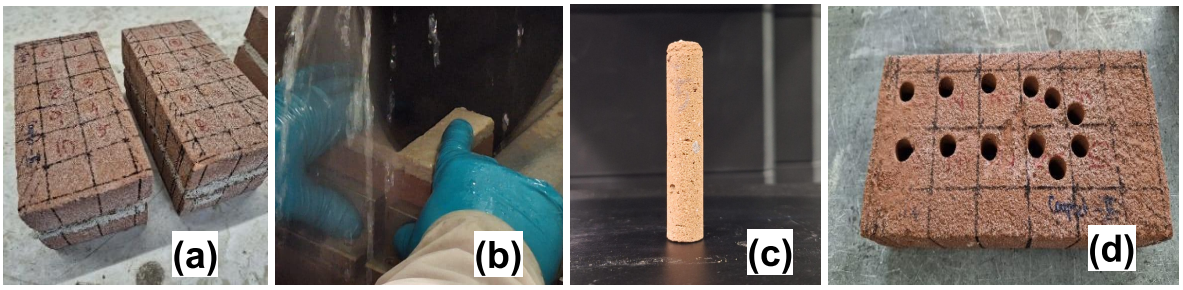

Figure 7 (a-d, clockwise): (a) Bonded couplets marked before specimen extraction, (b) Bottom specimen extraction using a rotating saw, (c) extracted cylindrical specimen, (d) The parent couplet after cylindrical specimen extract.

2.2.3 Procedure

Testing masonry specimens extracted from a brick-mortar unit, on the tribometer requires an unconventional approach. The reciprocating tribometer is modified to accommodate the extracted brittle specimen, such that failure due to buckling and the bending of the specimen

instead of sliding is ruled out. The reciprocating tribometer employs: (i). cylindrical metal holder with an extracted interface (hereby referred to as top specimen) through which normal load P is applied, and (ii). A reciprocating plate, on which the other surface of significance is mounted (hereby referred to as the bottom specimen). The tribometer offers many test parameters that can be opted for based on engineering assumptions for each scenario. The options offered are displacement range, reciprocating frequency, logging frequency, acceleration-deceleration control, and normal load control. The logging frequency adopted across the study is 4000 Hz. This would enable the study to have a higher resolution of data to pick up small variations in forces. However noise accompanies the high rate of logging, this must be considered while processing the measured data. The loading and friction test were performed in two steps, (a) the sample was loaded to the required normal load and was held in position for 60 seconds, (b) this was followed by the test. This way the variation in normal force, caused by the preset and feedback were minimised.

The bottom sample can be mounted into the holder with relative ease. The extracted specimen is placed between the holder's restraining blocks and is fastened. Mounting the top specimen requires the use of an HMA Glue (Heat Melt Adhesive). This glue does not chemically influence the brick specimen and does not soften the brick specimen due to the absence of moisture in any form. Therefore, a few more steps are to be carried out before it can be mounted into the tribometer to commence the pre-experiment checks: (i). The steel/metal holders are pre-heated in a kiln/oven. This would prevent the glue from drying out quickly, preventing the brick cylinder from being encased inside the metal holder. (ii). A thin layer of glue is applied, after which the brick cylinder is lowered into the opening. The sample is pushed so that any excess glue can flow out, ensuring good contact. (iii). The unit is left out to cool. (iv). After the experiment, the holder is placed on a container and back into the kiln/oven to heat and remove the mounted sample. (v). This cycle is repeated for all samples.The results were analysed (discussed in section 2.3) and a few parameters were revised for a second set of experiments. The test parameters are detailed in Table 2.4. The choice of test frequency is explained in section 2.3.1.

Parameter	Pre-compression -I	Pre-compression -II	Pre-compression -III	Pre-compression -IV	Pre-compression -V	Frequency	Sliding distance	Number of Cycles	Test Duration
Unit	MPa	MPa	MPa	MPa	MPa	Hz	mm		seconds
Exp - I	-	-	0.2	0.4	0.6	3	0.3 - 0.4	180	60
Exp - II	0.05	0.1	0.2	0.4	0.6	0.2			900

Table 2.4: Test parameters considered for the experiments.

2.3 Experiments and Results

During each cycle of reciprocating sliding, the changes in normal and tangential forces, their relation to each other, the energy dissipation and the resistance to the sliding by the interface at extremities were studied. The parameter corresponding to the relation between forces and energy is the coefficient of friction. To study the changes in forces and energy the Coefficient of friction was broken down into (i) the mean coefficient of friction (Mean CoF, μ) and (ii)

the Energy coefficient of friction (ECoF, μ_e). The mean coefficient of friction is derived from (I. Llavori et al 2019) [21], Eq(2):

$$Mean\ Coefficient\ of\ Friction\ (CoF, \mu) = \frac{Max\left(\frac{Q}{P}\right) - Min\left(\frac{Q}{P}\right)}{2} \quad (2)$$

In the presence of wear, the Q/P ratio is not appropriate to characterise friction as it is not representative in case of a Non-Coulomb behaviour, which is characterised by predominant peak values during velocity reversals [29]. The peak is non-coulomb and nonlinear, which can be understood from the observation of "hook" like features being present in the peaks of the fretting loops, [21] Fouvry 2004, developed the energy coefficient of friction to provide a more realistic method to calculate coefficient of friction. The method was developed to minimise the effect of wear-scar interaction and is based on the energy dissipation over the fretting loop to calculate the Coefficient of Friction (CoF), now called ECoF[29,27].

The energy coefficient of friction (ECoF, μ_e) gives the ratio of the measured loss in energy during the cycles to the hypothetical Coulomb energy loss which is approximated as four times the product of slip distance d and normal load P in the reciprocating translation [27]. This method is stable and is recommended for material characterisation. The energy coefficient of friction Eq(3) utilises the tangential force hysteresis instead of the Q/P hysteresis [28,29]. The area inside the hysteresis curve is equal to the energy dissipation

$$Energy\ Coefficient\ of\ Friction\ (ECoF, \mu e) = \frac{Energy\ Dissipated}{4 * slip\ distance * Normal\ load} \quad (3)$$

Contact stiffness is the change in tangential force at contact interface for a unit change in relative tangential displacement of the surface in contact in the sticking or velocity reversal phase, i.e. an instantaneous tangent at a specific load value associated with the velocity reversal region [31]. Contact stiffness was the third key parameter identified and analysed throughout this study.

2.3.1 Experimental observations

An initial set of experiments was performed across three pre-compression levels of: 0.2 MPa, 0.4 MPa and 0.6 MPa at a frequency of 3Hz. This was chosen based on the response of masonry structures to loading investigated in [34], the test structure is seen to have higher response between time periods of 0.2 seconds and 0.4 seconds. Three samples were tested in each case as per the parameters laid down in Table 2.4. The logged data was processed to obtain, (1) A Tangential/Normal force vs. displacement curve and (2) a Tangential force vs. displacement curve . Both the curves were observed to be hysteresis curves with 180 cycles. The data was analysed through two methods: (i) each cycle was analysed and (ii) the hysteresis (Fig.8c) was averaged across cycles to obtain a mean curve (figure 6a). The mean curves across a specific pre-compression level were averaged again to obtain a representative mean curve for a given pre-compression level[Appendix C, Appendix D].

The summary of mean Q/P (Tangential Force 'Q'/ Normal Load 'P') frictional hysteresis observed across different compression levels is represented in Fig 8a, 8b. The frictional behaviour is non-Coulomb in nature with a loss of symmetry with decreasing precompression levels and sharp peaks are observed in the extremes of the hysteresis. A curved profile of the hysteresis is observed between the peaks, i.e., the sliding region. The profile tends towards a smoother curved profile with an increase in pre-compression level.

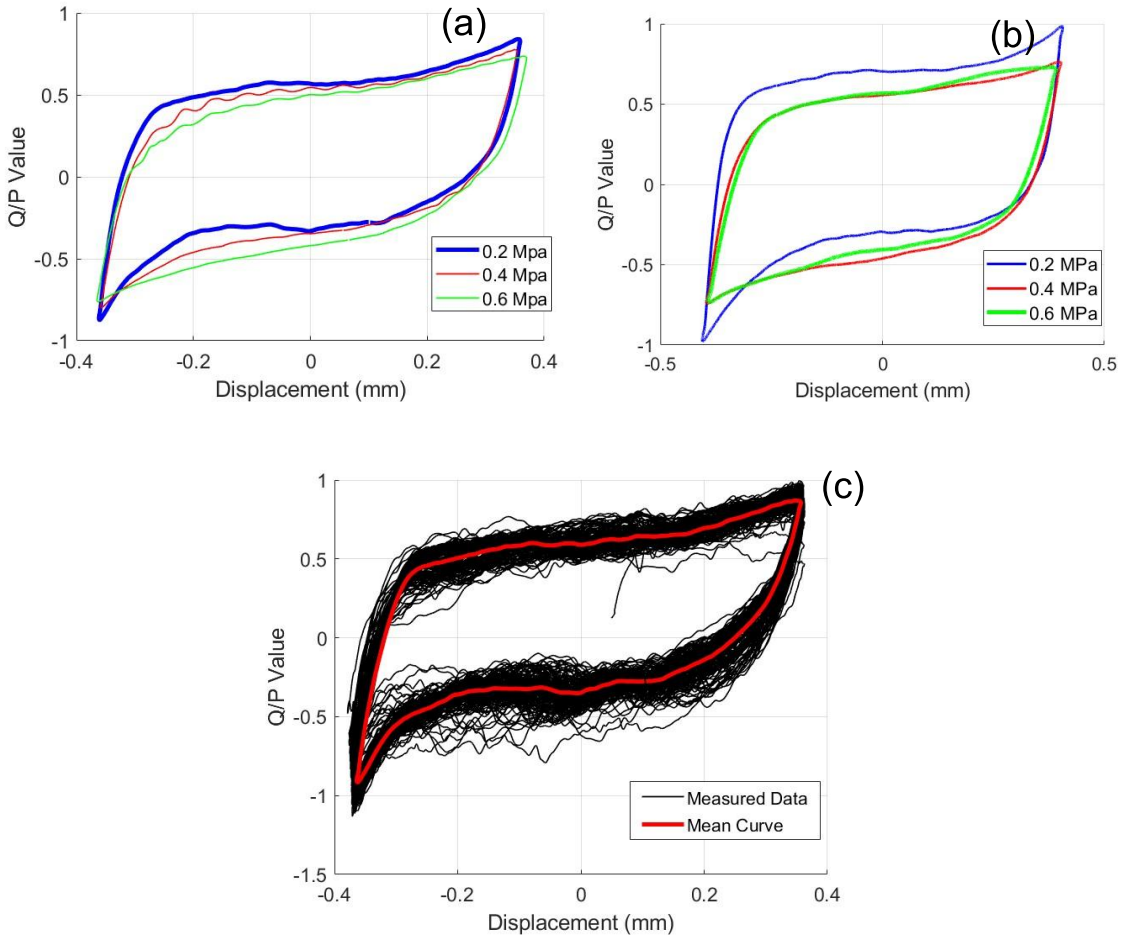

Figure 8 (a-c): (a) Mean representative curves across different precompression levels for 3Hz. (b) Mean representative curves across different precompression levels for 0.2Hz. (c) An example (3 Hz) of measured Q/P hysteresis and averaged mean curve.

The second set of experiments was performed across five pre-compression levels of: 0.05 MPa, 0,1 MPa, 0.2 MPa, 0.4 MPa and 0.6 MPa. This set of tests were performed at a low frequency, 0.2 Hz aimed at investigating the quasi-static frictional behaviour and influence of velocity in masonry tribometer tests.

The time averaged, mean Q/P frictional hysteresis observed across different compression levels is represented in Fig 8a,b . Similar to the previous results, the frictional behaviour is non-Coulomb in nature and sharp peaks are observed in the extremes of the hysteresis, this phenomenon is visible in the measured unaveraged data and in the averaged mean curves. It is to be noted that the sliding phase has a relatively linear path (between the peaks). The hysteresis curve tends to approach a linear trend with less distinct peaks when the pre-compression level is increased.

An observation from the mean curves across the frequencies (both 3Hz and 0.2Hz) indicates that the mean curves obtained from the lower frequency analysis have a more visible and distinct static and kinetic friction behaviour. This could be partly due to lower damping forces on the interface due to the reduced acceleration involved in the experiment. A plot of frictional force against sliding velocity Fig 9(a-b) illustrates this observation.The sliding velocity at each instant was obtained from time derivative of sliding distance and analytical time interval, which is then plotted against the instantaneous frictional force from the logged

data. The precompression level of 0.2 MPa was chosen to illustrate this observation, the peaks at extremities are less prominent with an increase in precompression level, similar to the peaks being less significant in the Q/P hysteresis with increase in precompression levels. The tests at 0.05MPa was an exception observed to this hypothesis. This deviation could be due to the combination of low normal load and low frequency. The significant noise in 0.05 MPa which contributes to the deviation observed could be due to the influence of low normal load and frequency on displacement controlled equipment. A noticeable level of noise is visible in the low frequency- low precompression loops. This could be possibly due to the high sampling rate and the feedback in the displacement-controlled apparatus picked up by the sensitive measurement array (piezometric sensors).

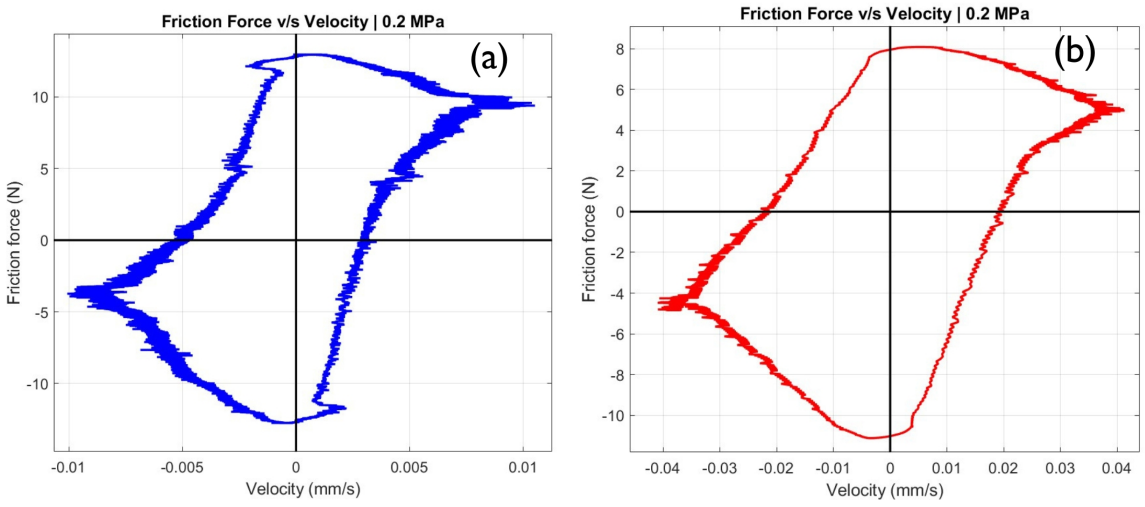

Figure 9 (a-b): Frictional Force v/s velocity (a) at 0.2 Hz with normal load 12.8 N, and (b) at 3 Hz with normal load 8 N

2.3.2 Coefficient of Friction

The mean coefficient of friction CoF observed across the hysteresis loop from each cycle. CoF was calculated for both: (i) per cycle and (ii) mean curve cases using Eq(2). The CoF calculated from each hysteresis cycle was recorded to form a CoF distribution. The CoF distribution is an array containing the mean coefficient of friction for all 180 cycles. A mean for the distribution ($CoF_{distribution}$) is determined from the parameters of a normal curve fitted onto the distribution . The mean of the $CoF_{distribution}$ is compared with the CoF obtained from the mean curve (average loop of the hysteresis) in Table2.5. In most cases, both the values (CoF of mean curve and $CoF_{distribution}$) were observed to be in close range. This indicates that the mean curve is a simpler and relatively accurate way to represent the frictional behaviour of an interface in the considered case. The results of the CoF calculation are shown in the table. No clear and systematic dependency between CoF and number of cycles is observed, this can be inferred from Fig.10(a-c) which illustrates the time evolution and distribution of CoF across cycles for the test frequency of 3 Hz. The distribution estimates the mean and standard deviation of CoF associated to a particular precompression level (the distribution parameters of the fitted curve are indicated in: red- standard deviation, blue- mean of distribution).

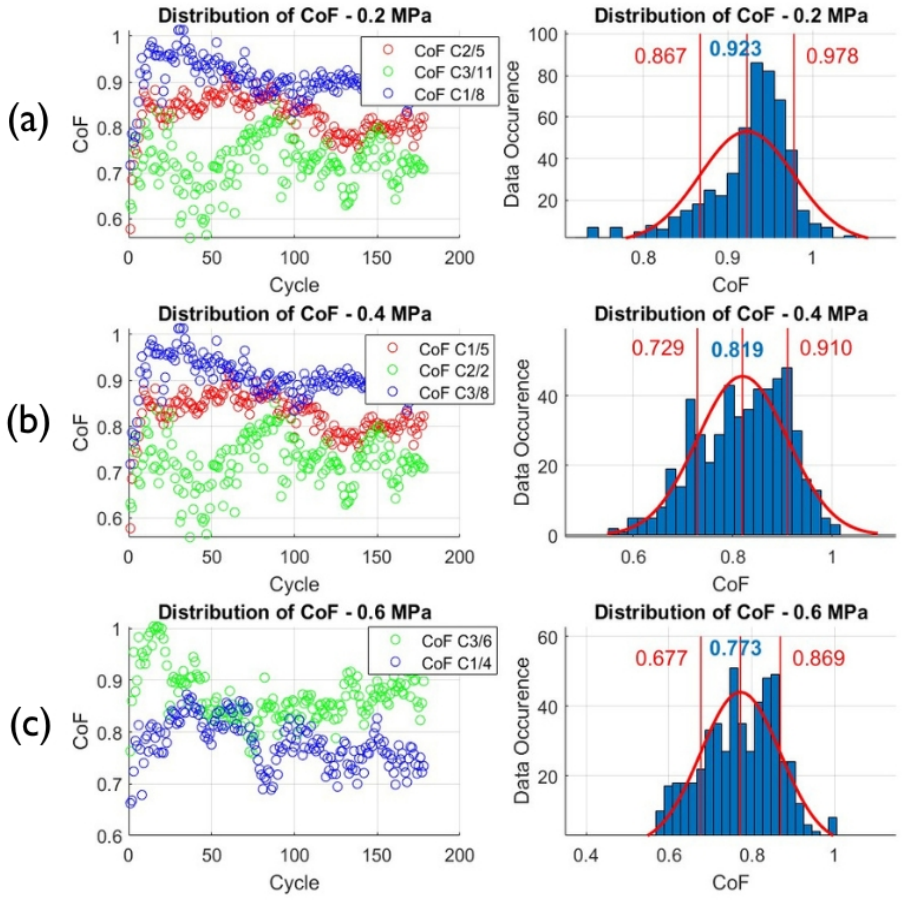

Figure 10 (a-c): Evolution and distribution of CoF as measured from tests with 3 Hz frequency plotted along with the distribution.

The Energy Coefficient of Friction (ECoF) was calculated in a similar way (i.e. both per cycle and mean curve) using Eq(3). The energy dissipated for each cycle was calculated by calculating the area enclosed under the Tangential force hysteresis curve (shear force v/s displacement). A similar trend was found between the $ECoF_{distribution}$ and ECoF of the mean curve. The ECoF has an initial high value, followed by a systematic decrease over time (Fig.11). This is further discussed in section 2.3.3.

However, it was important to note that the variation in the calculated ECoF across each precompression level was much less than the variation between mean CoF across different precompression levels as similar to the prediction in [21]. The table encompasses the values of mean CoF and ECoF for each precompression level.

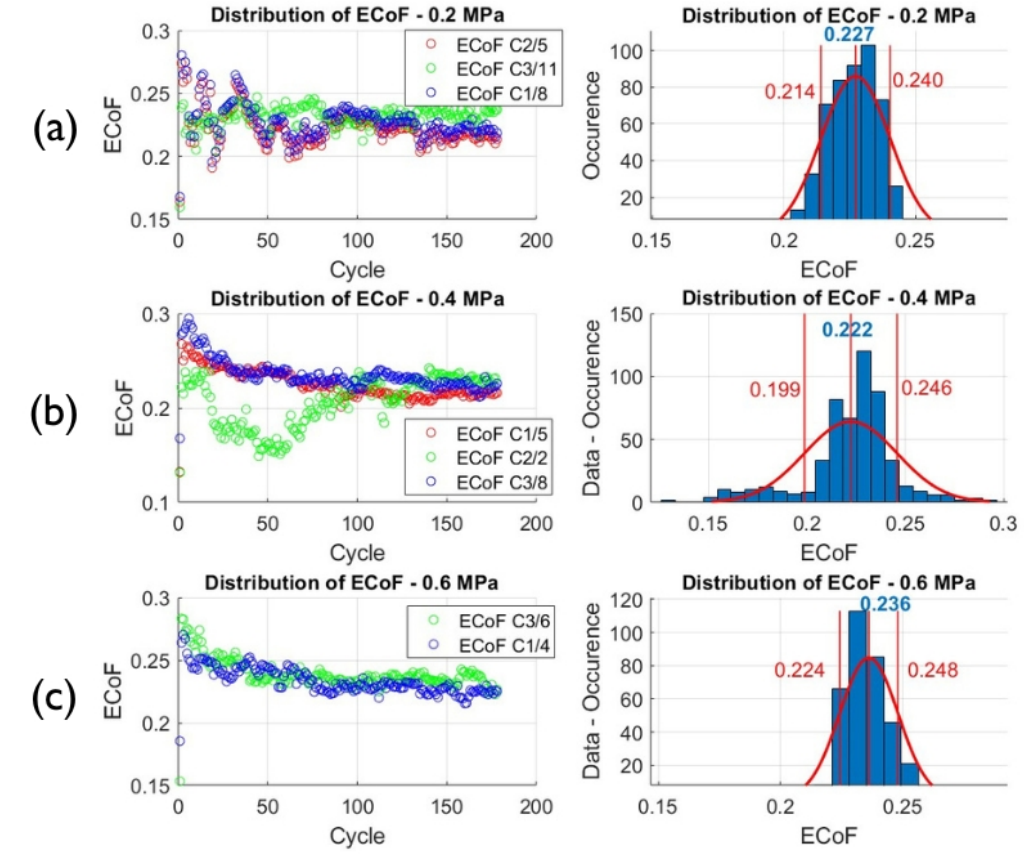

Figure 11: Evolution and distribution of ECoF as measured from tests with 3 Hz frequency.

A similar trend was observed for measurements from tests of 0.2 Hz (see Appendix D).

Parameters		**Frictional Coefficients**					
Frequency	***Precompression***	***mean CoF***	***mean $CoF_{distribution}$***	***Standard deviation $CoF_{distribution}$ (+/-)***	***mean ECoF***	***mean $ECoF_{distribution}$***	***Standard deviation $ECoF_{distribution}$(+/-)***
3 Hz	0.2 MPa	0.839	0.923	0.0856	0.217	0.227	0.013
	0.4 MPa	0.776	0.819	0.09	0.211	0.222	0.023
	0.6 MPa	0.736	0.773	0.096	0.209	0.218	0.012
0.2 Hz	0.2 MPa	0.985	1.003	0.185	0.250	0.258	0.023
	0.4 MPa	0.765	0.767	0.109	0.242	0.242	0.026
	0.6 MPa	0.729	0.746	0.049	0.243	0.243	0.028

Table 2.5 Comparison of CoF and ECoF

2.3.3 Energy Dissipation

Fouvry [29], studied fretting damage due to wear and crack nucleation of specific metal surfaces. It was found that the energy coefficient of friction exhibited an increasing trend for the first few hundred cycles. Although this refers to metals, and the formation of a tribologically transformed structure, a similar observation was made in this study of brick-mortar interfaces (Fig.11). A high ECoF value was observed briefly followed by a

downward trend. Fretting of asperities and lubrication can be hypothesised as probable mechanisms, but this is not considered in the current scope of the study.

The progression of hysteresis loops was investigated across the experiments. This enabled to track the trend of energy dissipation through the frictional hysteresis. By observing the change in shape of the hysteresis area and its trend (Fig.12), a correlation to the decay of ECoF can be understood. The decrease in the dissipated energy is directly proportional to the ECoF, as established earlier through Eq.(3).

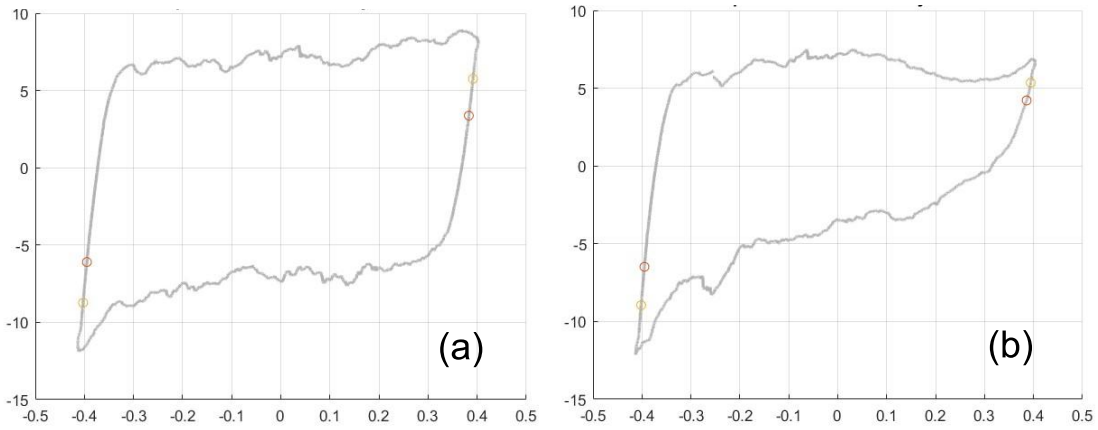

Figure 12 (a-b): Shape of tangential force hysteresis curve, (a) initial phase and (b) end of the test.

The dependency of energy dissipation on the applied precompression levels were also analysed. The total energy lost across 180 cycles was calculated as per Eq.(4) and the slip distance used was obtained from the measurements of each cycle. The energy dissipation showed a proportional trend to increasing precompression levels. This is illustrated in Fig.13.

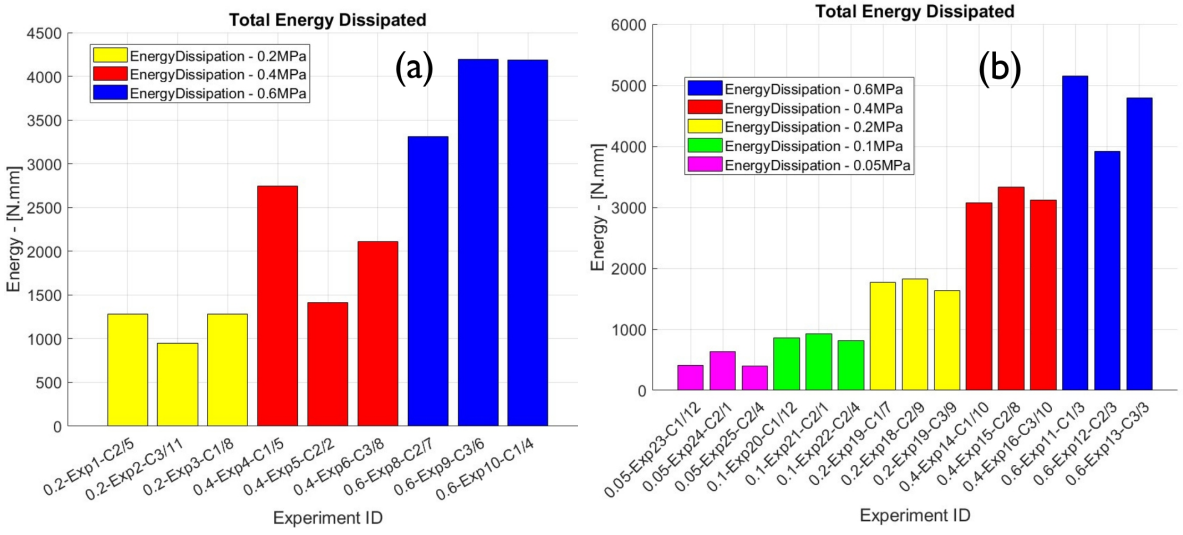

Figure 13(a-b): Energy dissipation across precompression levels in : (a) 3 Hz frequency and (b) 0.2 Hz frequency

2.3.5 Contact Stiffness

Contact stiffness is the change in tangential force at contact interface for a unit change in relative tangential displacement of the surface in contact in the micro-slip region, i.e. an instantaneous tangent at a specific load value [31]. The contact stiffness (k_t) was computed at either end of the displacement amplitude. The contact stiffness was analysed across cycles in an experiment and an average contact stiffness was also calculated from the mean curve of the experiment.

In order to exclude the possibility of the measured contact stiffness being influenced by the deformation of the top part of the specimen, which was partially held in the steel casing, a linear elastic analysis was performed. The stiffness of the interface and top specimen assembly were represented as a spring in series combination (Fig.16). The experimental value was subsequently juxtaposed with the numerical simulation results obtained for the top specimen under confinement conditions.

The stiffness provided by the top specimen was numerically simulated using a linear analysis (Fig.17). It was assumed that the steel casing, in conjunction with a 4.5 cm segment of a 5 cm long brick specimen, supported by heat melt adhesive glue (HMA glue), provided a rigid support for the embedded section. A unit load was applied to the 0.5 cm protrusion's surface, and the resulting displacement was calculated. Subsequently, the stiffness was derived from this computed displacement which was found to be 12150.67 N/mm (Table 2.6).

$$\frac{1}{k_{measured}} = \left(\frac{1}{k_b}\right) + \left(\frac{1}{k_{interface}}\right) \tag{4}$$

The measured stiffness can be illustrated as a series combination of springs involving the assembly (k_b) and interface ($k_{interface}$) [Eq 4]. The numerically estimated stiffness value of the assembly was then applied to the parameter k_b in the Eq(4) and was approximated to approach zero. Consequently, it was deduced that the observed experimental value could be attributed to the behaviour of the interface, since the measured value of stiffness is finite and $k_{measured} << k_b$.

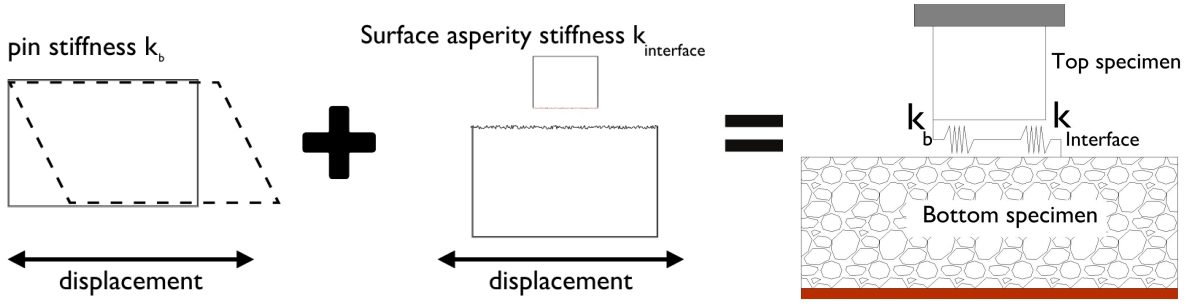

Figure 16: Spring model of the interface (series combination)

A 2D plane stress model features specimen total length of 50 mm embedded in a steel casing with a 5 mm protrusion supported at the base. Material properties include a Young's Modulus (E) of 6902 N/mm² and a Poisson's Ratio of 0.18. The element type employed is "Plane Stress 2D" with a thickness of 9 mm, using a mesh size of 0.1 mm.

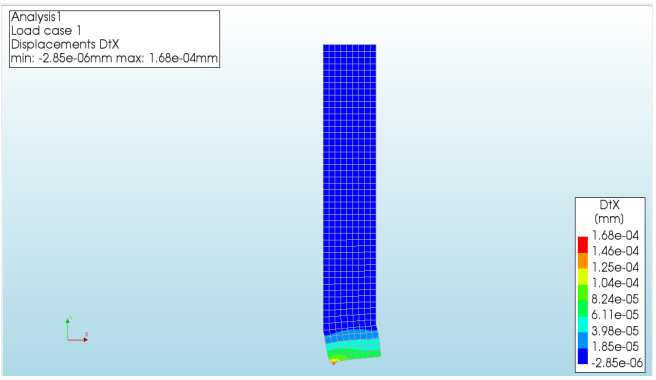

Figure 17: Numerical analysis of the horizontal displacement of the top specimen assembly

Load Applied	Displacement Node 470	Displacement Node 471	Average displacement	Stiffness of Pin
1 N	0.0000815 mm	0.0000764 mm	0.000079 mm	12150.67 N/mm

Table 2.6 Numerical estimation of Pin stiffness k_b

The following mathematical model [35] that lays down the relation between contact stiffness ($k_{b,i}$) and the normal force (N) is given by the equation:

$$dN/d\delta = k_{b,i} \equiv \kappa N^{\alpha} , \quad (5)$$

here δ is the linear elastic displacement and α is an exponent based on the type of contact (Cabboi et al, 2016 [35]). It can be inferred in general that the contact stiffness is proportional to the normal load applied. The contact stiffness was calculated and compared across different pre-compression levels for both frequencies. Generally, an increase in contact stiffness was observed increasing the pre-compression levels, which is in accordance with the assumption.(Fig 18a,b)

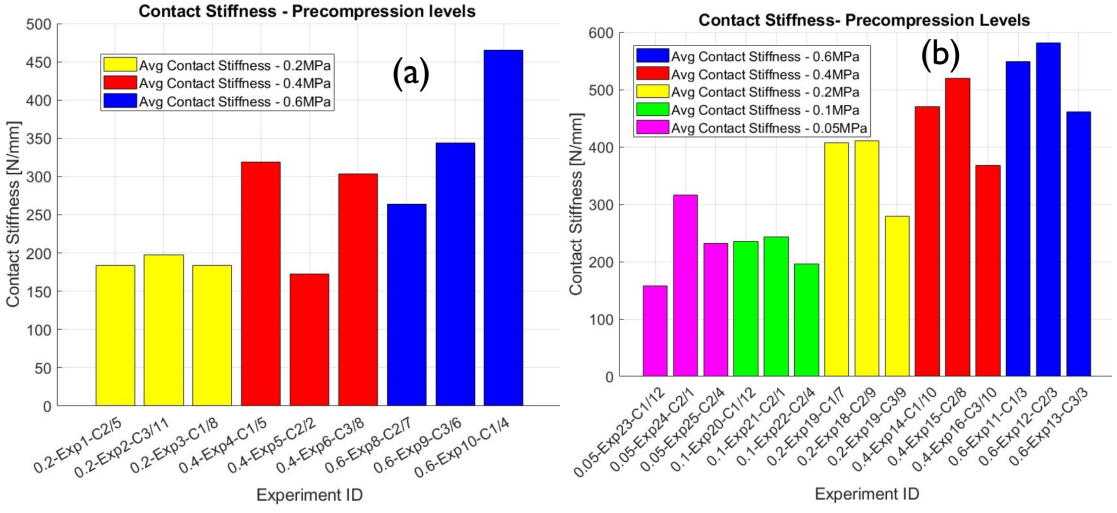

Figure 18 (a-b): Contact stiffness across precompression levels: (a) test with frequency of 3 Hz, (b) tests with frequency of 0.2 Hz

2.3.4 Preliminary Constitutive Modelling

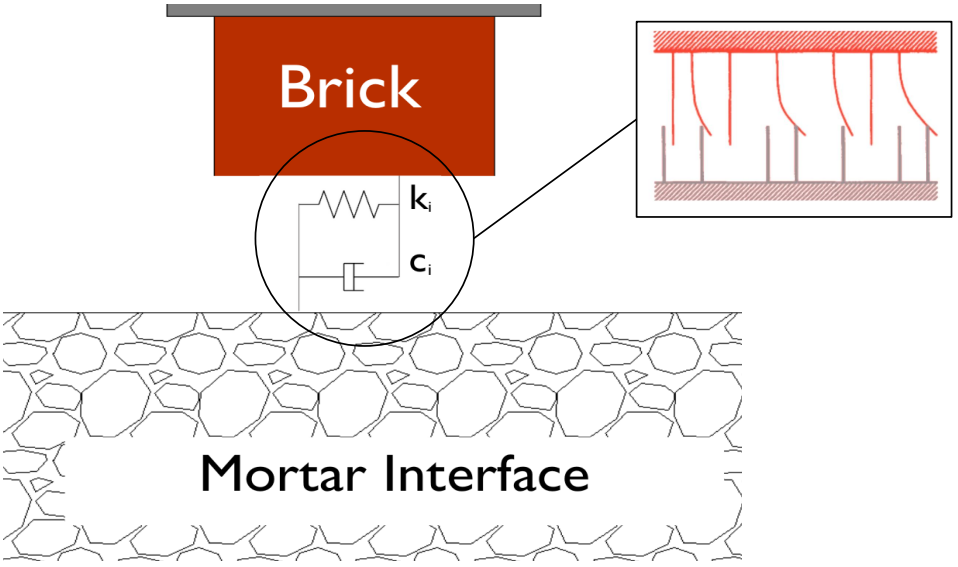

Figure 14: Spring-dashpot schematic of the interface.

Observing the profile of the frictional force vs relative velocity (Fig.9), a possible dependency on the test frequency was investigated (Schematised as spring-dashpot in Fig.14). The tribometer being a dynamic test, the equation of motion can be defined as Eq(6),

$$MX'' + CX' + KX = F(v) \quad , \tag{6}$$

the v in Eq.(5) corresponds to the relative velocity. The LuGre's friction model was used in identifying the influence of velocity. The asperities are considered as microscopic bristles with a certain stiffness and damping[32,33]. LuGre's model can be written down as Eq(7,8):

$$f_f(v) = \sigma_0 \hat{Z} + \sigma_1 (d\hat{Z}/d\tau) + \sigma_2 v \ , \tag{7}$$

$$d\hat{Z}/d\tau = v_r[1 - \sigma_0 \hat{Z}/g(v_r)sgn(v_r)] \tag{8}$$

here σ_0 is the bristle stiffness, σ_1 is the bristle damping and σ_2 is the viscous coefficient, $\hat{Z}$ is the average bristle deflection and $f_f(v)$is the frictional component such that $N_0 f_f(v) = F(v)$. The function $g(v_r)$ imparts the Stribeck effect into the model[32]. The constitutive model makes use of the Stribeck parameters [33]. These parameters σ_1, $\sigma_2$and v_s were calibrated considering the experiments with a frequency of 3 Hz and a pre-compression of 0.2 MPa. This was chose since the experimental hysteresis curve shoed a distinct velocity peak. The values used were: $\sigma_1 = 100, \sigma_2 = 0.02$, F_c=3.5, F_s=7 and v_s=0.04. The σ_0 refers to the measured contact stiffness of the interface, which was 220 N/mm.

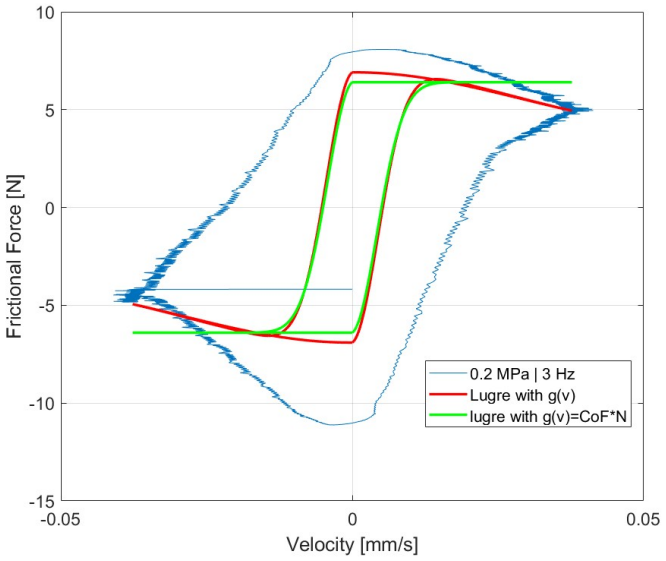

Figure 15: LuGre model compared to a frictional force hysteresis.

The deviations shown in Fig. 15 between the LuGre model with a g(v) function (red) and the LuGre model with μ*Normal load (green), both using the same input parameters, suggest a dependency on velocity for predicting the frictional behaviour at the interface.

2.4 Conclusions

Through employing a novel sampling and testing approach using a reciprocating tribometer, this study examined the behaviour of friction between unit-joint interfaces by assessing the frictional measurements at different precompression stress (normal stress) and for two ranges of frequencies.

The experiments carried out with the modified tribometer setup highlighted the deviation coefficient of friction from the assumed Coulomb behaviour, which is generally used in different models to estimate the contribution of friction and cohesion to the shear strength of brick-mortar interfaces. The experimental measurements were analysed in the form of (i) Tangential force 'Q'/ Normal load 'P' (Q/P) hysteresis curve and a (ii) Tangential force hysteresis curve. Two estimates for the coefficients relating the normal and tangential forces were considered: (i) mean coefficient of friction (CoF, μ) and (ii) the energy coefficient of friction (ECoF, μe). Tangential contact stiffness was also identified as a key parameter in characterising frictional behaviour. The feasibility of the test setup is influenced by both contact stiffness and stiffness of the top specimen assembly. When the contact stiffness exceeds the assembly stiffness, there is a tendency for the interface to stick instead of sliding, initiating undesirable bending on the top specimen, due to the applied displacement.

The primary observation in the analysis of the frictional coefficients was the dependency of the mean coefficient of friction (CoF) on the applied normal load. On comparing the results of CoF's across the three primary investigated precompression levels, a decrease in CoF with an increase in precompression levels was observed. This observation was prevalent in both the experimental frequencies, reinforcing the notion of a dependency of CoF on normal loads. CoF was computed from both the mean curve (obtained from averaging the hysteresis) and CoF distribution (a distribution of CoF evaluated from each cycle) for each precompression level, and both approaches gave the same result.

The Energy Coefficient of Friction, ECoF was calculated from the ratio of energy dissipated in friction to the hypothetical Coulomb energy loss. ECoF exhibited a slight dependency on the applied precompression level. The generally observed trend was similar to the behaviour observed between CoF and precompression levels (decrease in ECoF value with increase in precompression). However, it is important to note that the difference in ECoF across precompression levels was relatively small, in comparison to the difference between CoF values across precompression levels.

Both the coefficients contain limitations to characterise friction. The CoF is an overestimated data, since it is obtained from the non-linear peaks of the Q/P hysteresis to define the relation between normal load and friction. However, no clear and systematic dependency between CoF and number of cycles is observed. The variation is small and almost negligible, the ECoF is dependent on the hysteresis and interface behaviour which is affected over time or increased frequency (affected by the number of cycles). From the current study which uses 180 cycles, it may be concluded that the ECoF offers a better approximation for the overall frictional behaviour.

Contact stiffness, the rate of change of tangential force with tangential displacement, was calculated for the mean tangential hysteresis curves. An increase in the contact stiffness with an increase in the applied precompression level was observed. This is in accordance with the existing mathematical models and is an integral part in frictional behaviour.

The applied experimental frequencies resulted in observable changes in the hysteresis behaviour. The higher frequency, 3Hz resulted in hysteresis profiles with sharp peaks, a lower degree of symmetry, and non-linear behaviour in the gross-sliding region. The effects were less significant with an increase in precompression levels. At a lower experimental frequency, 0.2Hz the hysteresis profiles of precompression levels above 0.2MPa showed less significant peaks with linear profiles in the gross sliding region. The lower precompression levels had noise, possibly due to the high feedback in the displacement-controlled apparatus. The preliminary constitutive modelling approach using the LuGre model was used to study the influence of frequency on the tribometer experiments. The deviations between the LuGre model with a g(v) function and the LuGre model with constant value (CoF* Normal force), for the same input parameters, suggest a dependency on velocity for predicting the frictional behaviour at the interface.

In conclusion, the experimental results from the modified tribometer test highlight a deviation from the Coulomb behaviour, raising concerns about the current methodology used to evaluate and model shear response at brick-mortar interface . Although the estimated value of friction is similar to the range predicted by a standard triplet test, the behaviour of interfaces is to be better understood to unearth the governing mechanisms of friction in masonry. Based on the current study, few recommendations for future research are suggested. The current study uses an apparent area of contact (equal to cross-sectional area) approach to input the normal force required for a certain precompression level. The profilometer data indicates that the actual area of contact is often smaller due to surface imperfections. The researcher recommends precise contact area measurements for further research. Likewise, the sample preparation method needs refinement to accurately extract the interlocking unit-mortar interface. The current approach, which involves separate extraction for the top and bottom specimens, results in a notable misalignment of the interface.The experimental results were derived for a single masonry type. To further validate the conclusions, an extensive testing campaign considering different types of brick and mortar combinations is recommended.

3 CONCLUSIONS & RECOMMENDATIONS

The indistinguishable contribution of cohesion and friction to the shear strength of the unit-joints and the deduction of friction analytically from the results of such a test based on the Coulomb criterion, calls for the requirement of assessing friction independently. The study aimed at developing a standalone test for the study of frictional interfaces between unit-joints. Through this study, the following conclusions on the frictional behaviour of unit-joint interfaces can be inferred:

- The experiments carried out with the modified tribometer setup highlighted the deviation of friction from the assumed Coulomb behaviour, i.e.the frictional behaviour was non-Coulomb in nature. The Q/P hysteresis, obtained from the plot of Tangential to Normal force ratio against the sliding distance exhibits a non-linear profile, with hook-like features at the extremities.

- Factors influencing frictional behaviour were identified to be: (i) The Coefficient of Friction (CoF), (ii) Energy Coefficient of Friction (ECoF), and (iii) Tangential Contact Stiffness. Experimental measurements were utilised to construct (i) a Q/P hysteresis and (ii) a Tangential force hysteresis, forming the foundation for further investigations into frictional behaviour. The mean coefficient of friction (CoF, μ), was derived from the Q/P hysteresis, while the energy coefficient of friction (ECoF, μe) and tangential contact stiffness were obtained from the tangential force hysteresis. Tangential contact stiffness was also recognized as a crucial parameter characterising friction behaviour, influencing the feasibility of the test setup and contributing to the frictional mechanism.

- The primary observation was the dependency of the mean coefficient of friction (CoF) and energy coefficient of friction (ECoF) on the applied Precompression level.On comparing the results of CoF's and ECoF's across the three investigated precompression levels, a decrease in CoFand ECoF with an increase in precompression levels was observed. This observation was prevalent in both the experimental frequencies, indicating the dependency of CoF and ECoF on precompression levels.

- The Energy Coefficient of Friction (ECoF) exhibits a dependency on the number of cycles. ECoF shows a trend with high initial values followed by a systematic decrease with the progression of each cycle. However, no systematic dependance on the number of cycles was exhibited by mean coefficient of friction (CoF).

- The results obtained from the mean curve approach and cycle approach had little to no differences. Therefore, it can be concluded that the use of the mean curve to calculate CoF and ECoF does not affect the results.

- Contact stiffness the third key parameter can be defined as, rate of change of tangential force with tangential displacement, it was calculated for the mean tangential hysteresis curves of each precompression level across both the experimental frequencies. An increase in the contact stiffness with an increase in the applied precompression level was observed. This is in accordance with the contact stiffness modelled by using a power law of normal force.The interface undergoes two primary stages of frictional behaviour during the reciprocatory test: the partial slip phase (also known as micro slip) and gross sliding phase. The material stiffness of the top assembly plays an important role. During high levels of precompression, the tangential stiffness could be higher than the material stiffness causing the interface to stick while the top specimen undergoes a bending motion under the imposed deformation. This would result in erroneous data and misinterpretation of the mechanics (refer to appendix A).

- Surface roughness is often considered an important parameter in frictional study. The works of Rabinowicz, points out the presence of both regions where friction is dependent and independent of surface roughness. However, masonry being a very rough material generally, there is limited knowledge on these regions. Therefore the study proceeded without accounting for the influence of surface roughness on the value of coefficient of friction.

- The applied experimental frequencies resulted in observable changes in the hysteresis behaviour. The higher frequency, 3Hz resulted in hysteresis profiles with sharp peaks, a lower degree of symmetry, and non-linear behaviour in the gross-sliding region. The effects were less significant with an increase in precompression levels. At a lower experimental frequency, 0.2Hz the hysteresis profiles of precompression levels above 0.2MPa showed less significant peaks with linear profiles in the gross sliding region. The lower precompression levels had noise, possibly due to the high feedback in the displacement-controlled apparatus.

- In conclusion, the experimental results from the modified tribometer test highlight a deviation from the triplet test method. It was found that the coefficient of friction varies significantly with different precompression levels and questions the estimation of one global coefficient of friction estimated from the linear regression of data obtained by assuming a Coulomb behaviour, raising concerns about the current methods of evaluating friction based on the Coulomb criterion.
- Both the CoF and ECoF are parameters that define friction, however their estimation and reliability are to be considered for situation of use. Although the estimated value of friction (CoF) is similar to the range predicted by a standard triplet test, the behaviour of interfaces is to be better understood to unearth the governing mechanisms of friction in masonry thereby providing a deeper understanding of its shear strength.

The following recommendations are put forward by the researcher:

- The experimental results were derived for a single masonry type. To further validate the conclusions, an extensive testing campaign considering different types of brick and mortar combinations is recommended.
- The specimens are mechanically extracted from bond wrenched couplet elements. The current sampling method utilised the complete removal of the couplet unit, which causes an irreversible interface mismatch, meaning the interface can no longer align exactly. This was looked into, but with limited extraction opportunities a tolerance zone/region was adopted. Future studies may look into precise extraction techniques.
- Surface roughness impacts the frictional behaviour significantly. However, there exists a vacuum of information about the influence of surface roughness on the coefficient of friction. Like metal interfaces, this can be further explored and incorporated into the study.
- Fretting was observed at the beginning of the test. The presence of fretting may influence the conclusions of this study. The occurrence of fretting curves in certain hysteresis loops, calls for the consideration of fretting models in assessing coefficient of friction and the frictional behaviour in future studies.
- The fretting loss and change in the asperities of the surface can be investigated using equipment like a profilometer at each stage of the experiment, especially with the focus to investigate the dependency of CoF on surface damage and ECoF on material loss.
- The variation in ECoF over extended cycles or the variation of ECoF under high frequency can be investigated in addition to the fretting loss. Since fretting and wear mechanisms have been observed to play a part in the variation of ECoF.
- The apparent area approach was used for experiments, it is important to know that the true area of contact varies to the assumed/ apparent area of contact. This is an important setup related parameter, since smaller areas can easily lead to higher precompression levels.

REFERENCES

[1]Gooch, L. J., Masia, M. J., Stewart, M. G., & Lam, C. Y. (2023). Statistical assessment of tensile and shear properties of unreinforced clay brick masonry. Construction and Building Materials, 386, 131578.

[2]Taha, M. R., El-Dieb, A. S., & Shrive, N. G. (2001). Sorptivity: a reliable measurement for surface absorption of masonry brick units. Materials and Structures, 34, 438-445.

[3]Taha, M. R., & Shrive, N. G. (2001, June). The use of pozzolans to improve bond and bond strength. In 9 th Canadian masonry symposium. Canadá.

[4]Madhavi, K., Renukadevi, M. V., Jagadish, K. S., & Basutkar, S. M. (2023). Studies on shear strength and stiffness of brick masonry walls. Materials Today: Proceedings.

[5]Gaetano, D., Greco, F., Leonetti, L., Lonetti, P., Pascuzzo, A., & Ronchei, C. (2022). An interface-based detailed micro-model for the failure simulation of masonry structures. Engineering Failure Analysis, 142, 106753.

[6]Ferretti, F., Ferracuti, B., Mazzotti, C., & Savoia, M. (2019). Destructive and minor destructive tests on masonry buildings: experimental results and comparison between shear failure criteria. Construction and Building Materials, 199, 12-29.

[7]Montazerolghaem, M. A. H. D. I., & Jaeger, W. O. L. F. R. A. M. (2014, July). A comparative numerical evaluation of masonry initial shear test methods and modifications proposed for EN 1052-3. In Proceedings of the 9th international masonry conference.

[8]Riddington, J. R., & Jukes, P. (1994). A MASONRY JOINT SHEAR STRENGTH TEST METHOD. Proceedings of the Institution of Civil Engineers-Structures and Buildings, 104(3), 267-274.

[9]Bauschinger, J., & Föppl, A. (1873). Mitteilungen aus dem Mechanisch Technischen Laboratorium der Technischen Hochschule München (Vol. 1). Ackermann.

[10]Van der Pluijm, R. (1999). Out-of-plane bending of masonry behaviour and strength (Ph D thesis). Eindhoven, Netherland: Eindhoven University of Technology.

[11]Segura, J., Bernat, E., Mendizabal, V., Pelà, L., Roca, P., & Gil, L. (2021). Experimental comparison of two testing setups for characterizing the shear mechanical properties of masonry. Journal of Building Engineering, 44, 103277.

[12]Riddington, J. R., Fong, K. H., & Jukes, P. (1997). Numerical study of failure initiation in different joint shear tests. Masonry International, 11(2), 44-50.

[13]Popal, R., & Lissel, S. L. (2010, July). Numerical evaluation of existing mortar joint shear tests and a new test method. In Proc. 8th International Masonry Conference, Dresden.

[14]Barattucci, S., Sarhosis, V., Bruno, A. W., D'Altri, A. M., de Miranda, S., & Castellazzi, G. (2020). An experimental and numerical study on masonry triplets subjected to monotonic and cyclic shear loadings. Construction and Building Materials, 254, 119313.

[15]EN 1052-3: 2002-10. (2007). Methods of test for masonry. Part 3: Determination of initial shear strength. Beuth Verlag, Berlin. German version of EN 1052-3:2002.

[16]Maheri, M. R., Motielahi, F., & Najafgholipour, M. A. (2011). The effects of pre and post construction moisture condition on the in-plane and out-of-plane strengths of brick walls. Materials and Structures, 44, 541-559.

[17]Lourenço, P. B., & Rots, J. G. (1997). Multisurface interface model for analysis of masonry structures. Journal of engineering mechanics, 123(7), 660-668.

[18]Mulvihill, D. M., Kartal, M. E., Olver, A. V., Nowell, D., & Hills, D. A. (2011). Investigation of non-Coulomb friction behaviour in reciprocating sliding. Wear, 271(5-6), 802-816.

[19]Fouvry, S., Liskiewicz, T., Kapsa, P., Hannel, S., & Sauger, E. (2003). An energy description of wear mechanisms and its applications to oscillating sliding contacts. Wear, 255(1-6), 287-298.

[20]Hurricks, P. L. (1970). The mechanism of fretting—a review. Wear, 15(6), 389-409.

[21]Llavori, I., Zabala, A., Aginagalde, A., Tato, W., Ayerdi, J. J., & Gómez, X. (2020). Critical analysis of coefficient of friction derivation methods for fretting under gross slip regime. Tribology International, 143, 105988.

[22]Jafari, S., Rots, J. G., & Esposito, R. (2020). Core testing method to assess nonlinear shear-sliding behaviour of brick-mortar interfaces: A comparative experimental study. Construction and Building Materials, 244, 118236.

[23]Jafari, S. (2021). Material characterisation of existing masonry: a strategy to determine strength, stiffness and toughness properties for structural analysis. Delft University of Technology: TU Delft Applied Mechanics. https://repository. tudelft. nl Doctoral thesis.

[24]Rahman, A., & Ueda, T. (2014). Experimental investigation and numerical modeling of peak shear stress of brick masonry mortar joint under compression. Journal of Materials in Civil Engineering, 26(9), 04014061.

[25]Ferretti, F., Mazzotti, C., Esposito, R., & Rots, J. G. (2018, February). Shear-sliding behavior of masonry: numerical micro-modeling of triplet tests. In Conference on Computational Modelling of Concrete and Concrete Structures (pp. 941-952). CRC Press.

[26]JGonzález-Velázquez, J. L. (2020). A practical approach to fracture mechanics. Elsevier.2021, Pages 35-74, ISBN 9780128230206,

[27]G02 Committee, Guide for Determining Friction Energy Dissipation in Reciprocating Tribosystems, ASTM International; n.d, http://dx.doi.org/10.1520/G0203-10R16.

[28]Klaffke, D. (2006). Towards a tribological reference test–fretting test?. TriboTest, 12(2), 133-147.

[29]Fouvry, S., Duó, P., & Perruchaut, P. (2004). A quantitative approach of Ti–6Al–4V fretting damage: friction, wear and crack nucleation. Wear, 257(9-10), 916-929.

[30]Mulvihill, D. M., Brunskill, H., Kartal, M. E., Dwyer-Joyce, R. S., & Nowell, D. (2013). A comparison of contact stiffness measurements obtained by the digital image correlation and ultrasound techniques. Experimental Mechanics, 53, 1245-1263.

[31]Mulvihill, D. M., Brunskill, H., Kartal, M. E., Dwyer-Joyce, R. S., & Nowell, D. (2013). A comparison of contact stiffness measurements obtained by the digital image correlation and ultrasound techniques. Experimental Mechanics, 53, 1245-1263.

[32]Saha, A., Wahi, P., Wiercigroch, M., & Stefański, A. (2016). A modified LuGre friction model for an accurate prediction of friction force in the pure sliding regime. International Journal of Non-Linear Mechanics, 80, 122-131.

[33]De Wit, C. C., Olsson, H., Astrom, K. J., & Lischinsky, P. (1995). A new model for control of systems with friction. IEEE Transactions on automatic control, 40(3), 419-425.

[34]Graziotti, F., Tomassetti, U., Kallioras, S., Penna, A., & Magenes, G. (2017). Shaking table test on a full scale URM cavity wall building. Bulletin of earthquake engineering, 15, 5329-5364.

[35]Cabboi, A., Putelat, T., & Woodhouse, J. (2016). The frequency response of dynamic friction: enhanced rate-and-state models. Journal of the Mechanics and Physics of Solids, 92, 210-236.

[36]Rabinowicz E. Friction and Wear of Materials. 2nd ed. New York: Wiley; 1995.

APPENDIX A

I.Bending Failure

The assembly of the sample into the top specimen plays a significant role in the experiments. Due to the slenderness of the sample, the interfaces may "stick" and start bending instead of sliding on the onset of the displacement-controlled reciprocation. This would result in undesired results and can be diagnosed easily while processing the hysteresis. On a practical trial and error, 1cm of protrusion in the top specimen assembly resulted in the bending failure transpiring at 0.6 MPa. Therefore as a standard, the protrusion was reduced to 0.5 cm and this resulted in the top specimen being braced against such failure. The figure below is a typical note of bending failure:

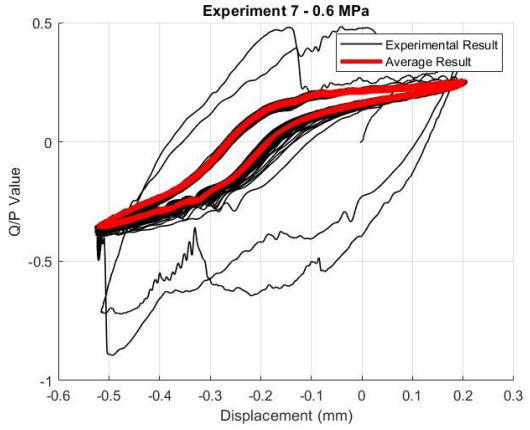

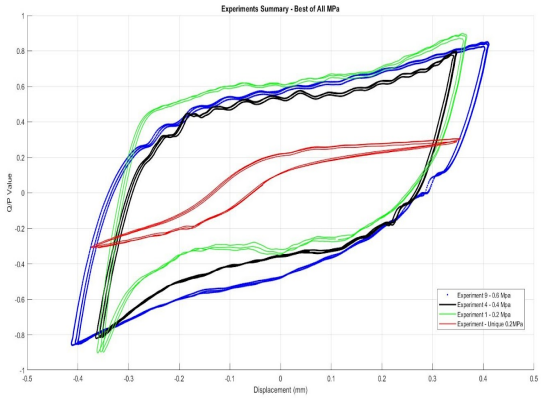

II. Specimens and experiments profile

The samples were extracted from three couplets The couplets were named: C1, C2 and C3. Each couplet was labelled, and grids were carefully drawn to identify the extracted specimens and later label them. Each couplet was marked with grids with each grid approximately yielding a 3 x 3 cm cut bottom specimen. The grids were numerically labelled in the range of 1-12, in an odd-even pattern. The specimens were labelled as:

$$Specimen\ ID\ =\ C'X'\_'Y'\_'Z'$$

X- refers to the couplet (1/2/3); Y- refers to the grid (1-12); Z- refers to the brick half [Top (T)/ Bottom (B)]. An example of this would be:

$$Specimen\ ID\ =\ C2\_7\_B$$

The specimen profiles and a summary of measured and analysed data of each experiment, is presented in Annex-B and Annex-C respectively.

APPENDIX B -

SAMPLE PROFILE

Please not in this appendix, comma is used as decimal separator

Experiment: 01

Specimen ID:	*C2_5*	*Precompression Stress:*	*0,2 MPa*	*Frequency:*	*3 Hz*

Bottom Specimen: C2_5_B

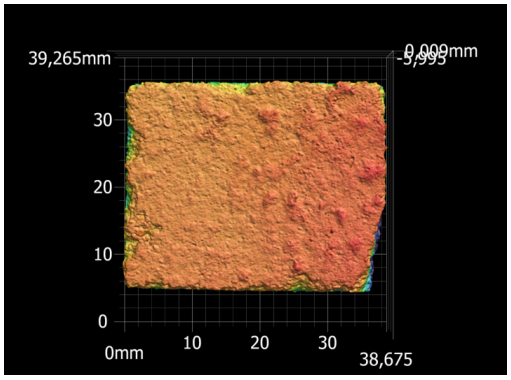

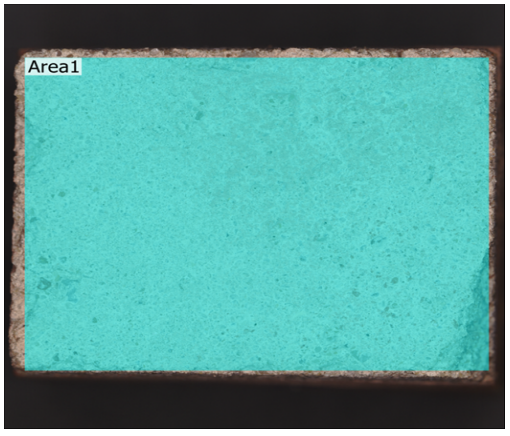

	Sa	Sz	Str	Spc
	µm	µm		1/mm
Max.	253,630	5604,600	0,243	6,510
Min.	253,630	5604,600	0,243	6,510
Ave.	253,630	5604,600	0,243	6,510
Std. DV	0,000	0,000	0,000	0,000
Area1	253,630	5604,600	0,243	6,510

Top Specimen: C2_5_T

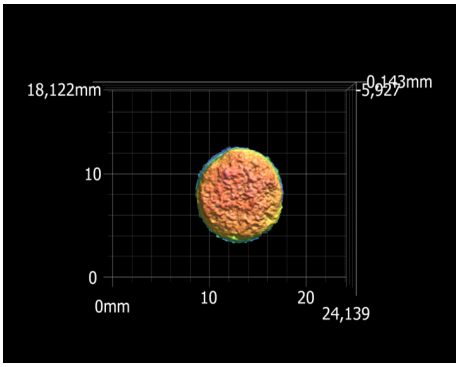

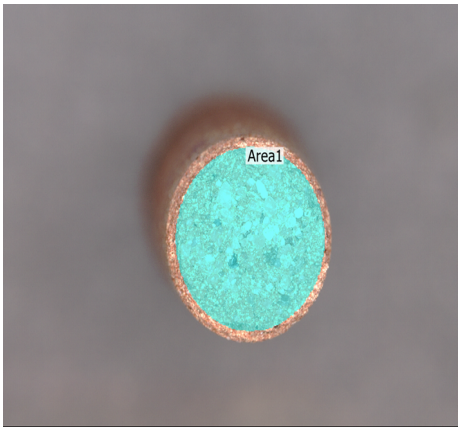

	Sa	Sz	Str	Spc
	µm	µm		1/mm
Max.	284,611	2495,200		13,758
Min.	284,611	2495,200		13,758
Ave.	284,611	2495,200		13,758
Std. DV	0,000	0,000		0,000
Area1	284,611	2495,200		13,758

Specimen location: Couplet C2

2	*4*	*6*	*8*	*10*	*12*
1	*3*	*5*	*7*	*9*	*11*

Experiment: 02

Specimen ID:	***C3_11***	***Precompression Stress:***	***0,2 MPa***	***Frequency:***	***3 Hz***

Bottom Specimen: C3_11_B

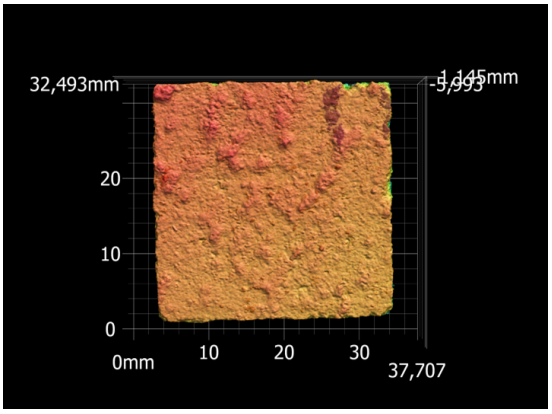

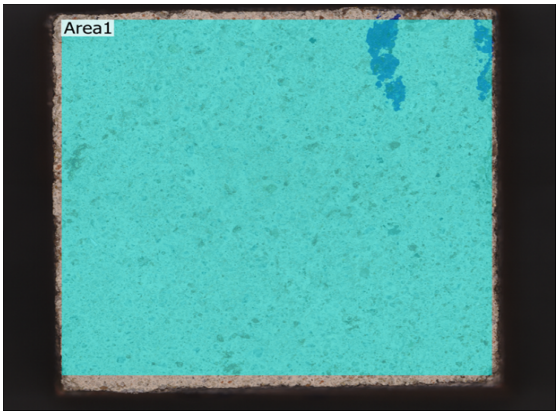

	Sa	Sz	Str	Spc
	µm	µm		1/mm
Max.	187,127	3376,700	0,387	7,503
Min.	187,127	3376,700	0,387	7,503
Ave.	187,127	3376,700	0,387	7,503
Std. DV	0,000	0,000	0,000	0,000
Area1	187,127	3376,700	0,387	7,503

Top Specimen: C3_11_T

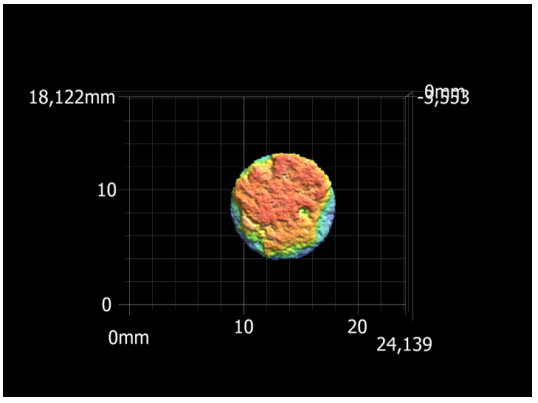

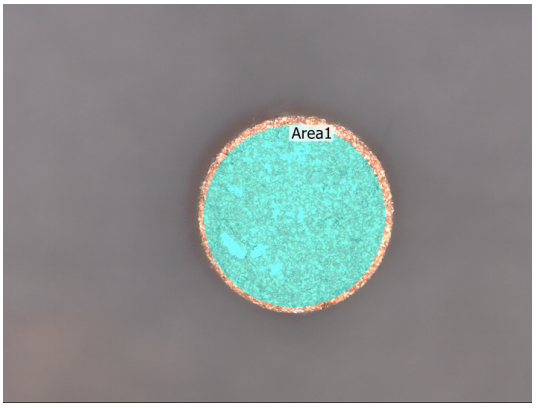

	Sa	Sz	Str	Spc
	µm	µm		1/mm
Max.	234,890	1330,600		9,032
Min.	234,890	1330,600		9,032
Ave.	234,890	1330,600		9,032
Std. DV	0,000	0,000		0,000
Area1	234,890	1330,600		9,032

2	***4***	***6***	***8***	***10***	***12***
1	***3***	***5***	***7***	***9***	***11***

Experiment: 03

Specimen ID:	***C1_8***	***Precompression Stress:***	***0,2 MPa***	***Frequency:***	***3 Hz***

Bottom Specimen: C1_8_B	***Top Specimen: C1_8_T***

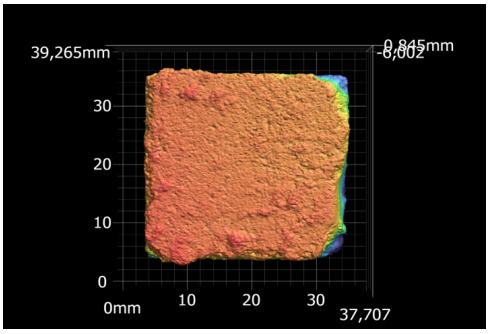

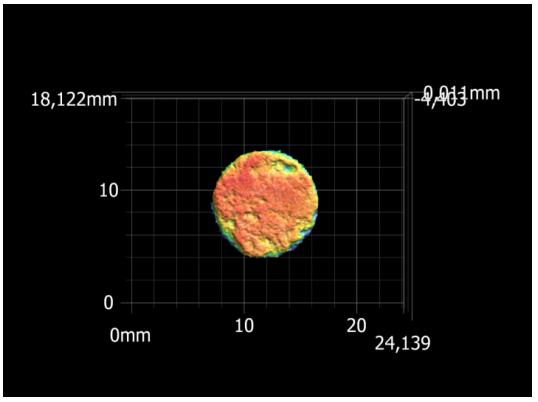

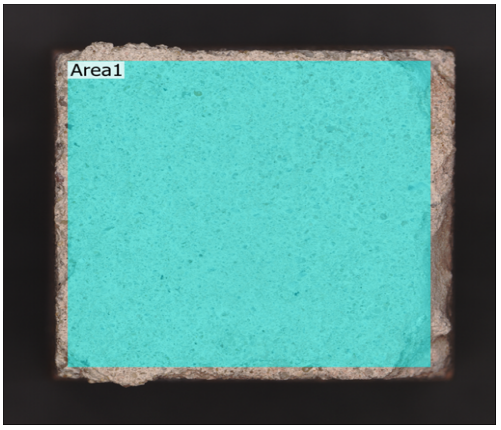

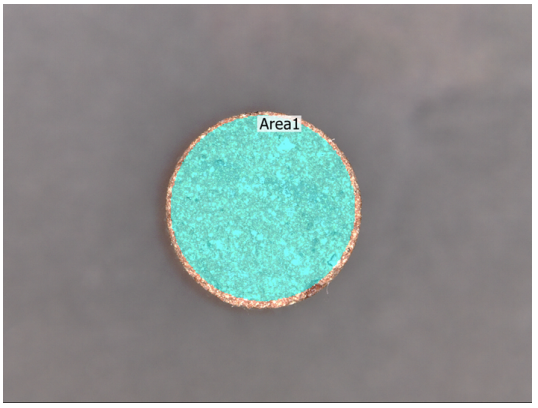

	Sa	Sz	Str	Spc
	µm	µm		1/mm
Max.	219,024	5525,400	0,161	6,218
Min.	219,024	5525,400	0,161	6,218
Ave.	219,024	5525,400	0,161	6,218
Std. DV	0,000	0,000	0,000	0,000
Area1	219,024	5525,400	0,161	6,218

	Sa	Sz	Str	Spc
	µm	µm		1/mm
Max.	93,477	833,700		5,005
Min.	93,477	833,700		5,005
Ave.	93,477	833,700		5,005
Std. DV	0,000	0,000		0,000
Area1	93,477	833,700		5,005

2	***4***	***6***	***8***	***10***	***12***
1	***3***	***5***	***7***	***9***	***11***

Experiment: 04

Specimen ID:	*C1_5*	*Precompression Stress:*	*0,4 MPa*	*Frequency:*	*3 Hz*
Bottom Specimen: C1_5_B			*Top Specimen: C1_5_T*		

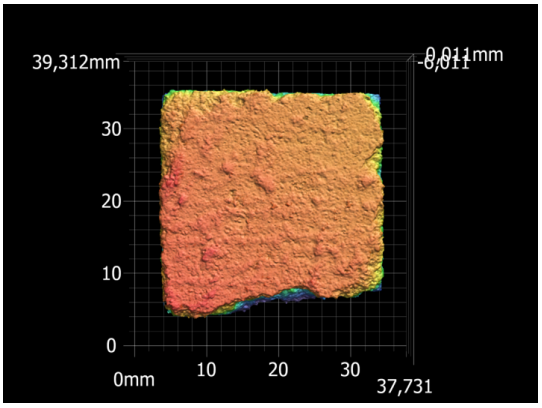

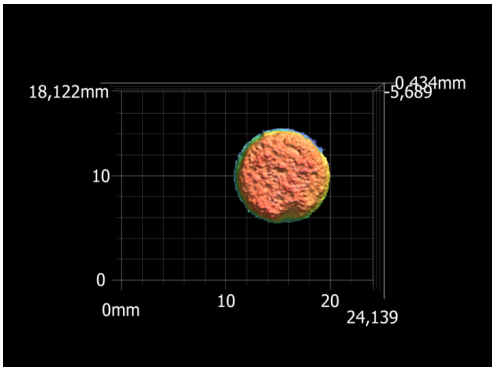

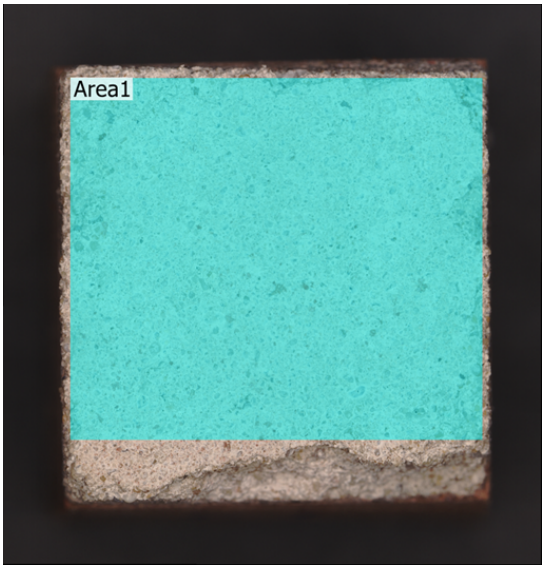

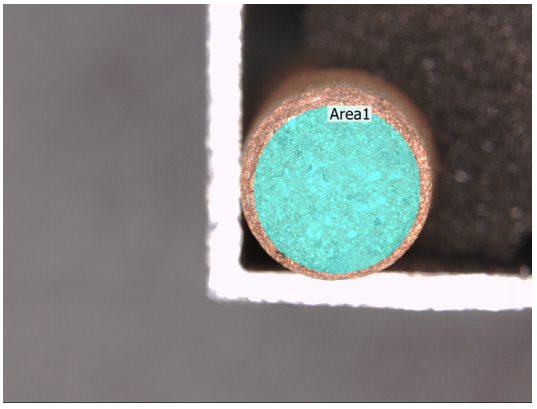

	Sa	Sz	Str	Spc
	µm	µm		1/mm
Max.	255,829	4102,500	0,257	5,974
Min.	255,829	4102,500	0,257	5,974
Ave.	255,829	4102,500	0,257	5,974
Std. DV	0,000	0,000	0,000	0,000
Area1	255,829	4102,500	0,257	5,974

	Sa	Sz	Str	Spc
	µm	µm		1/mm
Max.	236,145	2650,400		14,616
Min.	236,145	2650,400		14,616
Ave.	236,145	2650,400		14,616
Std. DV	0,000	0,000		0,000
Area1	236,145	2650,400		14,616

2	*4*	*6*	*8*	*10*	*12*
1	*3*	*5*	*7*	*9*	*11*

Experiment: 05

Specimen ID:	***C2_2***	***Precompression Stress:***	***0,4 MPa***	***Frequency:***	***3 Hz***

Bottom Specimen: C2_2_B

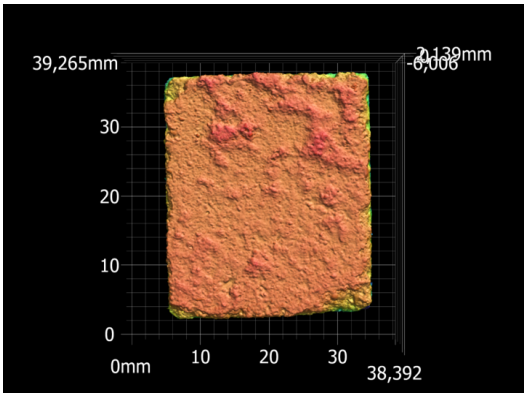

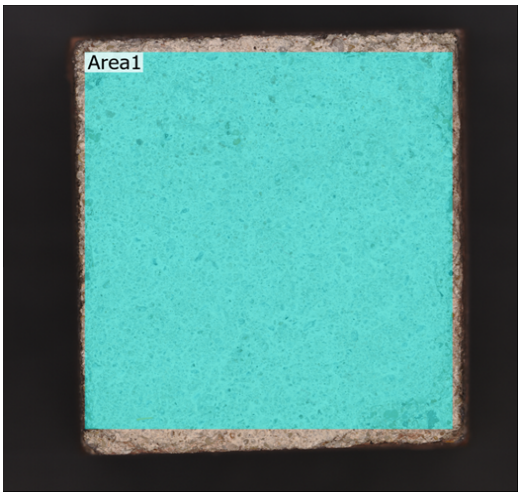

	Sa	Sz	Str	Spc
	µm	µm		1/mm
Max.	141,678	2787,500	0,443	6,149
Min.	141,678	2787,500	0,443	6,149
Ave.	141,678	2787,500	0,443	6,149
Std. DV	0,000	0,000	0,000	0,000
Area1	141,678	2787,500	0,443	6,149

Top Specimen: C2_2_T

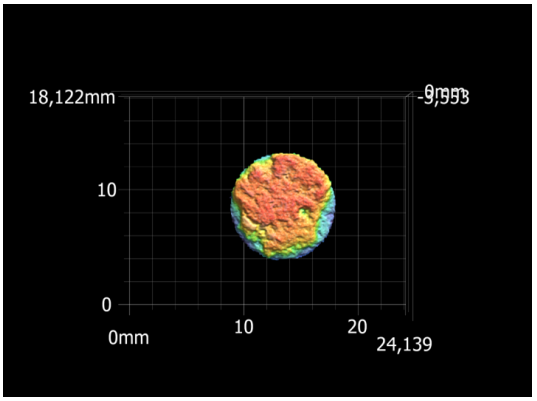

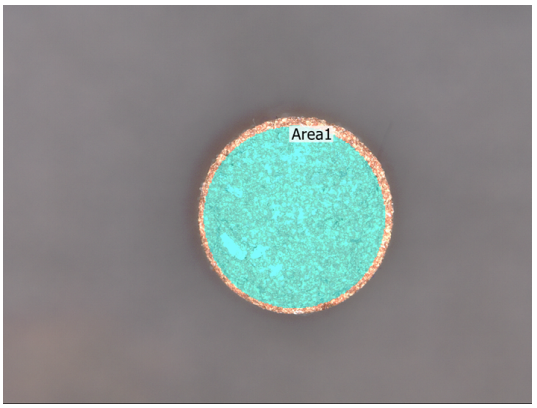

	Sa	Sz	Str	Spc
	µm	µm		1/mm
Max.	234,890	1330,600		9,032
Min.	234,890	1330,600		9,032
Ave.	234,890	1330,600		9,032
Std. DV	0,000	0,000		0,000
Area1	234,890	1330,600		9,032

2	***4***	***6***	***8***	***10***	***12***
1	***3***	***5***	***7***	***9***	***11***

Experiment: 06

Specimen ID:	*C3_8*	*Precompression Stress:*	*0,4 MPa*	*Frequency:*	*3 Hz*

Bottom Specimen: C3_8_B

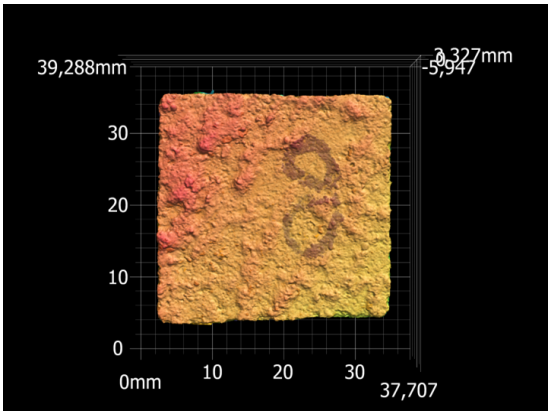

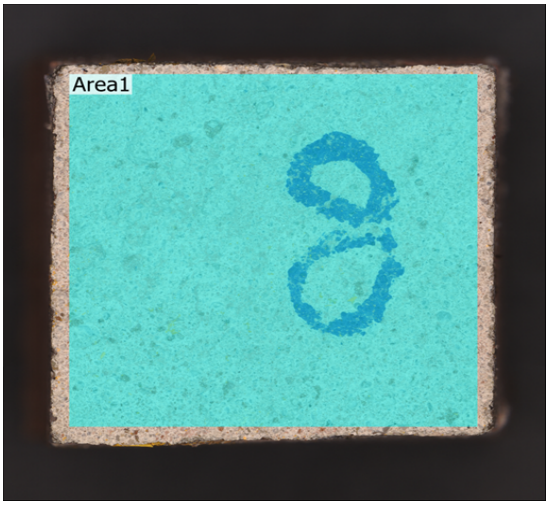

	Sa	Sz	Str	Spc
	µm	µm		1/mm
Max.	310,437	2550,200	0,525	6,368
Min.	310,437	2550,200	0,525	6,368
Ave.	310,437	2550,200	0,525	6,368
Std. DV	0,000	0,000	0,000	0,000
Area1	310,437	2550,200	0,525	6,368

Top Specimen: C3_8_T

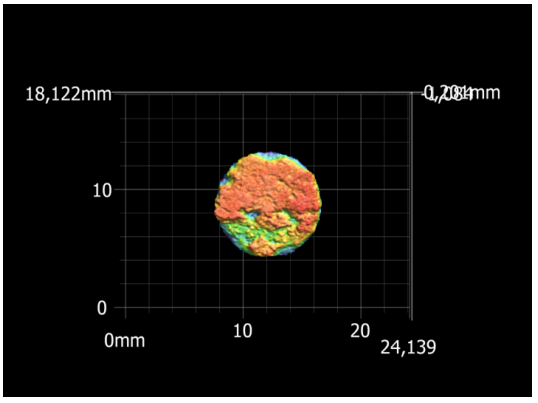

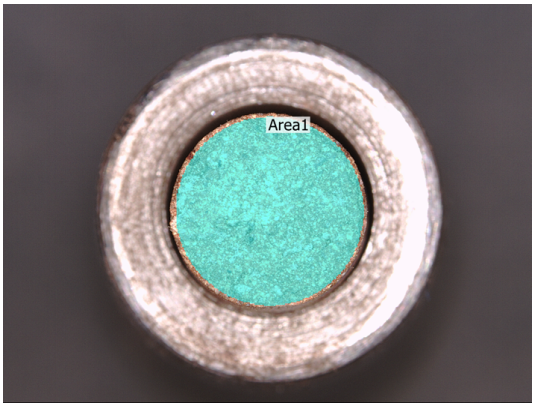

	Sa	Sz	Str	Spc
	µm	µm		1/mm
Max.	168,565	1059,400		6,751
Min.	168,565	1059,400		6,751
Ave.	168,565	1059,400		6,751
Std. DV	0,000	0,000		0,000
Area1	168,565	1059,400		6,751

2	*4*	*6*	*8*	*10*	*12*
1	*3*	*5*	*7*	*9*	*11*

Experiment: 07

Specimen ID:	***C2_10***	***Precompression Stress:***	***0,6 MPa***	***Frequency:***	***3 Hz***

Bottom Specimen: C2_10_B	***Top Specimen: C2_10_T***

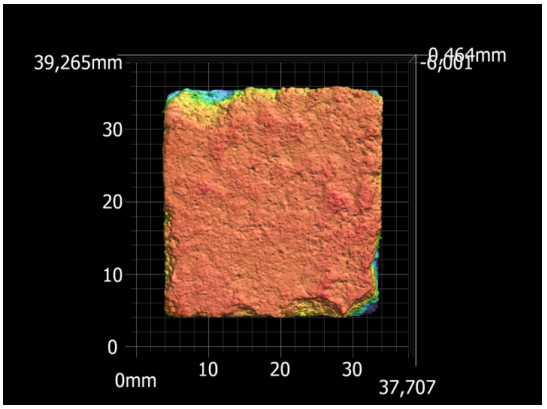

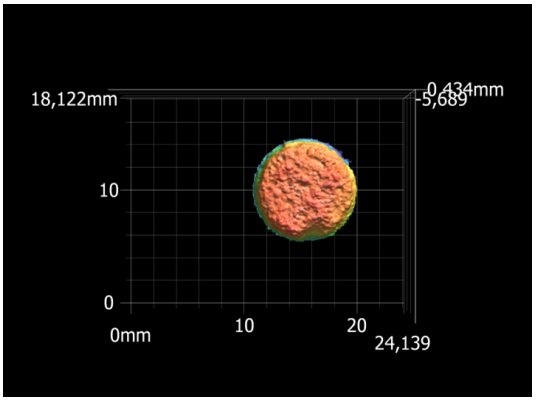

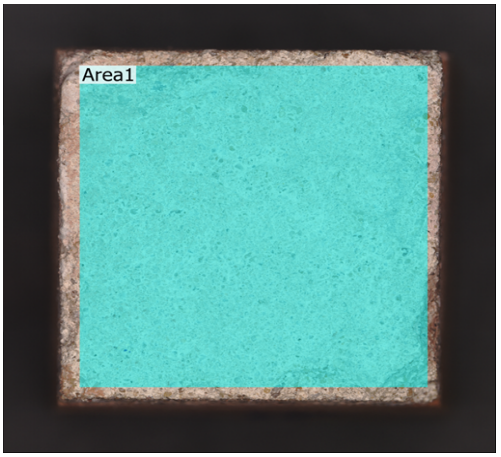

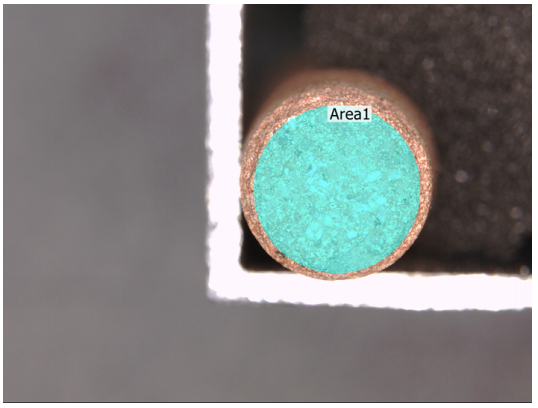

	Sa	Sz	Str	Spc
	µm	µm		1/mm
Max.	182,837	5350,100	0,144	6,052
Min.	182,837	5350,100	0,144	6,052
Ave.	182,837	5350,100	0,144	6,052
Std. DV	0,000	0,000	0,000	0,000
Area1	182,837	5350,100	0,144	6,052

	Sa	Sz	Str	Spc
	µm	µm		1/mm
Max.	236,145	2650,400		14,616
Min.	236,145	2650,400		14,616
Ave.	236,145	2650,400		14,616
Std. DV	0,000	0,000		0,000
Area1	236,145	2650,400		14,616

2	***4***	***6***	***8***	***10***	***12***
1	***3***	***5***	***7***	***9***	***11***

Experiment: 08

Specimen ID:	*C2_7*	*Precompression Stress:*	*0,6 MPa*	*Frequency:*	*3 Hz*

Bottom Specimen: C2_7_B

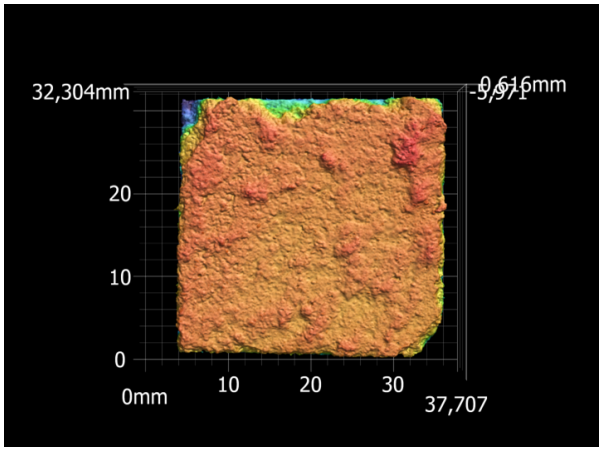

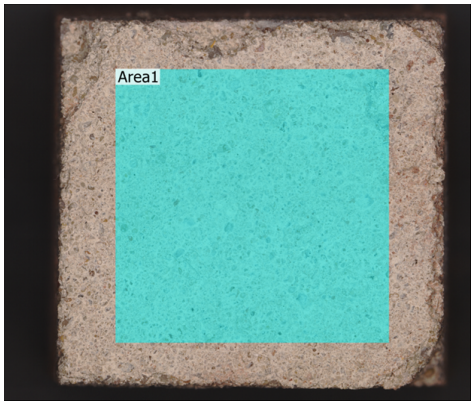

	Sa	Sz	Str	Spc
	µm	µm		1/mm
Max.	211,515	5079,300	0,479	7,484
Min.	211,515	5079,300	0,479	7,484
Ave.	211,515	5079,300	0,479	7,484
Std. DV	0,000	0,000	0,000	0,000
Area1	211,515	5079,300	0,479	7,484

Top Specimen: C2_7_T

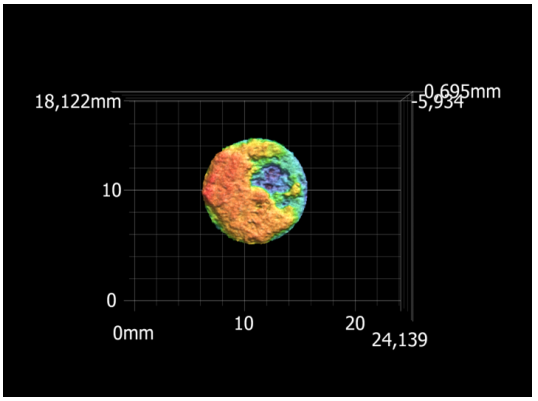

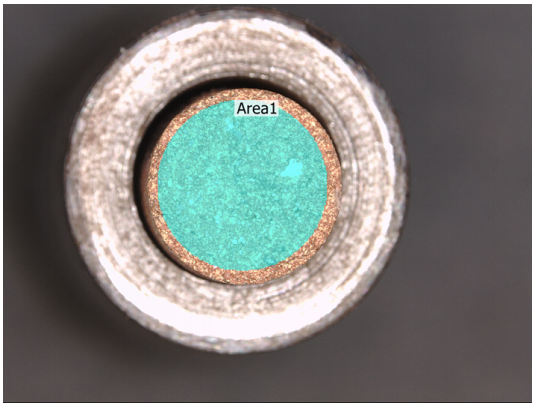

	Sa	Sz	Str	Spc
	µm	µm		1/mm
Max.	284,611	2495,200		13,758
Min.	284,611	2495,200		13,758
Ave.	284,611	2495,200		13,758
Std. DV	0,000	0,000		0,000
Area1	284,611	2495,200		13,758

2	*4*	*6*	*8*	*10*	*12*
1	*3*	*5*	*7*	*9*	*11*

Experiment: 09

Specimen ID:	*C3_6*	*Precompression Stress:*	*0,6 MPa*	*Frequency:*	*3 Hz*

Bottom Specimen: C3_6_B

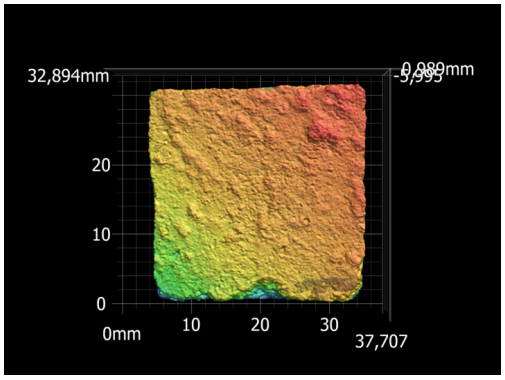

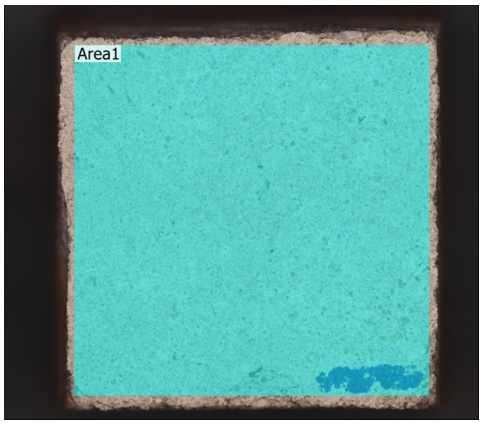

	Sa	Sz	Str	Spc
	µm	µm		1/mm
Max.	501,833	4429,900	0,419	7,189
Min.	501,833	4429,900	0,419	7,189
Ave.	501,833	4429,900	0,419	7,189
Std. DV	0,000	0,000	0,000	0,000
Area1	501,833	4429,900	0,419	7,189

Top Specimen: C3_6_T

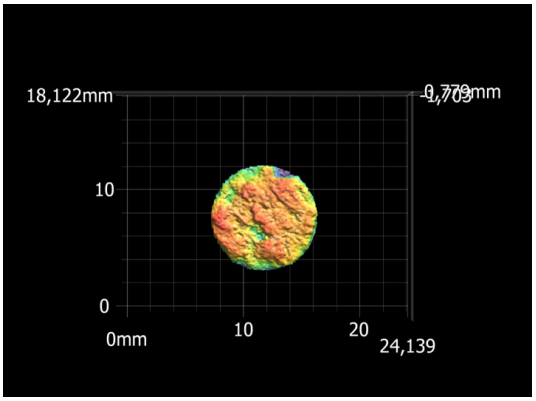

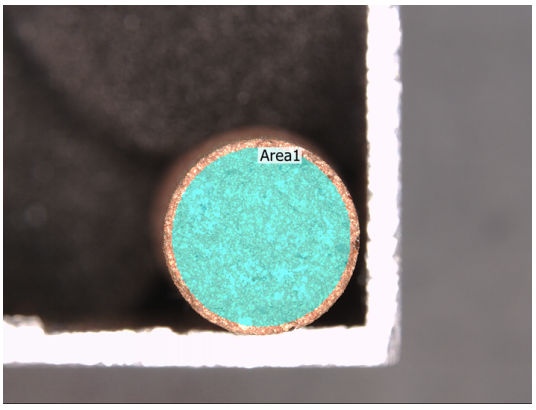

	Sa	Sz	Str	Spc
	µm	µm		1/mm
Max.	189,289	1978,500		13,213
Min.	189,289	1978,500		13,213
Ave.	189,289	1978,500		13,213
Std. DV	0,000	0,000		0,000
Area1	189,289	1978,500		13,213

2	*4*	*6*	*8*	*10*	*12*
1	*3*	*5*	*7*	*9*	*11*

Experiment: 10

Specimen ID:	***C1_4***	***Precompression Stress:***	***0,6 MPa***	***Frequency:***	***3 Hz***

Bottom Specimen: C1_4_B

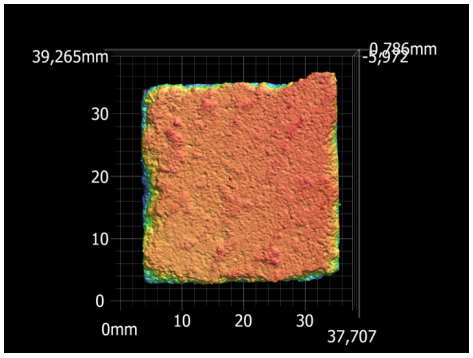

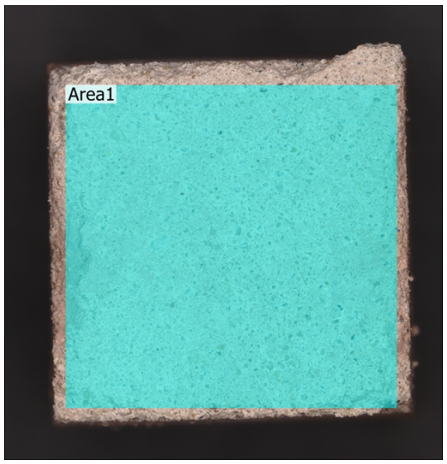

	Sa	Sz	Str	Spc
	µm	µm		1/mm
Max.	165,736	5497,000	0,200	6,150
Min.	165,736	5497,000	0,200	6,150
Ave.	165,736	5497,000	0,200	6,150
Std. DV	0,000	0,000	0,000	0,000
Area1	165,736	5497,000	0,200	6,150

Top Specimen: C1_4_T

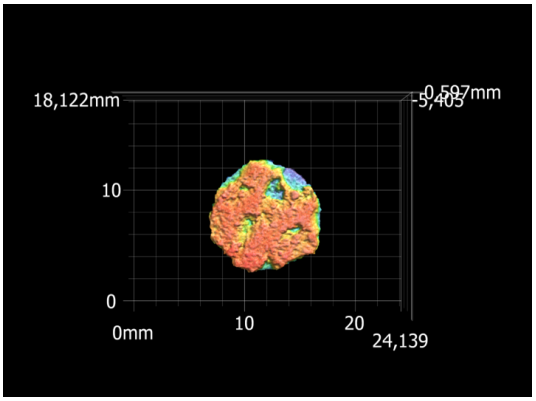

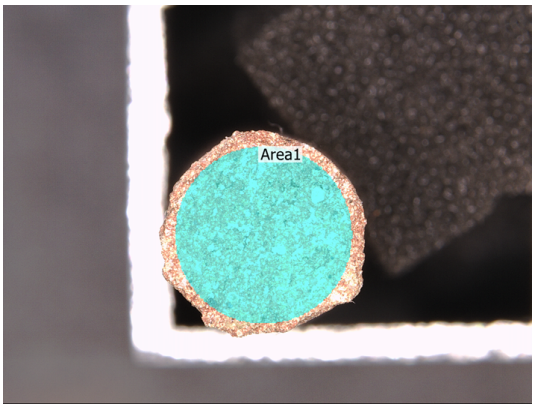

	Sa	Sz	Str	Spc
	µm	µm		1/mm
Max.	153,093	1154,300		8,617
Min.	153,093	1154,300		8,617
Ave.	153,093	1154,300		8,617
Std. DV	0,000	0,000		0,000
Area1	153,093	1154,300		8,617

2	***4***	***6***	***8***	***10***	***12***
1	***3***	***5***	***7***	***9***	***11***

Experiment: 11

Specimen ID:	***C1_3***	***Precompression Stress:***	***0,6 MPa***	***Frequency:***	***3 Hz***

Bottom Specimen: C1_3_B	***Top Specimen: C1_3_T***

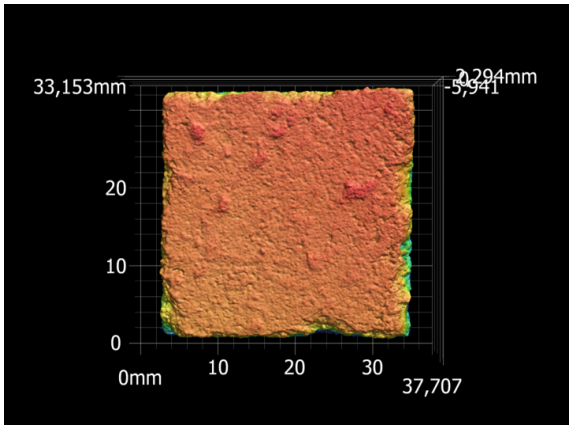

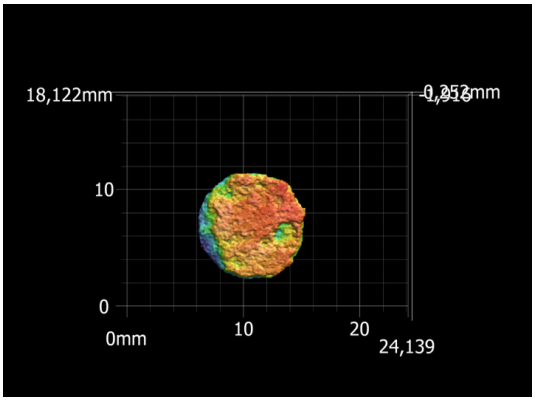

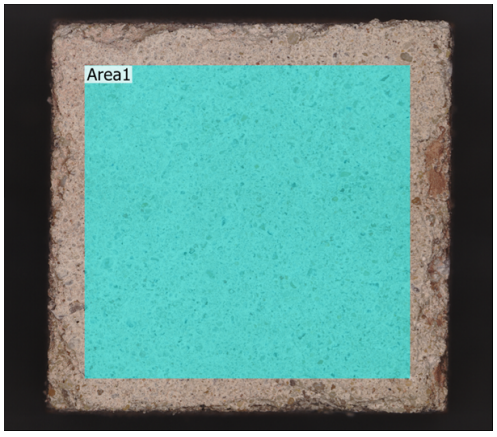

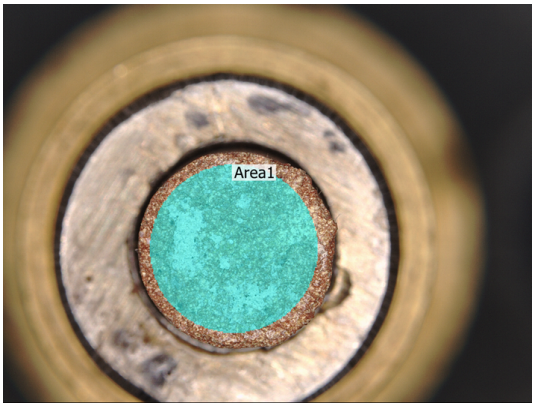

	Sa	Sz	Str	Spc
	µm	µm		1/mm
Max.	253,630	5604,600	0,243	6,510
Min.	253,630	5604,600	0,243	6,510
Ave.	253,630	5604,600	0,243	6,510
Std. DV	0,000	0,000	0,000	0,000
Area1	253,630	5604,600	0,243	6,510

	Sa	Sz	Str	Spc
	µm	µm		1/mm
Max.	160,204	1054,500		7,912
Min.	160,204	1054,500		7,912
Ave.	160,204	1054,500		7,912
Std. DV	0,000	0,000		0,000
Area1	160,204	1054,500		7,912

2	*4*	*6*	*8*	*10*	*12*
1	*3*	*5*	*7*	*9*	*11*

Experiment: 12

Specimen ID:	***C2_3***	***Precompression Stress:***	***0,6 MPa***	***Frequency:***	***3 Hz***

Bottom Specimen: C2_3_B

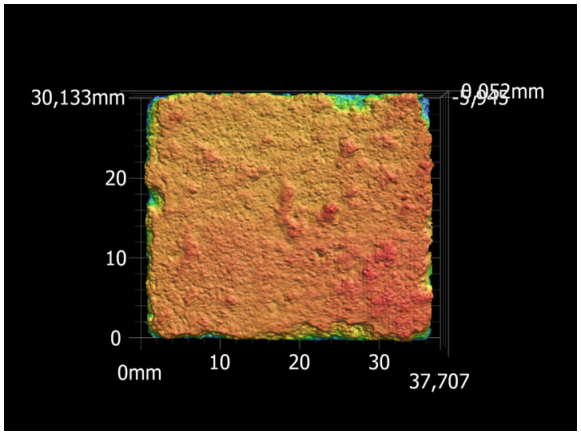

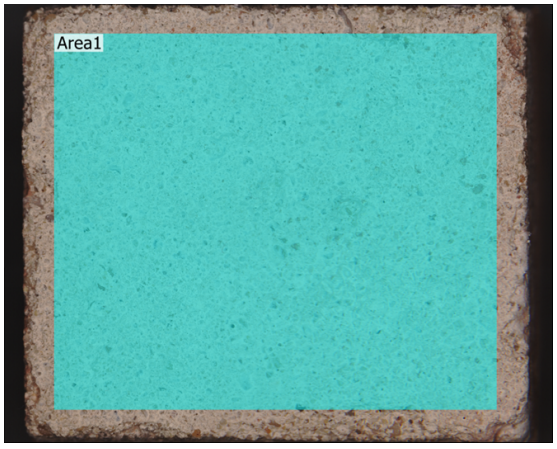

	Sa	Sz	Str	Spc
	µm	µm		1/mm
Max.	157,033	1724,700	0,326	6,403
Min.	157,033	1724,700	0,326	6,403
Ave.	157,033	1724,700	0,326	6,403
Std. DV	0,000	0,000	0,000	0,000
Area1	157,033	1724,700	0,326	6,403

Top Specimen: C2_3_T

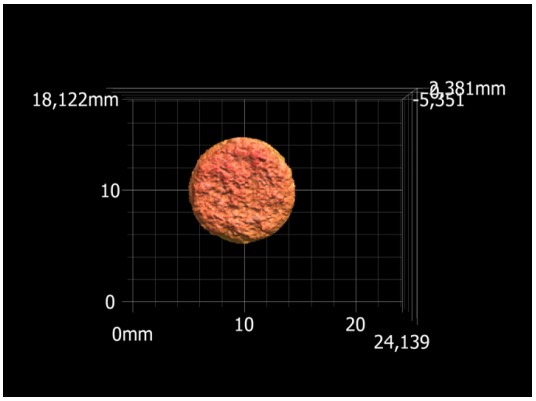

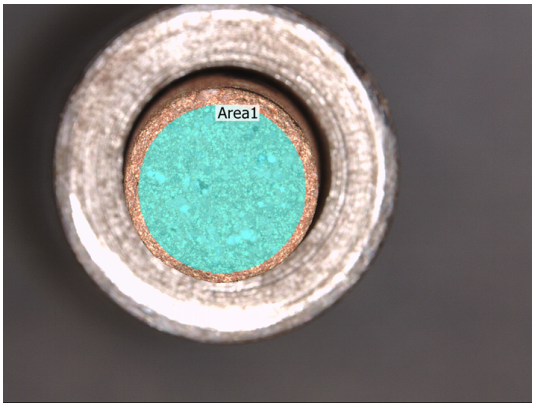

	Sa	Sz	Str	Spc
	µm	µm		1/mm
Max.	169,249	1363,400		13,369
Min.	169,249	1363,400		13,369
Ave.	169,249	1363,400		13,369
Std. DV	0,000	0,000		0,000
Area1	169,249	1363,400		13,369

2	***4***	***6***	***8***	***10***	***12***
1	***3***	***5***	***7***	***9***	***11***

Experiment: 13

Specimen ID:	***C3_3***	***Precompression Stress:***	***0,6 MPa***	***Frequency:***	***3 Hz***

Bottom Specimen: C3_3_B

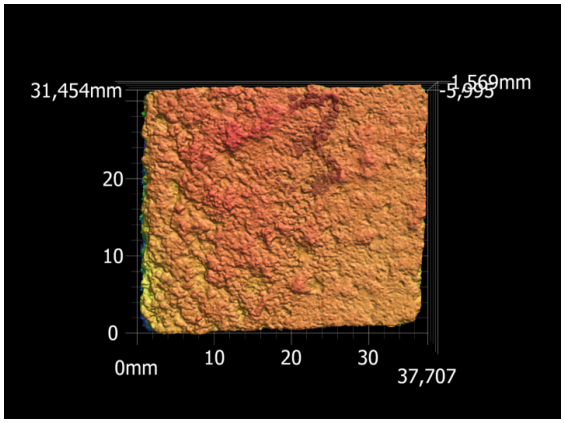

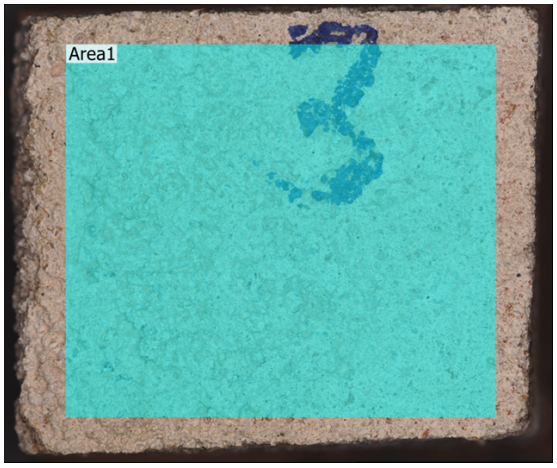

	Sa	Sz	Str	Spc
	µm	µm		1/mm
Max.	249,317	2419,600	0,402	7,442
Min.	249,317	2419,600	0,402	7,442
Ave.	249,317	2419,600	0,402	7,442
Std. DV	0,000	0,000	0,000	0,000
Area1	249,317	2419,600	0,402	7,442

Top Specimen: C3_3_T

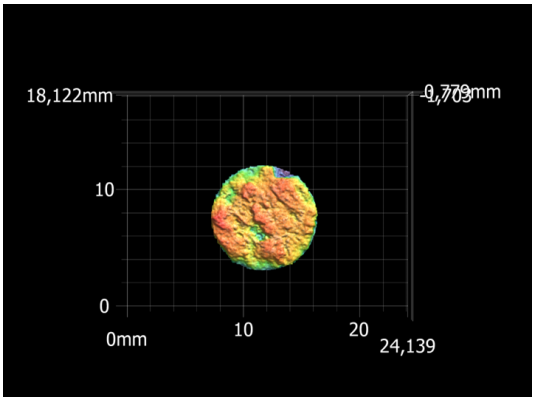

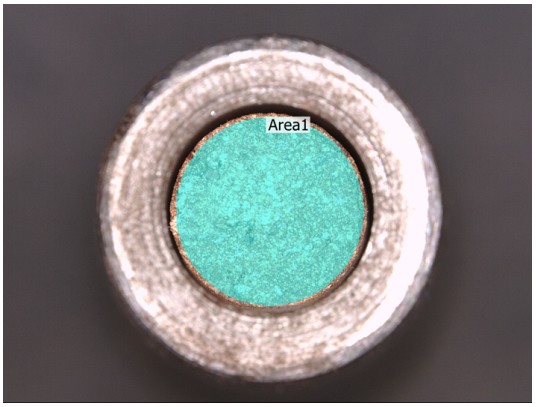

	Sa	Sz	Str	Spc
	µm	µm		1/mm
Max.	153,093	1154,300		8,617
Min.	153,093	1154,300		8,617
Ave.	153,093	1154,300		8,617
Std. DV	0,000	0,000		0,000
Area1	153,093	1154,300		8,617

2	*4*	*6*	*8*	*10*	*12*
1	*3*	*5*	*7*	*9*	*11*

Experiment: 14

Specimen ID:	***C1_10***	***Precompression Stress:***	***0,4 MPa***	***Frequency:***	***3 Hz***

Bottom Specimen: C1_10_B	***Top Specimen:C1_10_T***

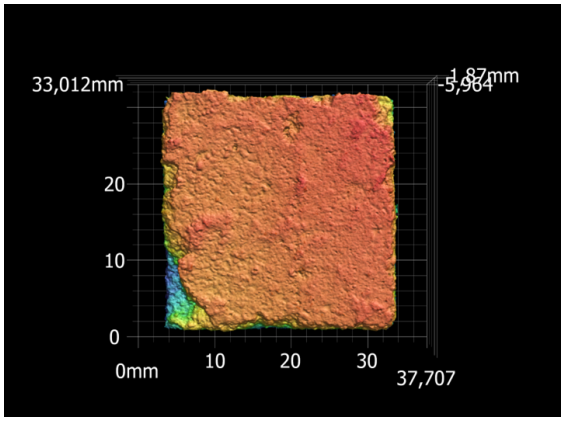

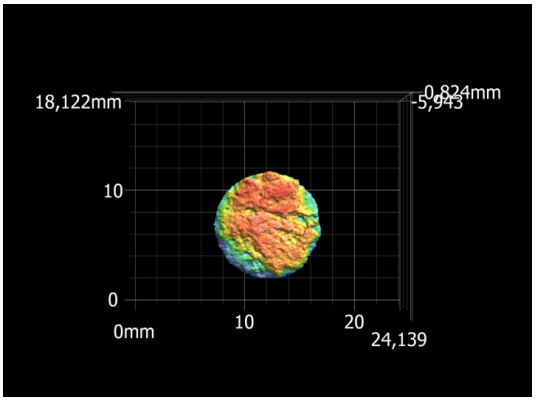

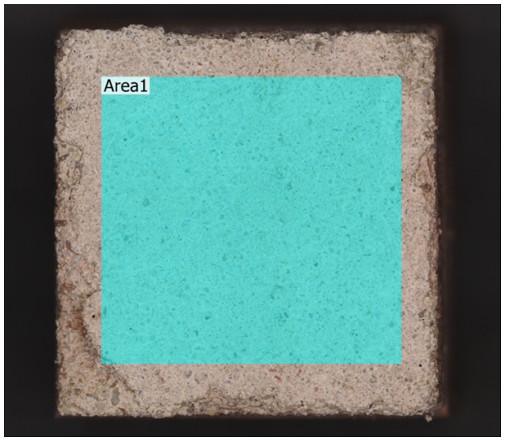

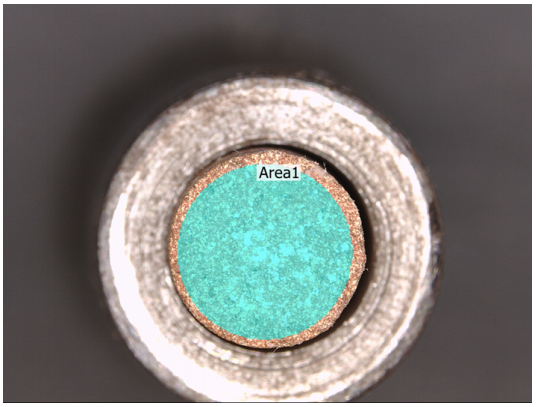

	Sa	Sz	Str	Spc
	µm	µm		1/mm
Max.	253,630	5604,600	0,243	6,510
Min.	253,630	5604,600	0,243	6,510
Ave.	253,630	5604,600	0,243	6,510
Std. DV	0,000	0,000	0,000	0,000
Area1	253,630	5604,600	0,243	6,510

	Sa	Sz	Str	Spc
	µm	µm		1/mm
Max.	191,729	1192,100		9,037
Min.	191,729	1192,100		9,037
Ave.	191,729	1192,100		9,037
Std. DV	0,000	0,000		0,000
Area1	191,729	1192,100		9,037

2	***4***	***6***	***8***	***10***	***12***
1	***3***	***5***	***7***	***9***	***11***

Experiment: 15

Specimen ID:	***C2_8***	***Precompression Stress:***	***0,4 MPa***	***Frequency:***	***3 Hz***

Bottom Specimen: C2_8_B

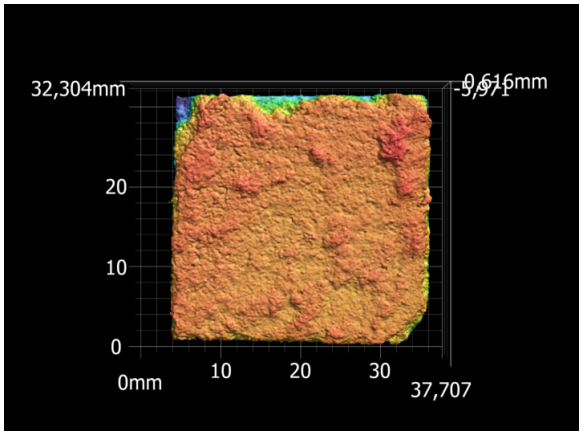

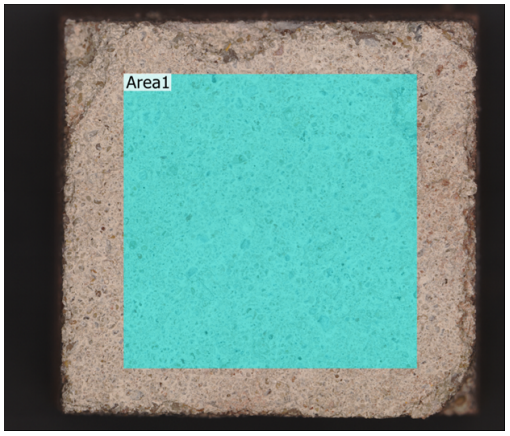

	Sa	Sz	Str	Spc
	µm	µm		1/mm
Max.	137,422	1607,000	0,586	6,150
Min.	137,422	1607,000	0,586	6,150
Ave.	137,422	1607,000	0,586	6,150
Std. DV	0,000	0,000	0,000	0,000
Area1	137,422	1607,000	0,586	6,150

Top Specimen: C2_8_T

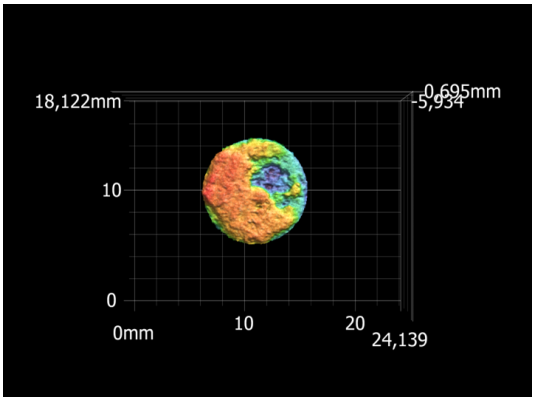

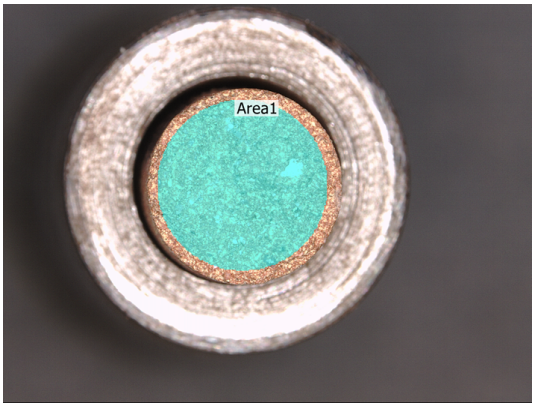

	Sa	Sz	Str	Spc
	µm	µm		1/mm
Max.	395,931	2206,900		8,517
Min.	395,931	2206,900		8,517
Ave.	395,931	2206,900		8,517
Std. DV	0,000	0,000		0,000
Area1	395,931	2206,900		8,517

2	***4***	***6***	***8***	***10***	***12***
1	***3***	***5***	***7***	***9***	***11***

Experiment: 16

Specimen ID:	*C3_10*	*Precompression Stress:*	*0,4 MPa*	*Frequency:*	*3 Hz*

Bottom Specimen: C3_10_B

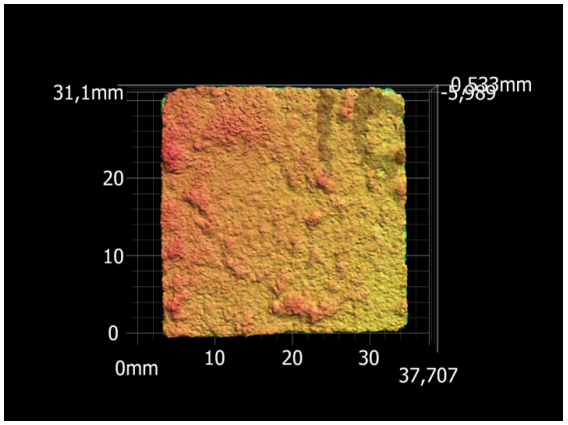

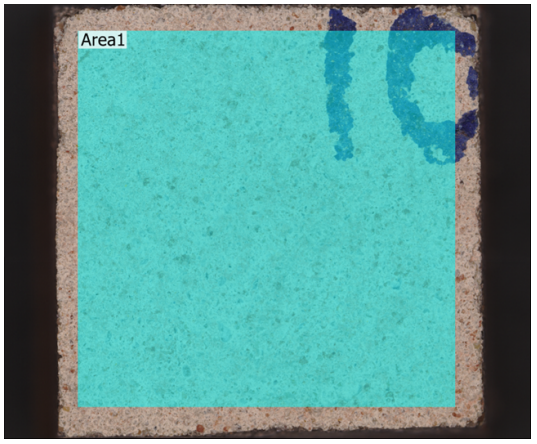

	Sa	Sz	Str	Spc
	µm	µm		1/mm
Max.	203,677	1759,700	0,265	7,970
Min.	203,677	1759,700	0,265	7,970
Ave.	203,677	1759,700	0,265	7,970
Std. DV	0,000	0,000	0,000	0,000
Area1	203,677	1759,700	0,265	7,970

Top Specimen: C3_10_T

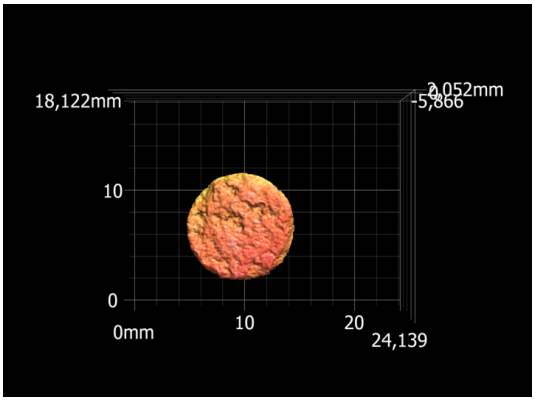

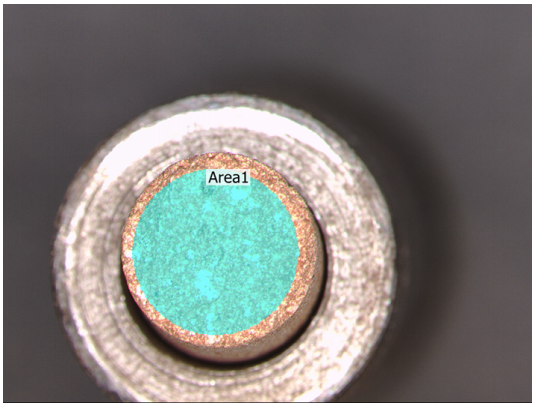

	Sa	Sz	Str	Spc
	µm	µm		1/mm
Max.	169,712	1385,100		8,039
Min.	169,712	1385,100		8,039
Ave.	169,712	1385,100		8,039
Std. DV	0,000	0,000		0,000
Area1	169,712	1385,100		8,039

2	*4*	*6*	*8*	*10*	*12*
1	*3*	*5*	*7*	*9*	*11*

Experiment: 17

Specimen ID:	***C1_7***	***Precompression Stress:***	***0,2 MPa***	***Frequency:***	***3 Hz***

Bottom Specimen: C1_7_B

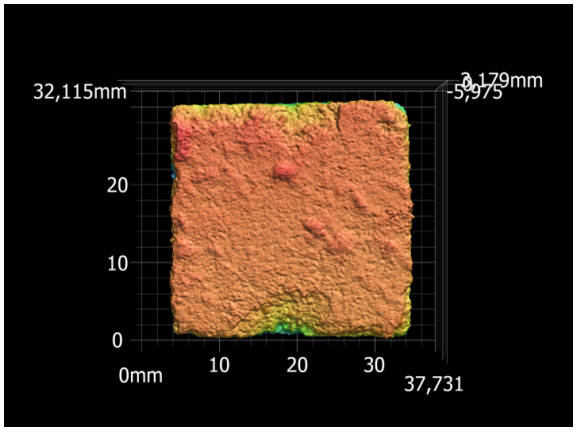

	Sa	Sz	Str	Spc
	µm	µm		1/mm
Max.	187,322	2429,200	0,247	5,917
Min.	187,322	2429,200	0,247	5,917
Ave.	187,322	2429,200	0,247	5,917
Std. DV	0,000	0,000	0,000	0,000
Area1	187,322	2429,200	0,247	5,917

Top Specimen: C1_7_T

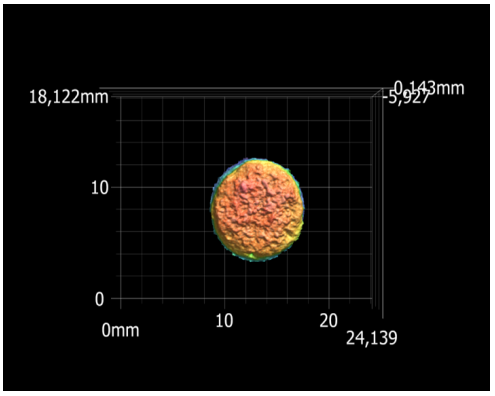

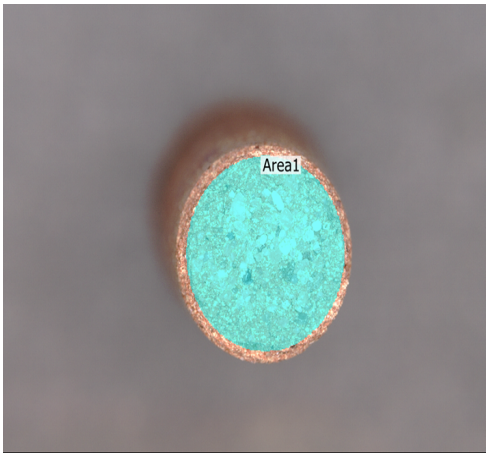

	Sa	Sz	Str	Spc
	µm	µm		1/mm
Max.	191,729	1192,100		9,037
Min.	191,729	1192,100		9,037
Ave.	191,729	1192,100		9,037
Std. DV	0,000	0,000		0,000
Area1	191,729	1192,100		9,037

2	***4***	***6***	***8***	***10***	***12***
1	***3***	***5***	***7***	***9***	***11***

Experiment: 18

Specimen ID:	***C2_9***	***Precompression Stress:***	***0,2 MPa***	***Frequency:***	***3 Hz***

Bottom Specimen: C2_9_B

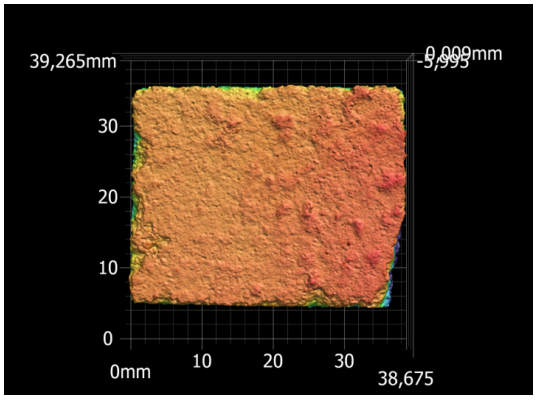

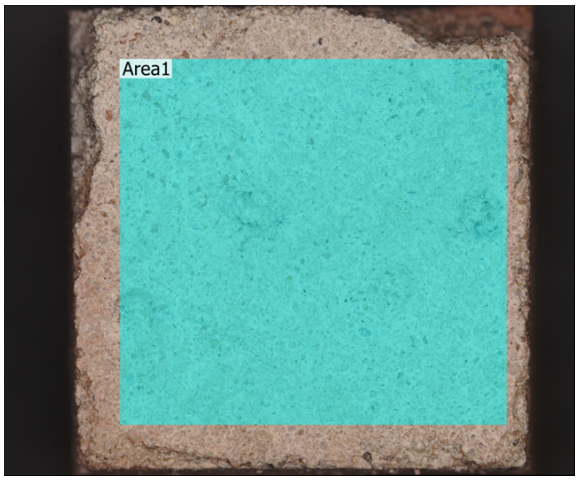

	Sa	Sz	Str	Spc
	µm	µm		1/mm
Max.	139,093	1594,800	0,879	6,731
Min.	139,093	1594,800	0,879	6,731
Ave.	139,093	1594,800	0,879	6,731
Std. DV	0,000	0,000	0,000	0,000
Area1	139,093	1594,800	0,879	6,731

Top Specimen: C2_9_T

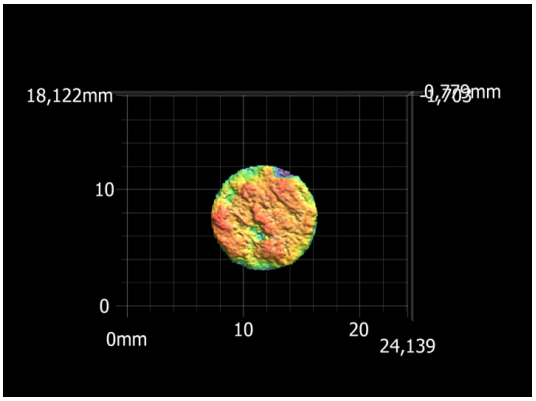

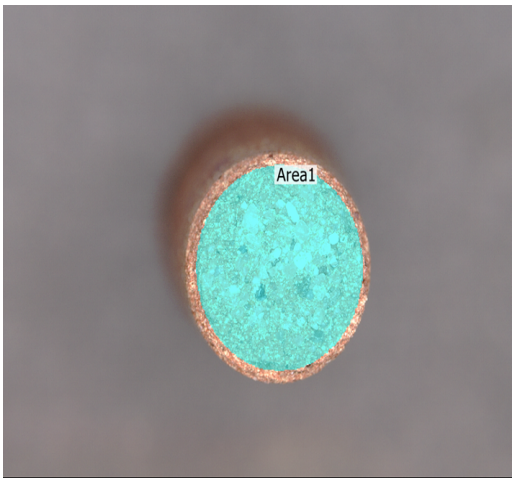

	Sa	Sz	Str	Spc
	µm	µm		1/mm
Max.	169,249	1363,400		13,369
Min.	169,249	1363,400		13,369
Ave.	169,249	1363,400		13,369
Std. DV	0,000	0,000		0,000
Area1	169,249	1363,400		13,369

2	***4***	***6***	***8***	***10***	***12***
1	***3***	***5***	***7***	***9***	***11***

Experiment: 19

Specimen ID:	*C3_9*	*Precompression Stress:*	*0,2 MPa*	*Frequency:*	*3 Hz*

Bottom Specimen: C3_9_B

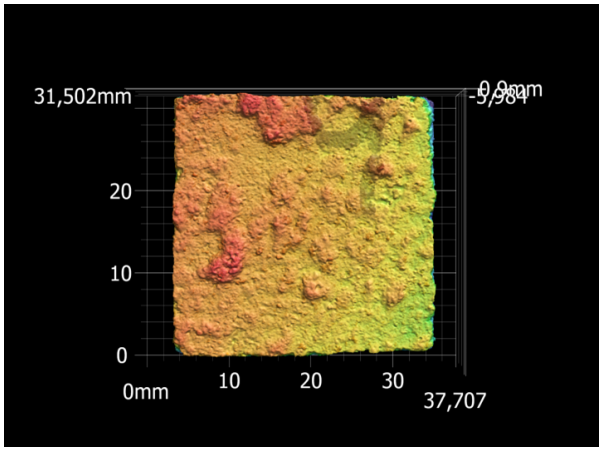

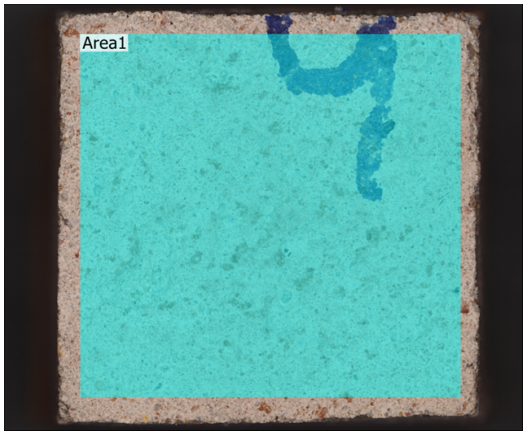

	Sa	Sz	Str	Spc
	µm	µm		1/mm
Max.	245,749	1930,700	0,311	7,277
Min.	245,749	1930,700	0,311	7,277
Ave.	245,749	1930,700	0,311	7,277
Std. DV	0,000	0,000	0,000	0,000
Area1	245,749	1930,700	0,311	7,277

Top Specimen: C3_9_T

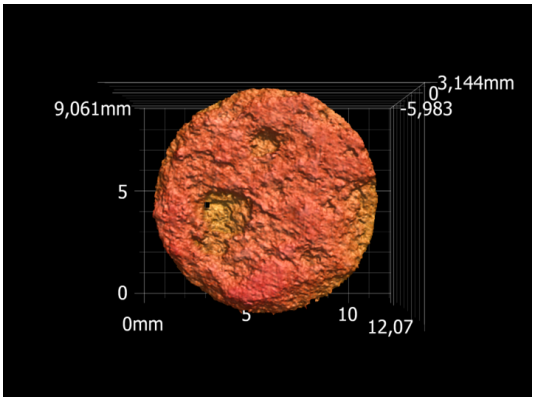

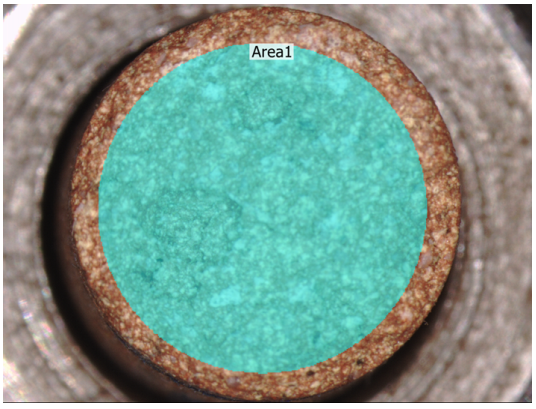

	Sa	Sz	Str	Spc
	µm	µm		1/mm
Max.	188,254	1728,500		36,742
Min.	188,254	1728,500		36,742
Ave.	188,254	1728,500		36,742
Std. DV	0,000	0,000		0,000
Area1	188,254	1728,500		36,742

2	*4*	*6*	*8*	*10*	*12*
1	*3*	*5*	*7*	*9*	*11*

Experiment: 20,23

Specimen ID:	***C1_12***	***Precompression Stress:***	***0,1 MPa***	***Frequency:***	***3 Hz***

Bottom Specimen: C1_12_B

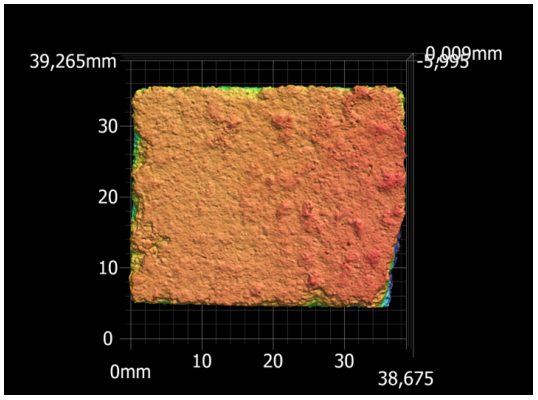

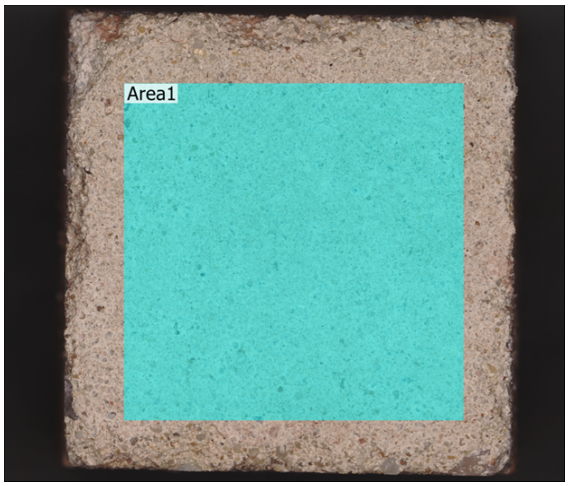

	Sa	Sz	Str	Spc
	µm	µm		1/mm
Max.	191,093	1419,400	0,405	5,608
Min.	191,093	1419,400	0,405	5,608
Ave.	191,093	1419,400	0,405	5,608
Std. DV	0,000	0,000	0,000	0,000
Area1	191,093	1419,400	0,405	5,608

Top Specimen: C1_12_T

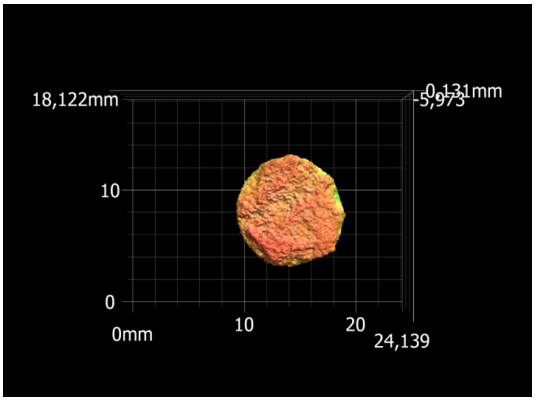

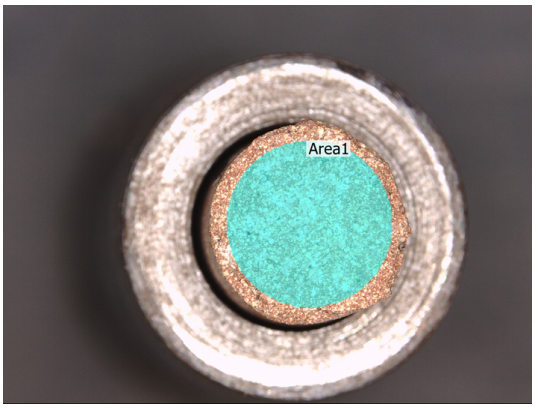

	Sa	Sz	Str	Spc
	µm	µm		1/mm
Max.	110,638	1047,700		13,337
Min.	110,638	1047,700		13,337
Ave.	110,638	1047,700		13,337
Std. DV	0,000	0,000		0,000
Area1	110,638	1047,700		13,337

2	***4***	***6***	***8***	***10***	***12***
1	***3***	***5***	***7***	***9***	***11***

Experiment: 21,24

Specimen ID:	***C2_1***	***Precompression Stress:***	***0,1 MPa***	***Frequency:***	***3 Hz***

Bottom Specimen: C2_1_B

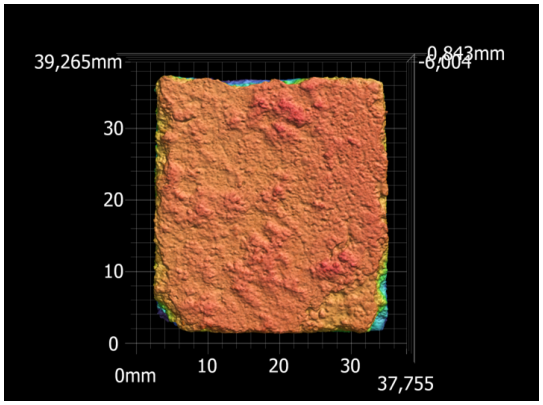

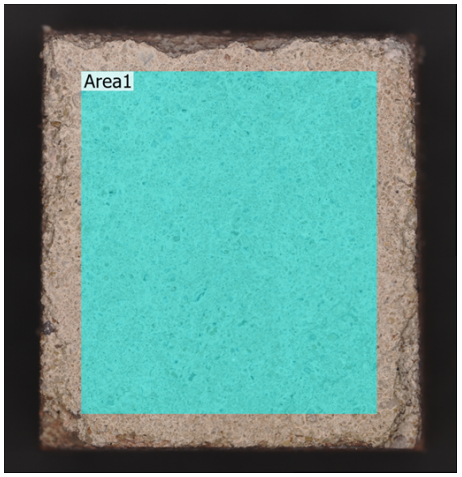

	Sa	Sz	Str	Spc
	µm	µm		1/mm
Max.	167,534	1785,200	0,623	5,774
Min.	167,534	1785,200	0,623	5,774
Ave.	167,534	1785,200	0,623	5,774
Std. DV	0,000	0,000	0,000	0,000
Area1	167,534	1785,200	0,623	5,774

Top Specimen: C2_1_T

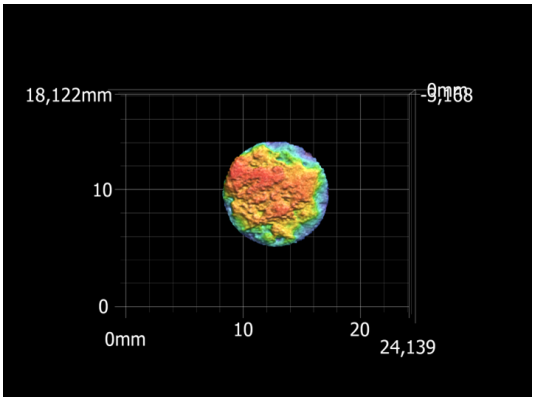

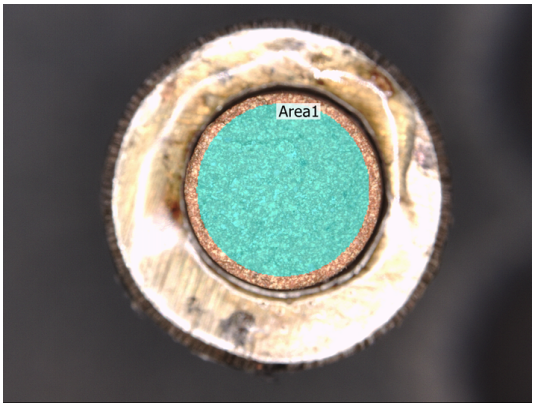

	Sa	Sz	Str	Spc
	µm	µm		1/mm
Max.	238,550	1366,100		9,579
Min.	238,550	1366,100		9,579
Ave.	238,550	1366,100		9,579
Std. DV	0,000	0,000		0,000
Area1	238,550	1366,100		9,579

2	*4*	*6*	*8*	*10*	*12*
1	*3*	*5*	*7*	*9*	*11*

Experiment: 22,25

Specimen ID:	***C2_4***	***Precompression Stress:***	***0,1 MPa***	***Frequency:***	***3 Hz***

Bottom Specimen: C2_4_B

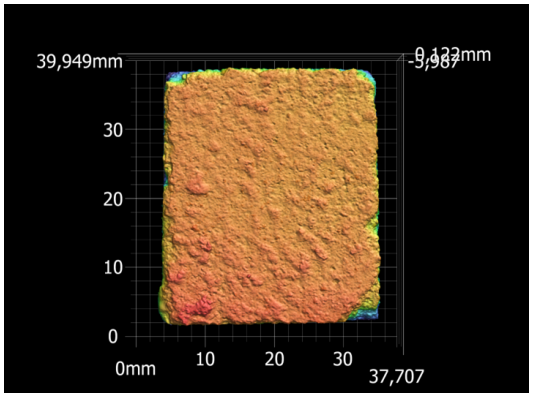

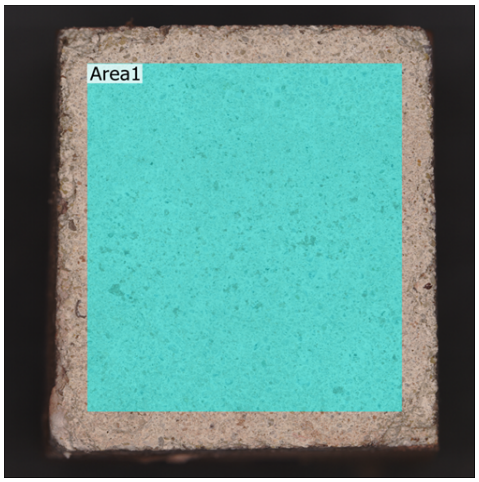

	Sa	Sz	Str	Spc
	µm	µm		1/mm
Max.	127,044	1439,400	0,388	6,109
Min.	127,044	1439,400	0,388	6,109
Ave.	127,044	1439,400	0,388	6,109
Std. DV	0,000	0,000	0,000	0,000
Area1	127,044	1439,400	0,388	6,109

Top Specimen: C2_4_T

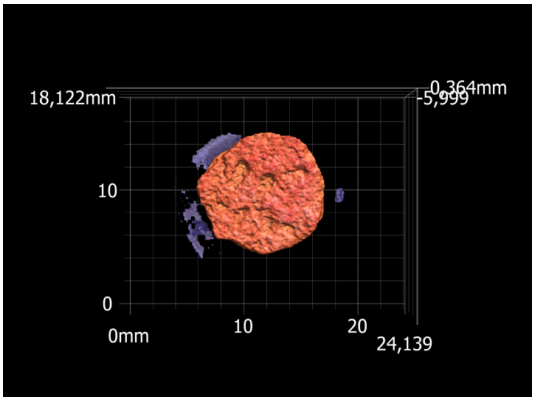

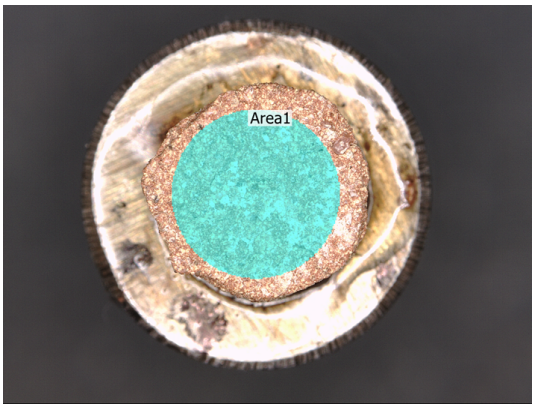

	Sa	Sz	Str	Spc
	µm	µm		1/mm
Max.	123,343	886,800		7,627
Min.	123,343	886,800		7,627
Ave.	123,343	886,800		7,627
Std. DV	0,000	0,000		0,000
Area1	123,343	886,800		7,627

2	***4***	***6***	***8***	***10***	***12***
1	***3***	***5***	***7***	***9***	***11***

APPENDIX C -

EXPERIMENT RESULTS

Experiment: 01

Specimen ID:	***C2_5***	***Precompression Stress:***	***0.2 MPa***	***Frequency:***	***3 Hz***
Bottom Specimen: C2_5_B			***Top Specimen: C2_5_T***		

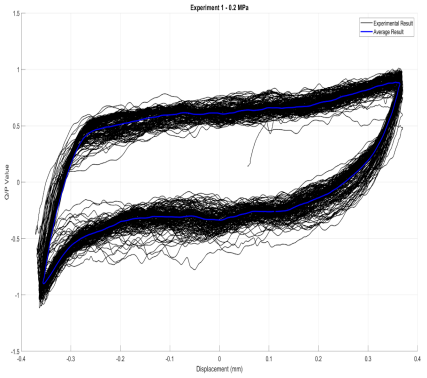

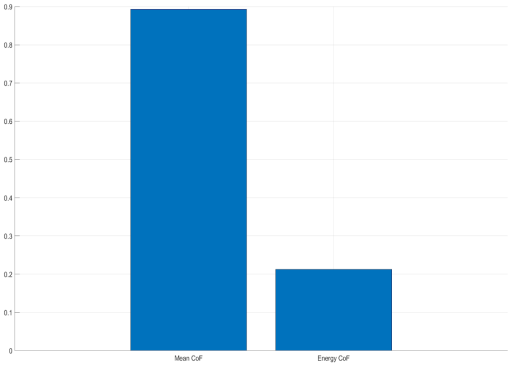

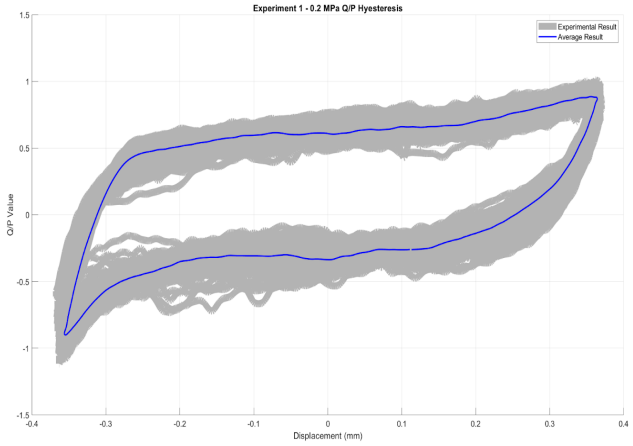

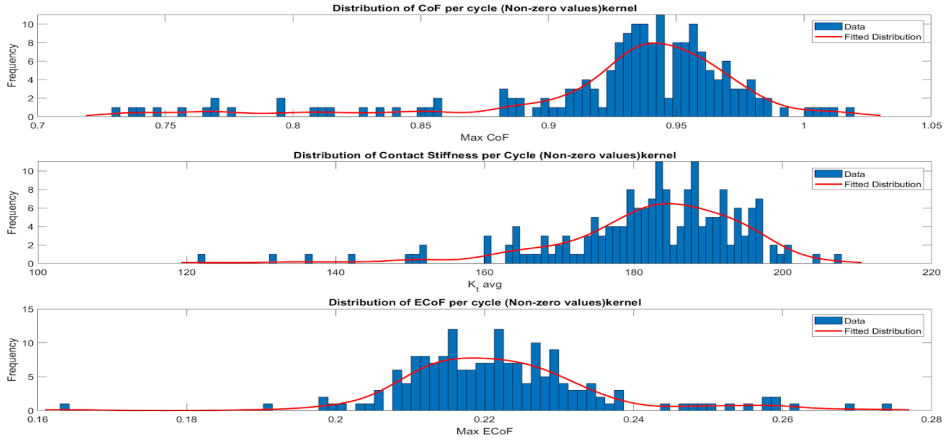

Experiment: 02

Specimen ID:	***C3_11***	***Precompression Stress:***	***0.2 MPa***	***Frequency:***	***3 Hz***
Bottom Specimen: C3_11_B			***Top Specimen: C3_11_T***		

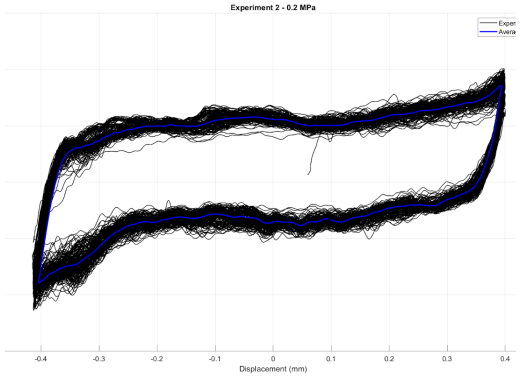

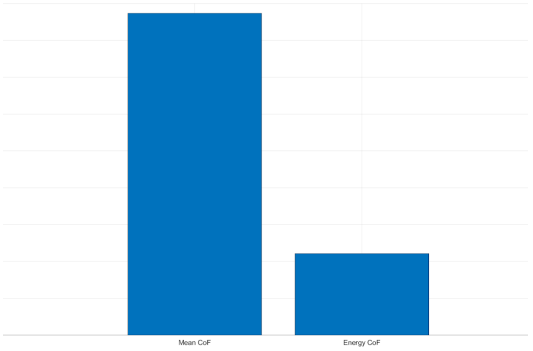

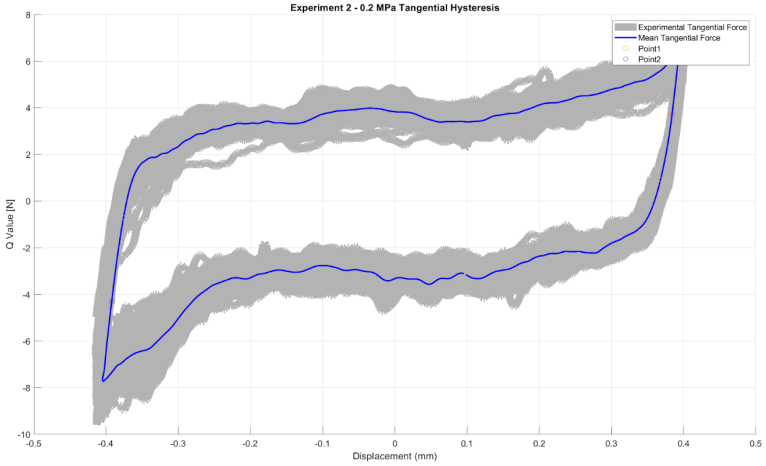

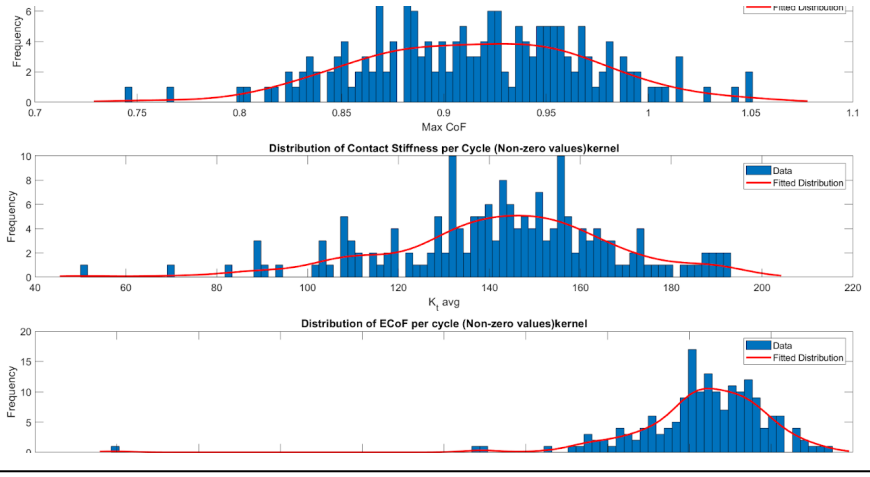

Experiment: 03

Specimen ID:	*C1_8*	*Precompression Stress:*	*0.2 MPa*	*Frequency:*	*3 Hz*

Bottom Specimen: C1_8_B	*Top Specimen: C1_8_T*

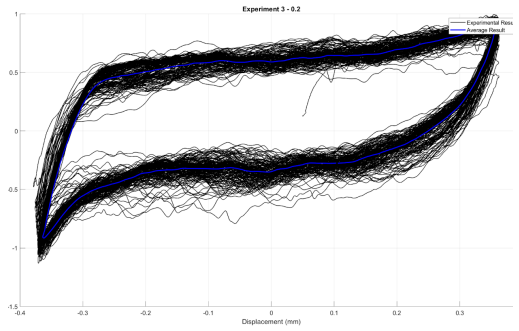

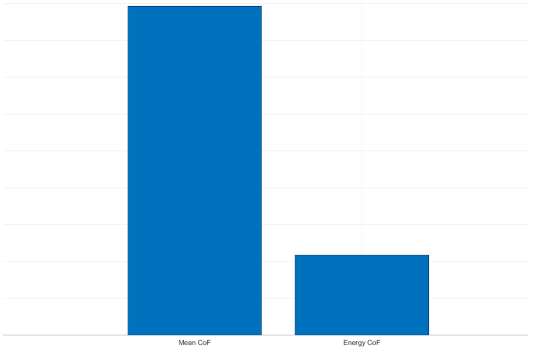

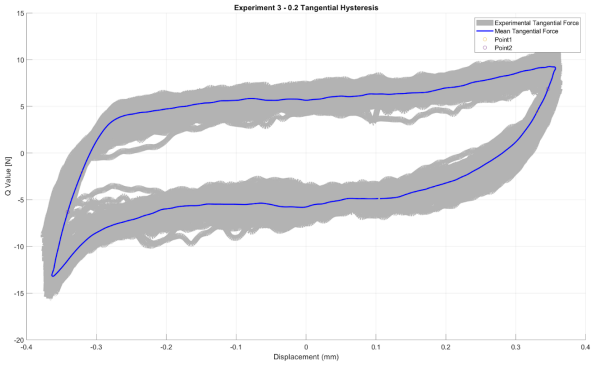

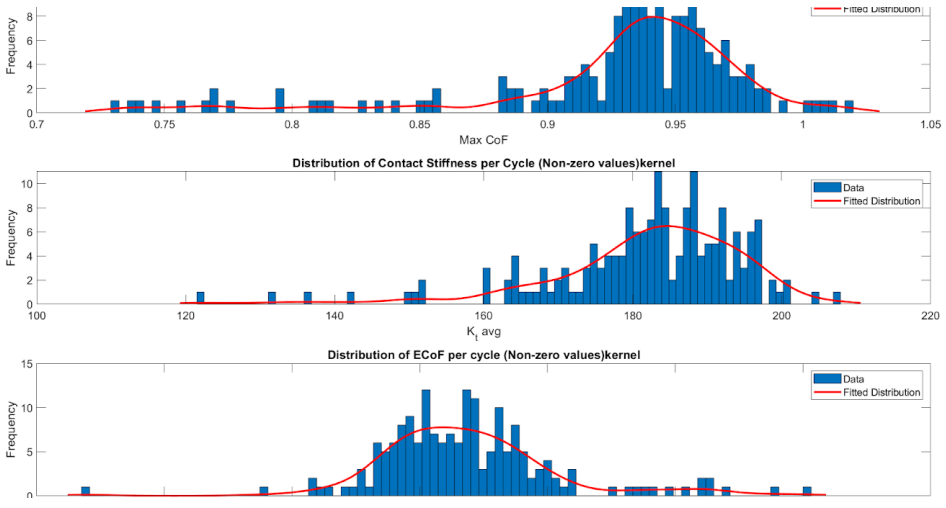

Experiment: 04

Specimen ID:	***C1_5***	***Precompression Stress:***	***0.4 MPa***	***Frequency:***	***3 Hz***
Bottom Specimen: C1_5_B			***Top Specimen: C1_5_T***		

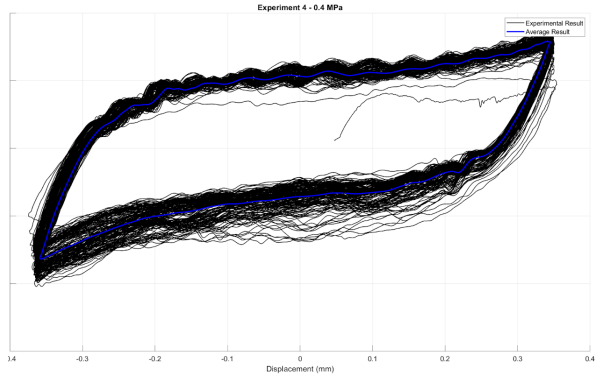

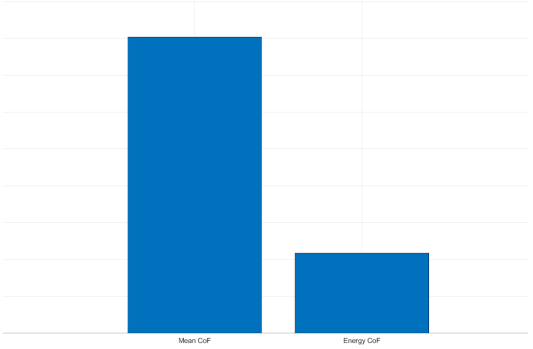

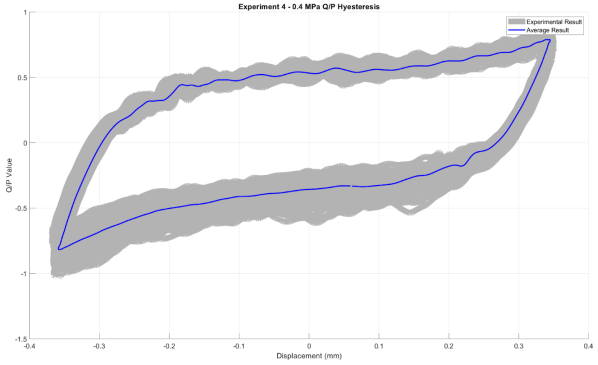

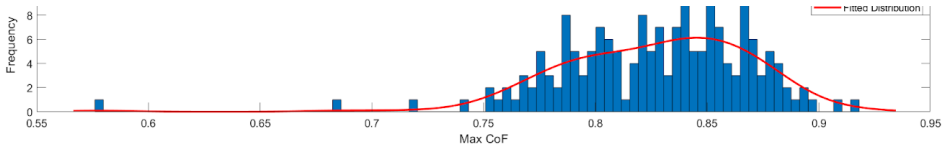

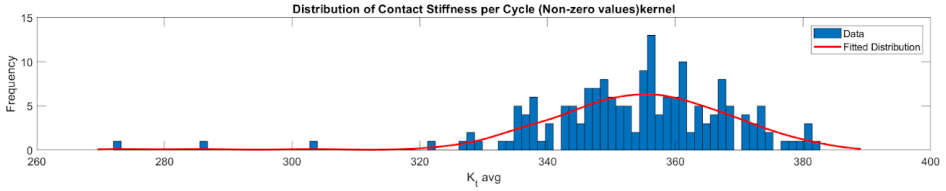

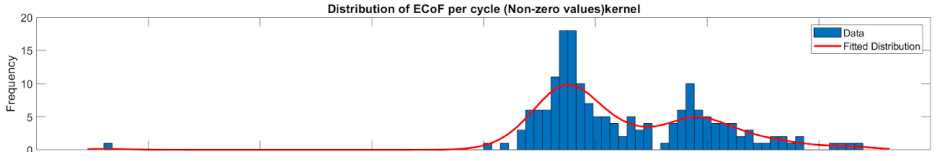

Experiment: 05

Specimen ID:	*C2_2*	*Precompression Stress:*	*0.4 MPa*	*Frequency:*	*3 Hz*

Bottom Specimen: C2_2_B	*Top Specimen: C2_2_T*

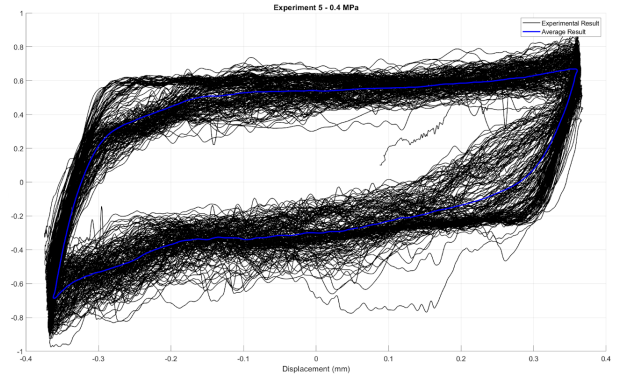

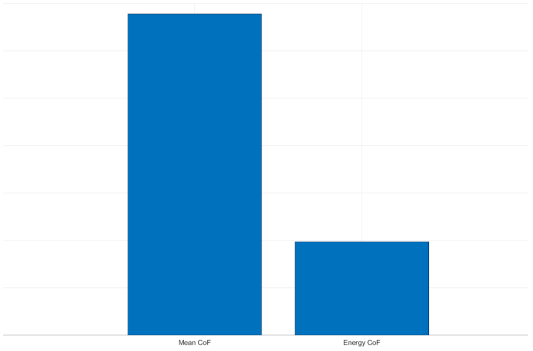

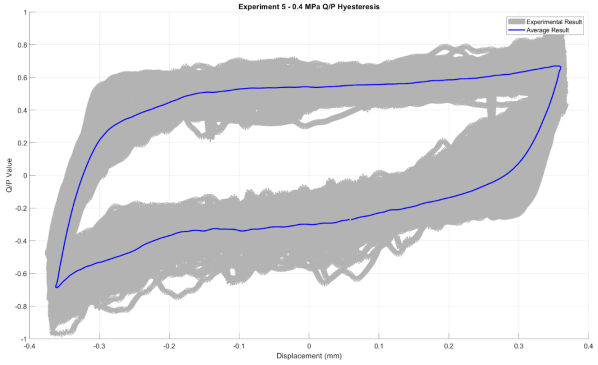

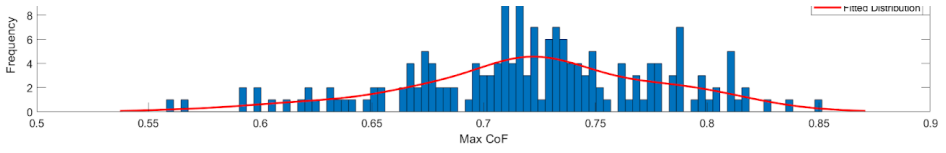

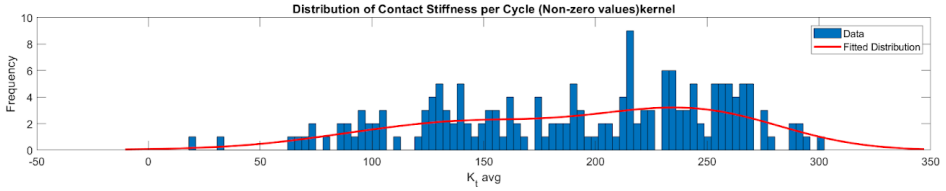

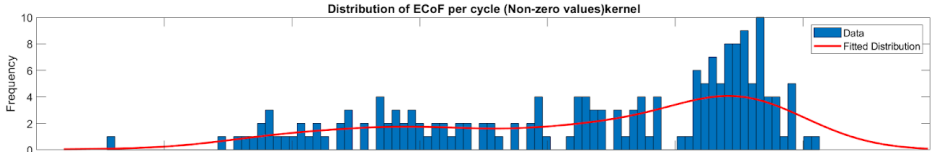

Experiment: 06

Specimen ID:	*C3_8*	*Precompression Stress:*	*0.4 MPa*	*Frequency:*	*3 Hz*

Bottom Specimen: C3_8_B	*Top Specimen: C3_8_T*

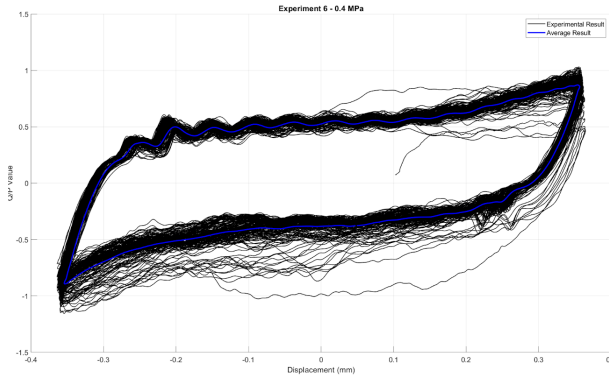

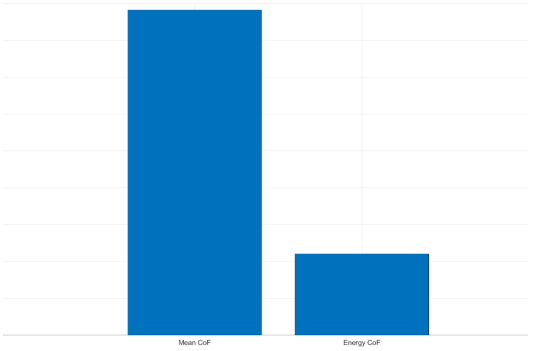

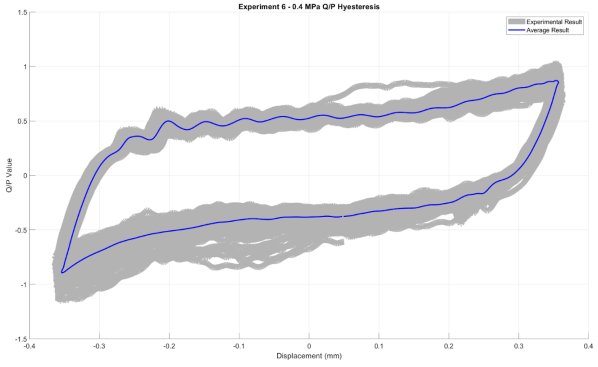

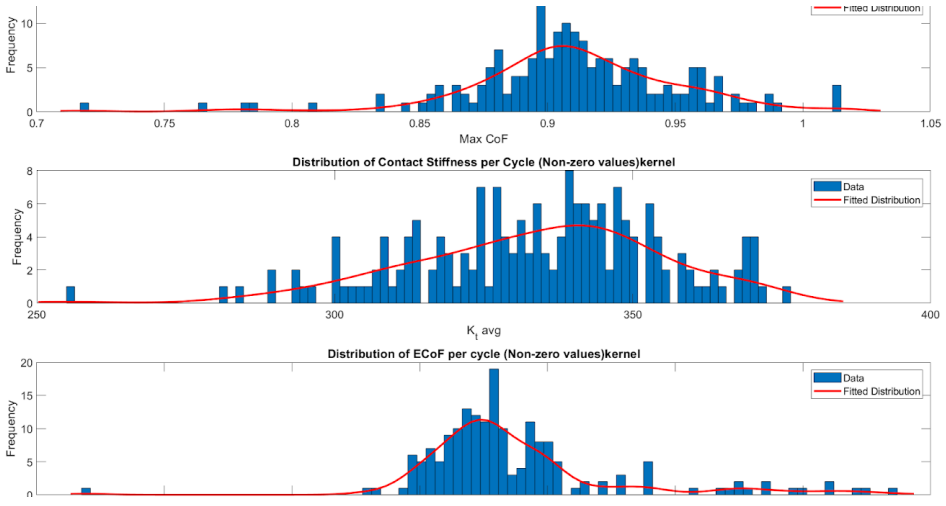

Experiment: 07

Specimen ID:	*C2_10*	*Precompression Stress:*	*0.6 MPa*	*Frequency:*	*3 Hz*
Bottom Specimen: C2_10_B			*Top Specimen: C2_10_T*		

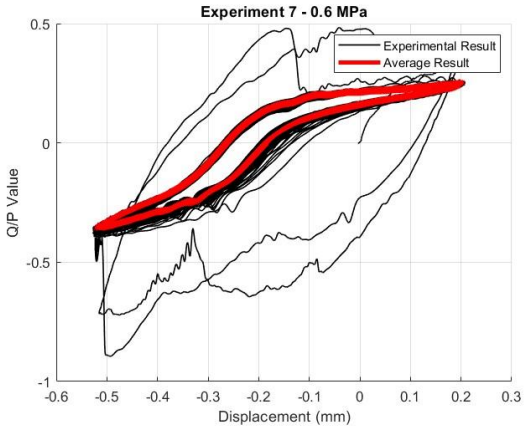

Results weren't obtained since the experiment failed and yielded erroneous data

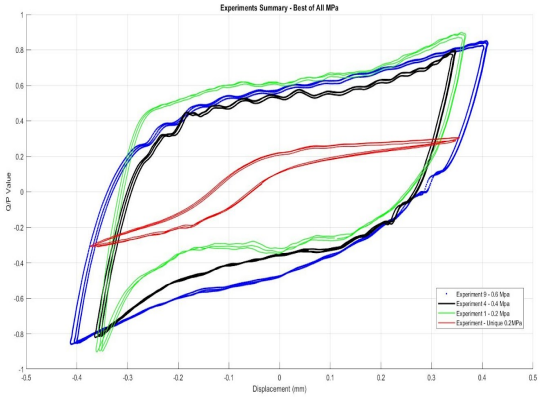

Bending failure. The specimen experienced a stick-bending phase

Experiment: 08

Specimen ID:	***C2_7***	***Precompression Stress:***	***0.6 MPa***	***Frequency:***	***3 Hz***
Bottom Specimen: C2_7_B			***Top Specimen: C2_7_T***		

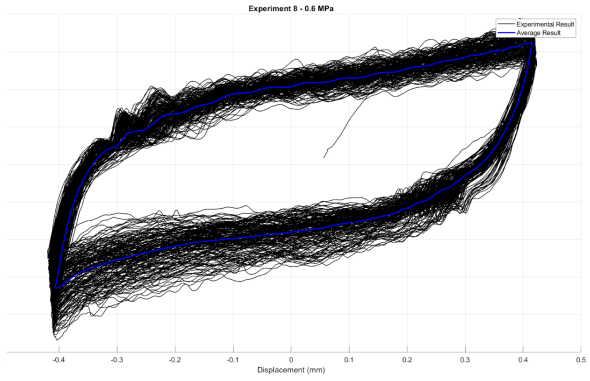

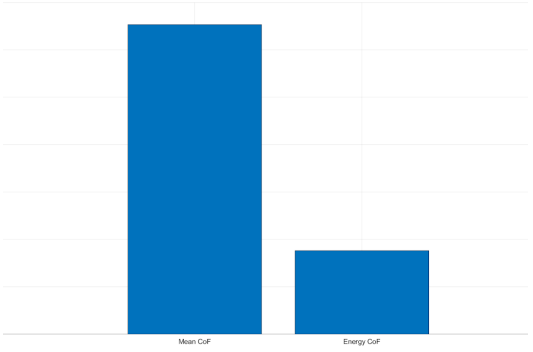

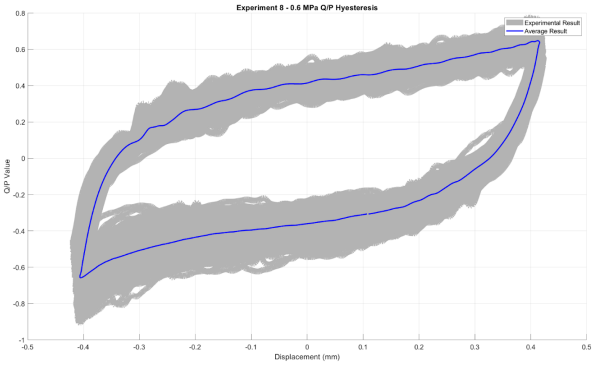

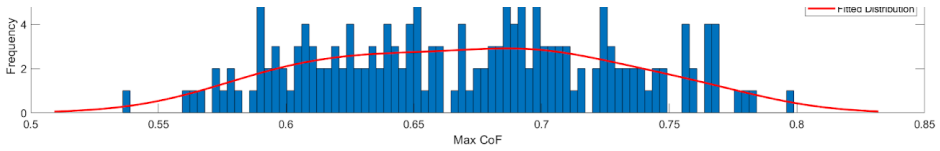

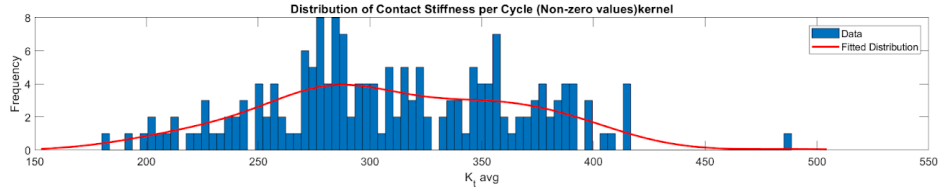

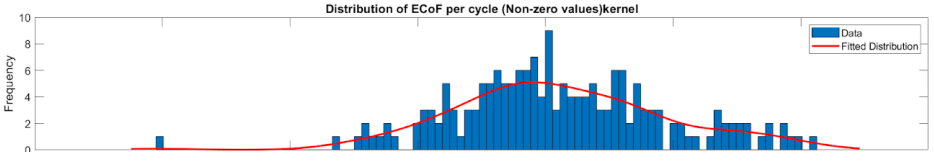

Experiment: 09

Specimen ID:	***C3_6***	***Precompression Stress:***	***0.6 MPa***	***Frequency:***	***3 Hz***
Bottom Specimen: C3_6_B			***Top Specimen: C3_6_T***		

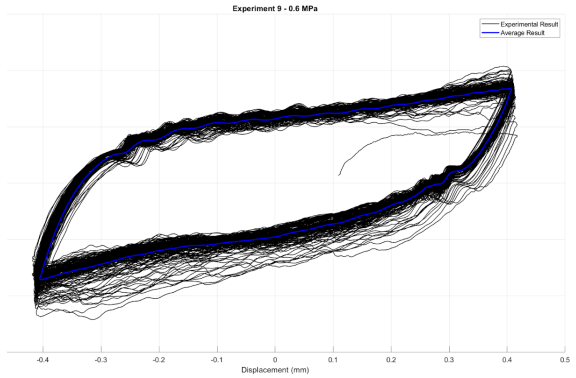

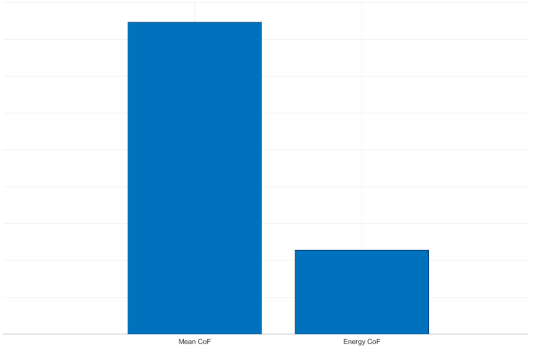

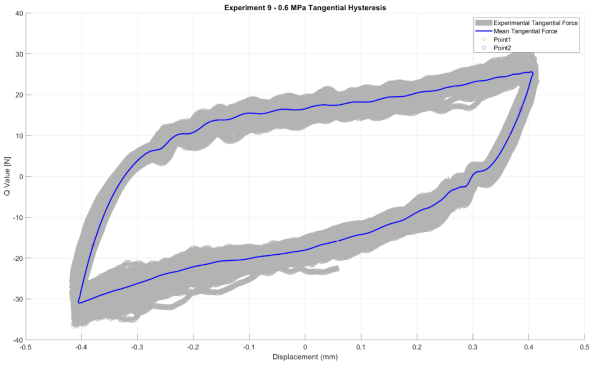

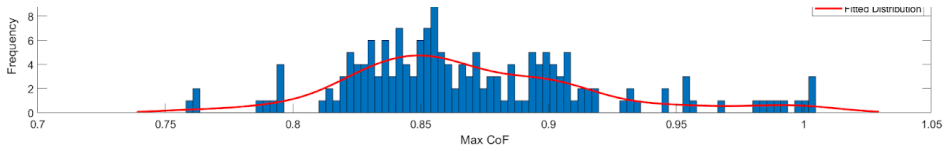

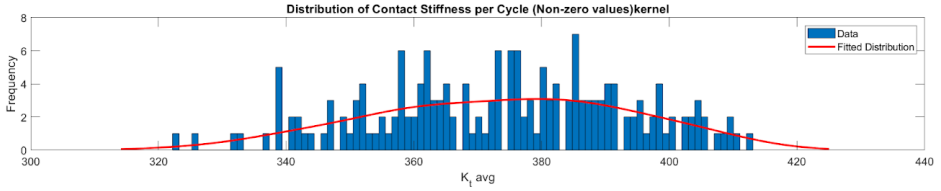

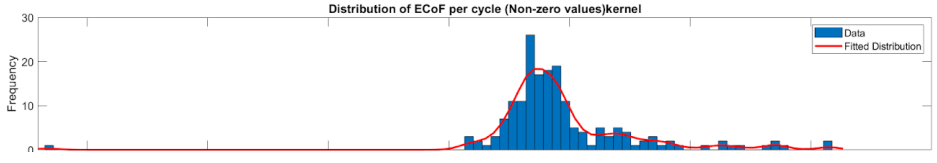

Experiment: 10

Specimen ID:	***C1_4***	***Precompression Stress:***	***0.6 MPa***	***Frequency:***	***3 Hz***

Bottom Specimen: C1_4_B

Top Specimen: C1_4_T

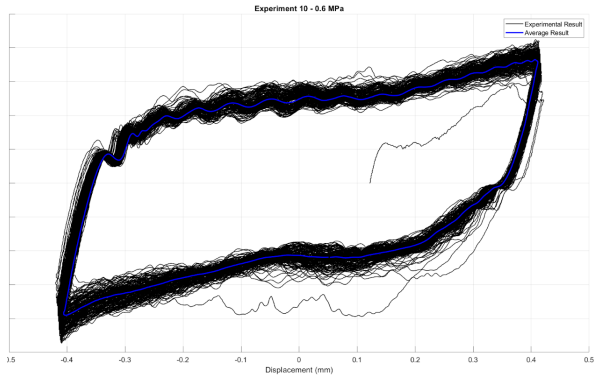

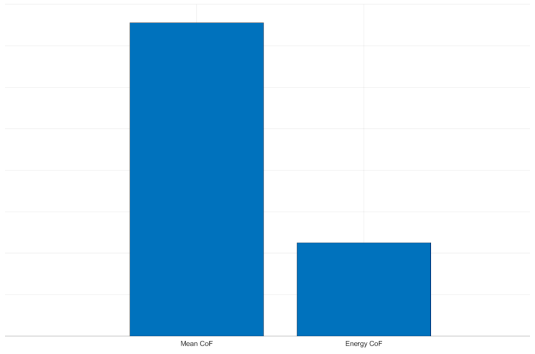

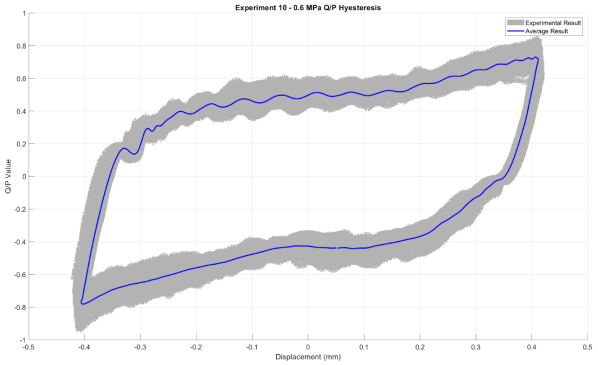

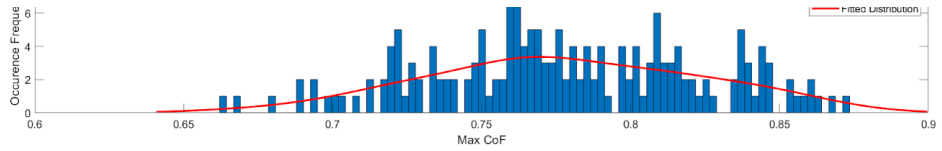

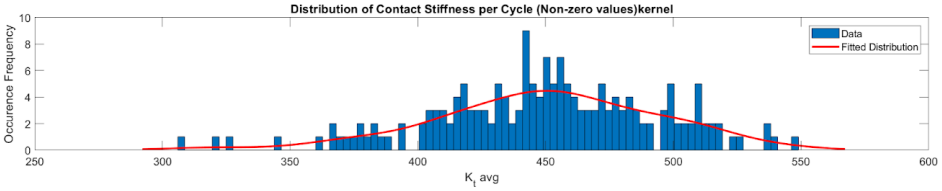

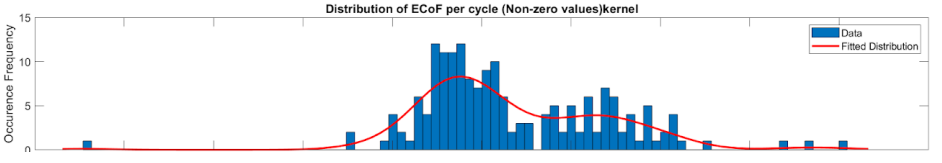

Experiment: 11

Specimen ID:	***C1_3***	***Precompression Stress:***	***0.6 MPa***	***Frequency:***	***0.2 Hz***

Bottom Specimen: C1_3_B

Top Specimen: C1_3_T

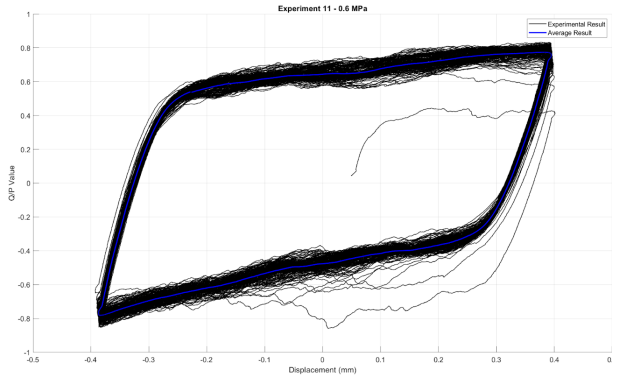

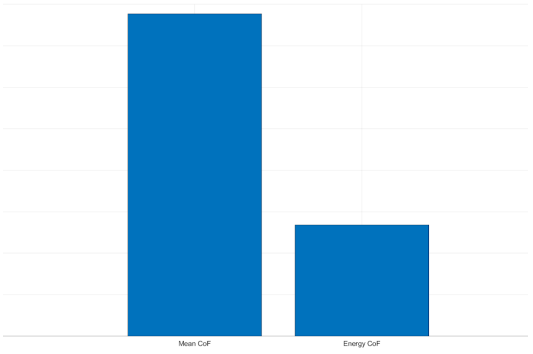

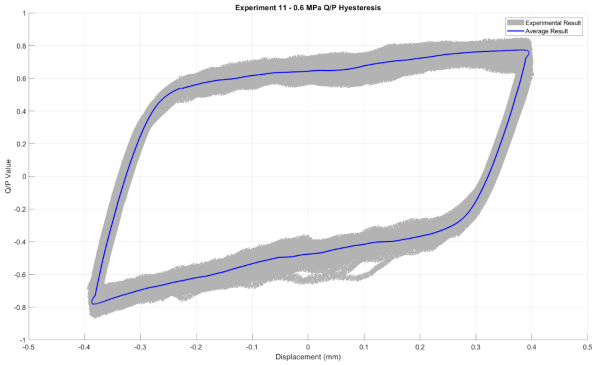

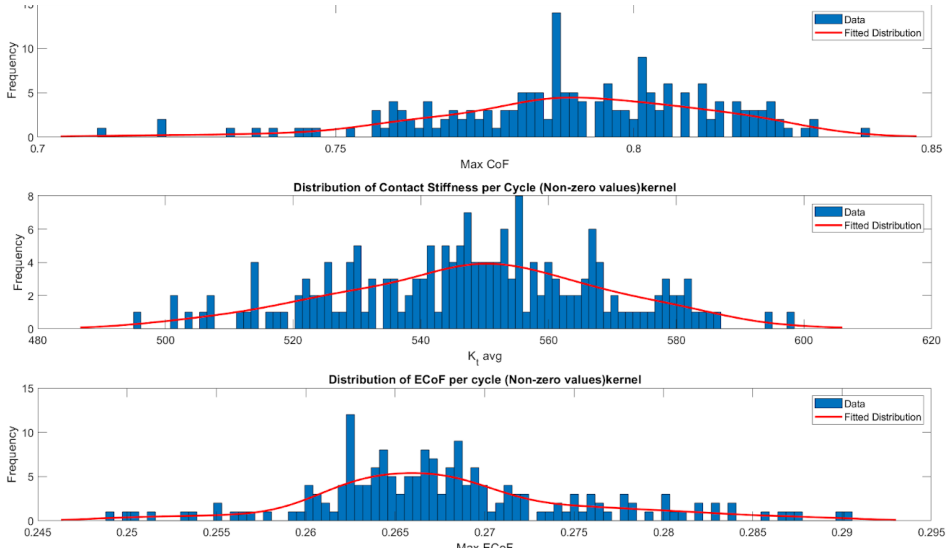

Experiment: 12

Specimen ID:	***C2_3***	***Precompression Stress:***	***0.6 MPa***	***Frequency:***	***0.2 Hz***
Bottom Specimen: C2_3_B			***Top Specimen: C2_3_T***		

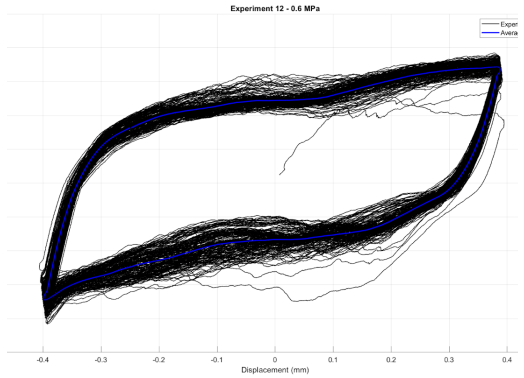

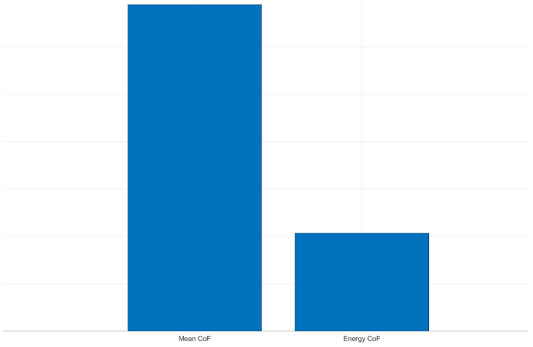

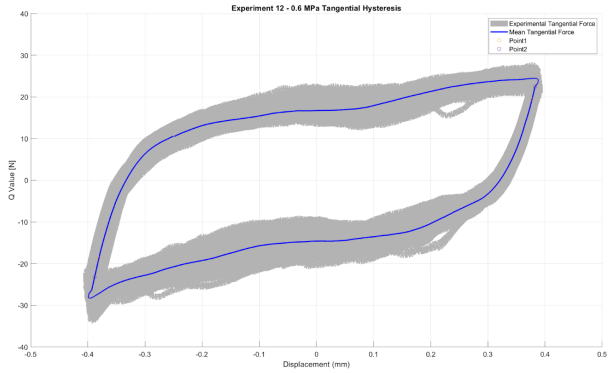

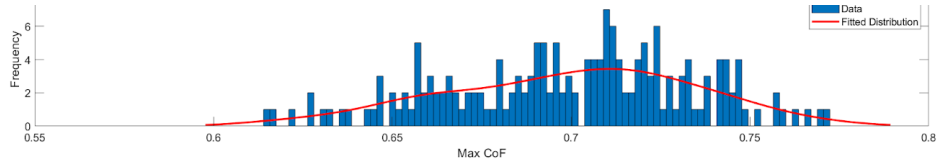

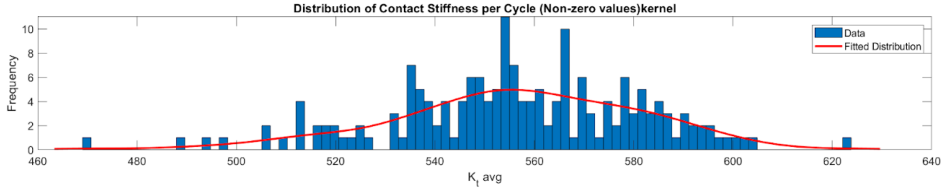

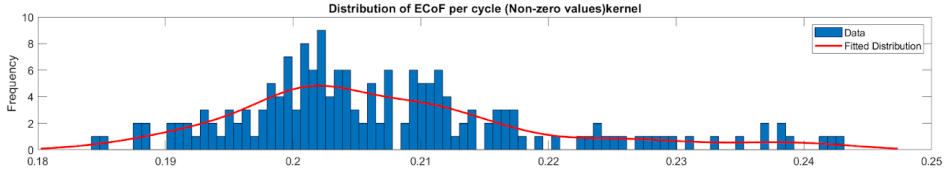

Experiment: 13

Specimen ID:	***C3_3***	***Precompression Stress:***	***0.6 MPa***	***Frequency:***	***0.2 Hz***
Bottom Specimen: C3_3_B			***Top Specimen: C3_3_T***		

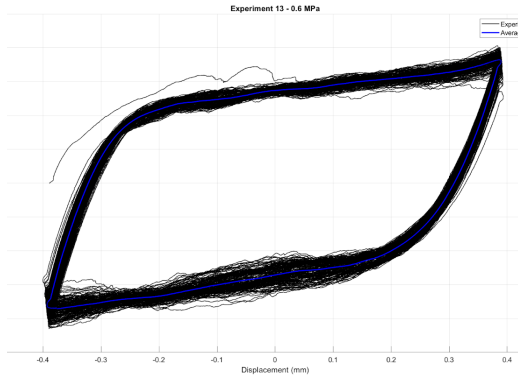

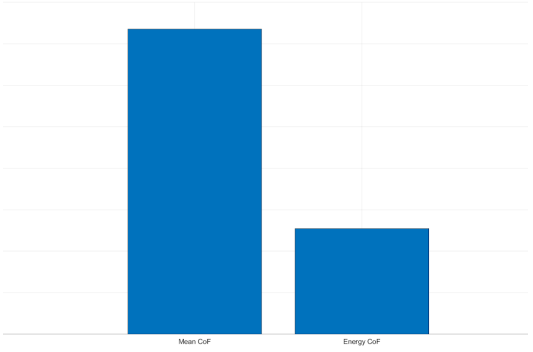

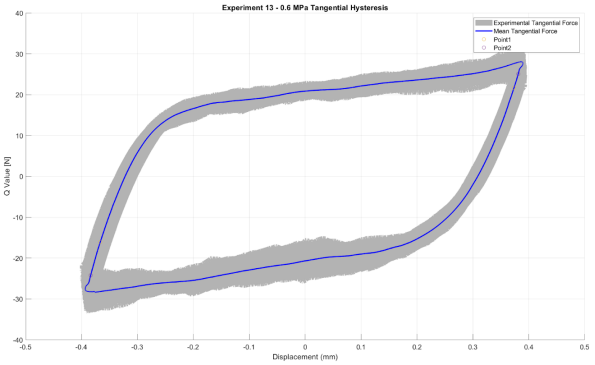

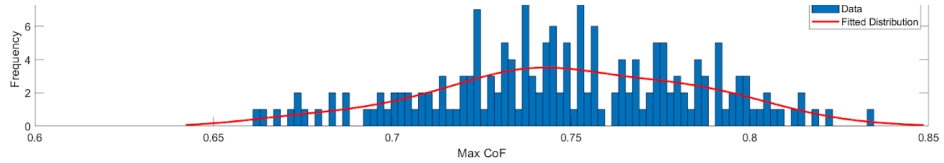

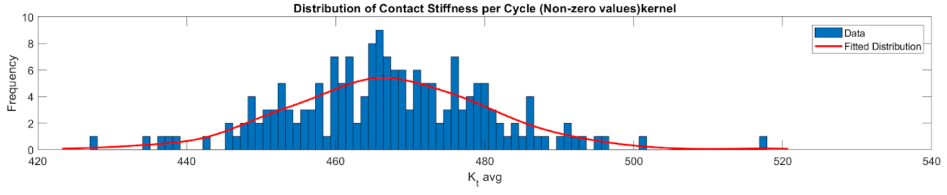

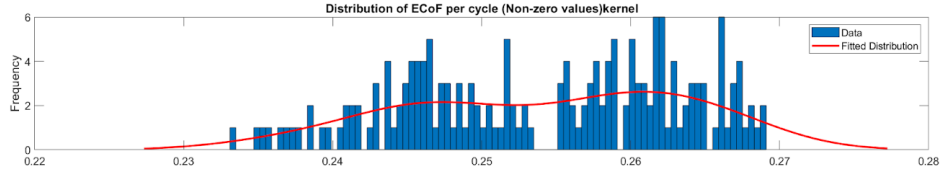

Experiment: 14

Specimen ID:	***C1_10***	***Precompression Stress:***	***0.4 MPa***	***Frequency:***	***0.2 Hz***
Bottom Specimen: C1_10_B			***Top Specimen:C1_10_T***		

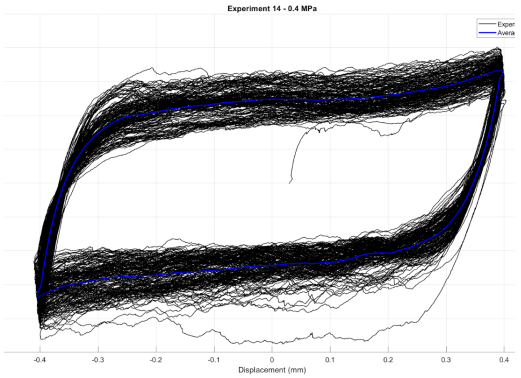

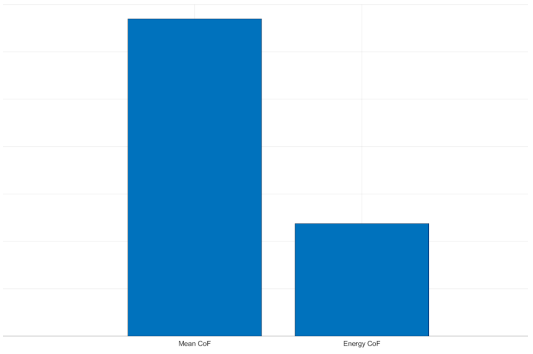

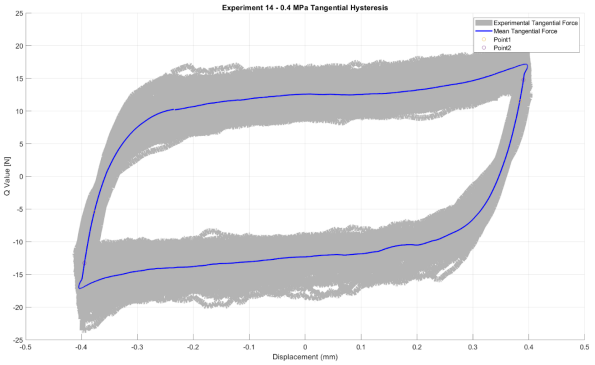

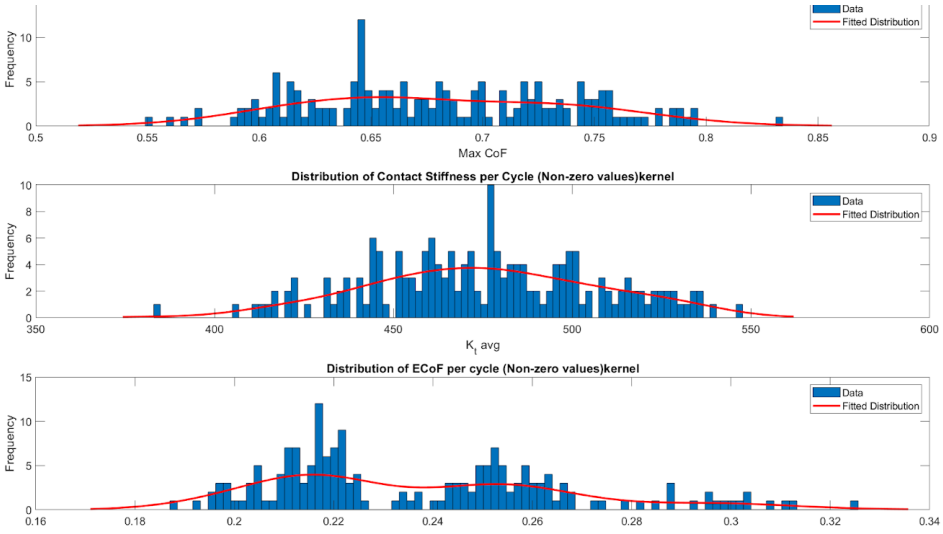

Experiment: 15

Specimen ID:	***C2_8***	***Precompression Stress:***	***0.4 MPa***	***Frequency:***	***0.2 Hz***
Bottom Specimen: C2_8_B			***Top Specimen: C2_8_T***		

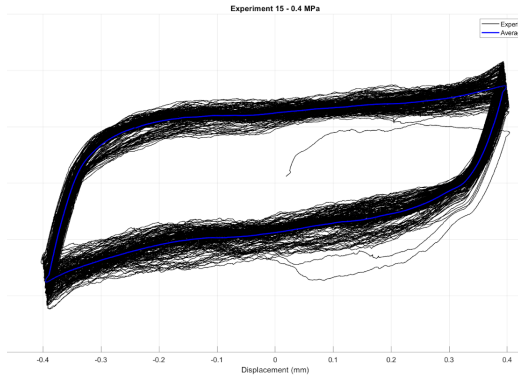

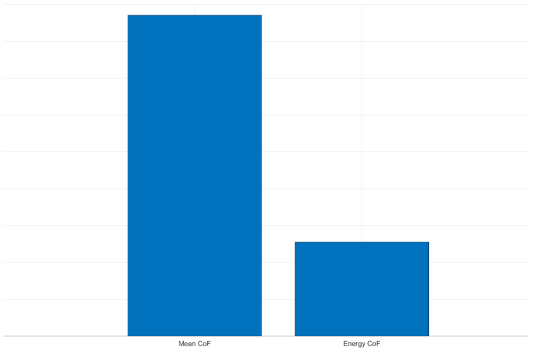

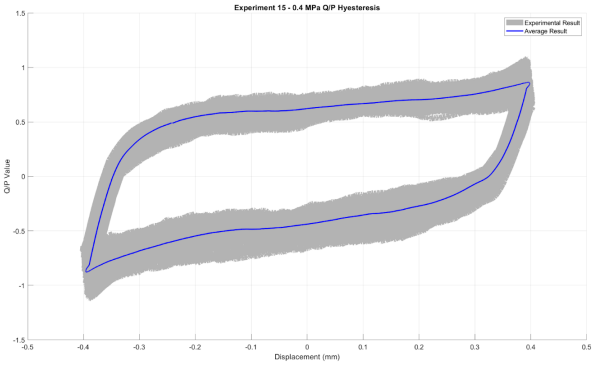

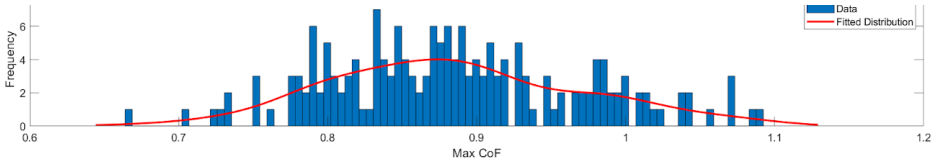

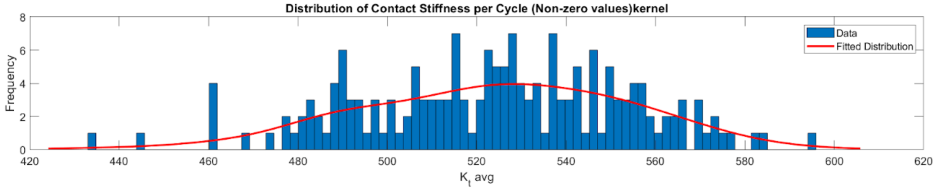

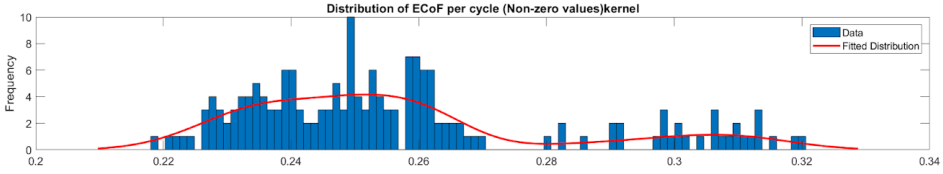

Experiment: 16

Specimen ID:	*C3_10*	*Precompression Stress:*	*0.4 MPa*	*Frequency:*	*0.2 Hz*

Bottom Specimen: C3_10_B

Top Specimen: C3_10_T

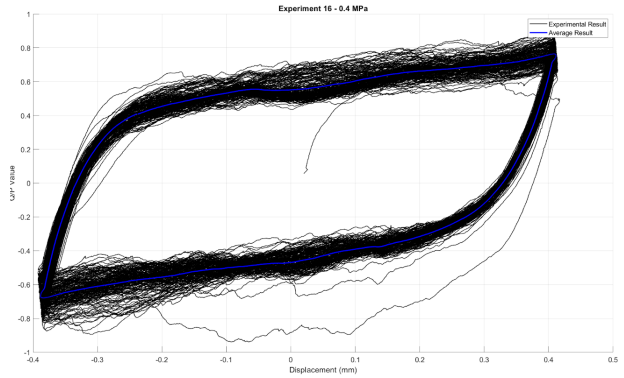

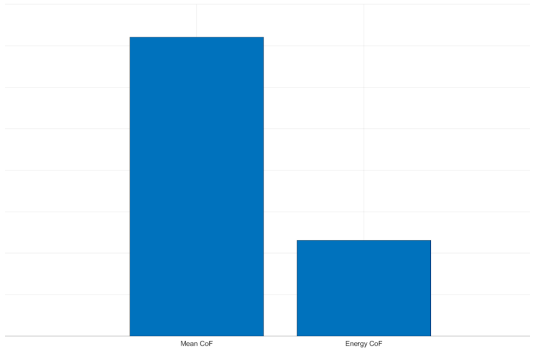

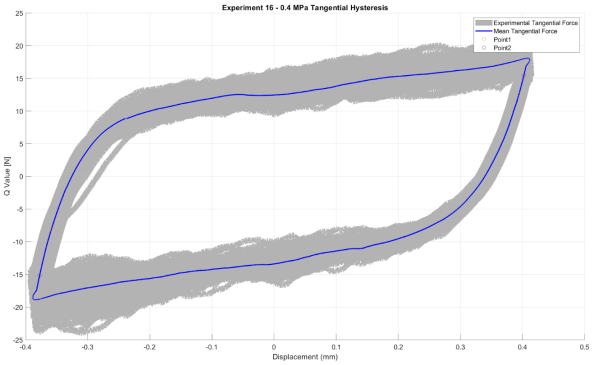

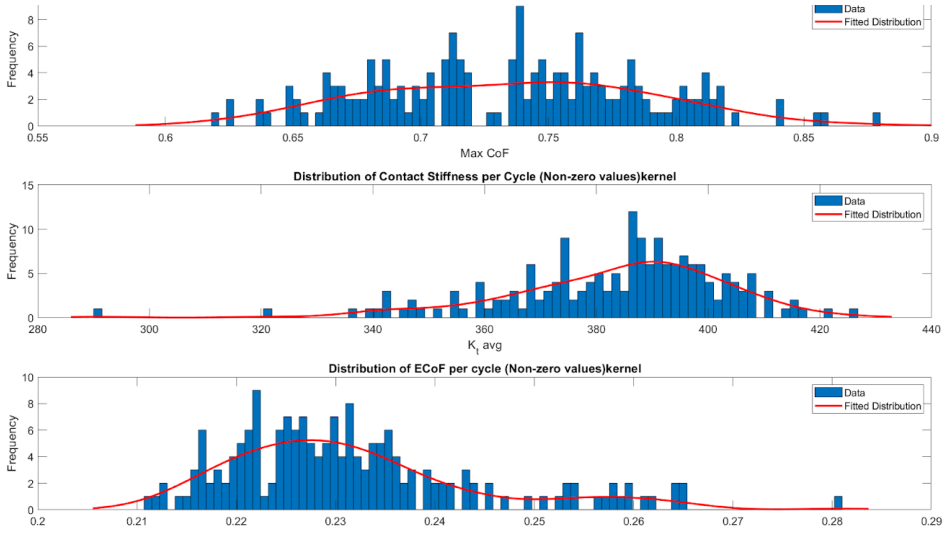

Experiment: 17

Specimen ID:	***C1_7***	***Precompression Stress:***	***0.2 MPa***	***Frequency:***	***0.2 Hz***
Bottom Specimen: C1_7_B			***Top Specimen: C1_7_T***		

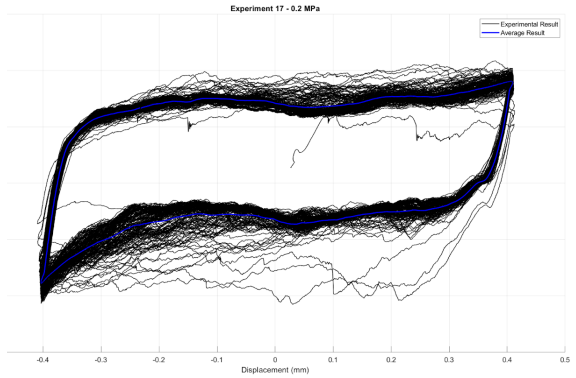

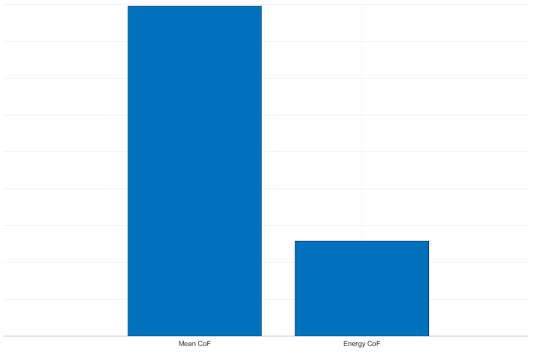

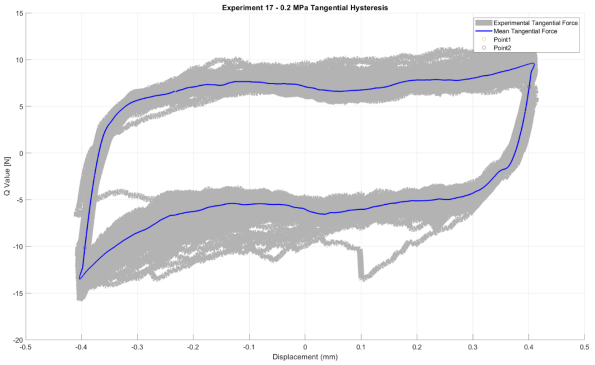

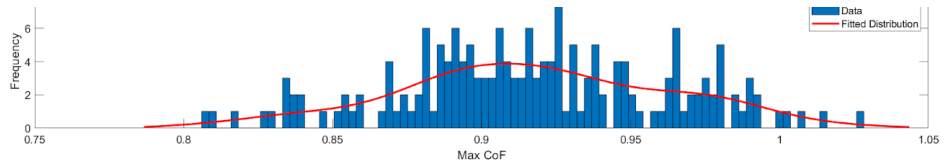

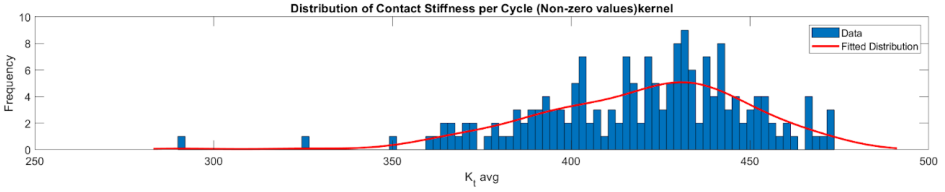

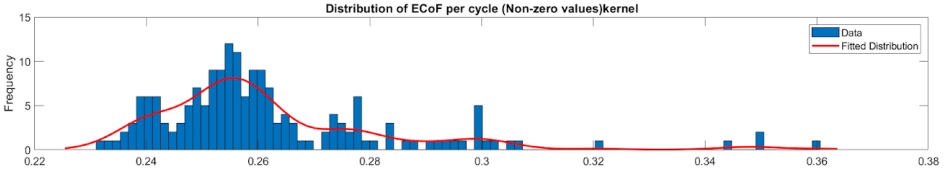

Experiment: 18

Specimen ID:	***C2_9***	***Precompression Stress:***	***0.2 MPa***	***Frequency:***	***0.2 Hz***
Bottom Specimen: C2_9_B			***Top Specimen: C2_9_T***		

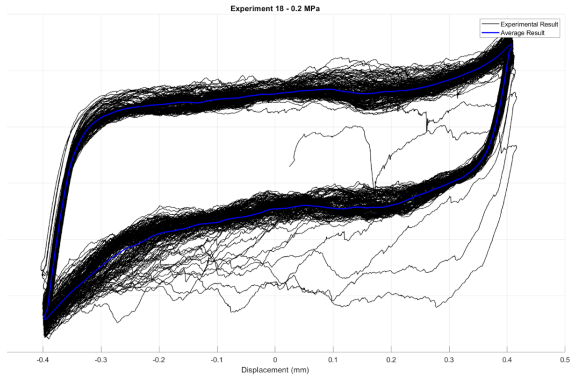

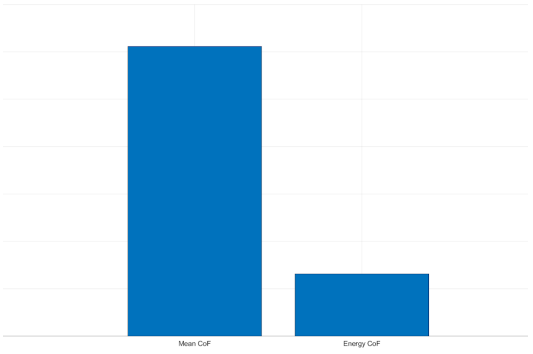

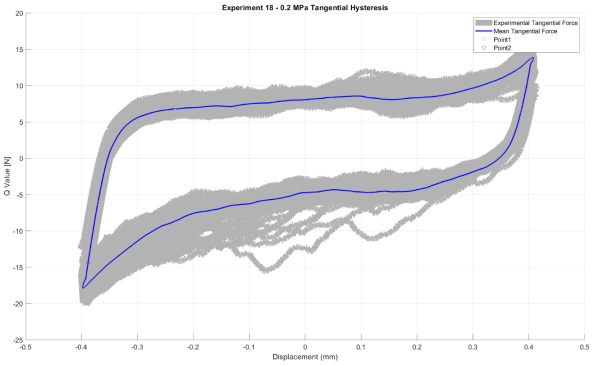

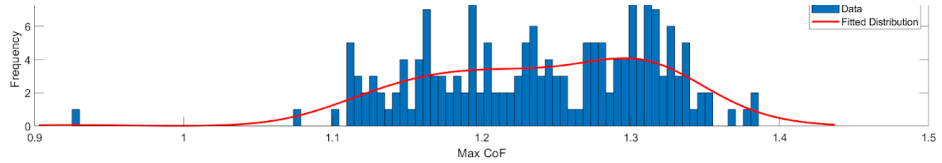

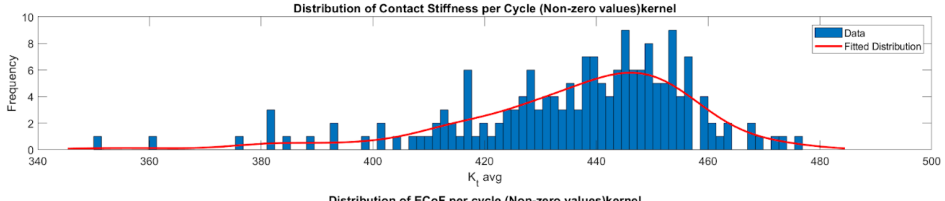

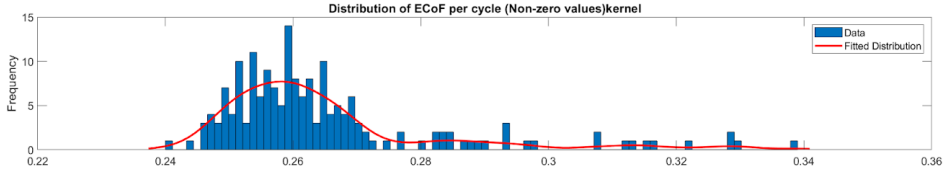

Experiment: 19

Specimen ID:	***C3_9***	***Precompression Stress:***	***0.2 MPa***	***Frequency:***	***0.2 Hz***

Bottom Specimen: C3_9_B

Top Specimen: C3_9_T

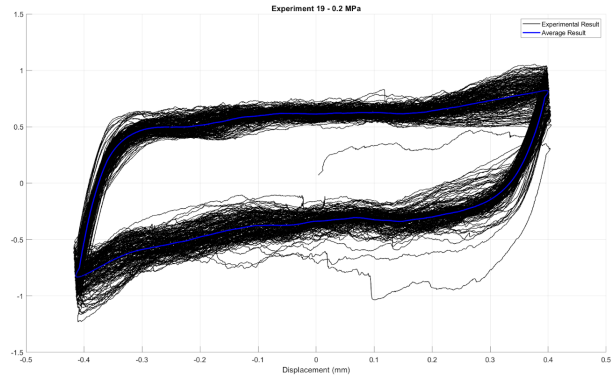

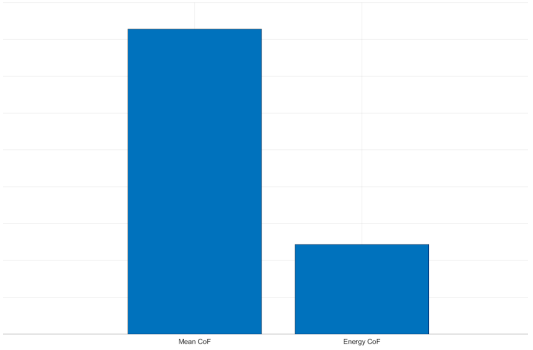

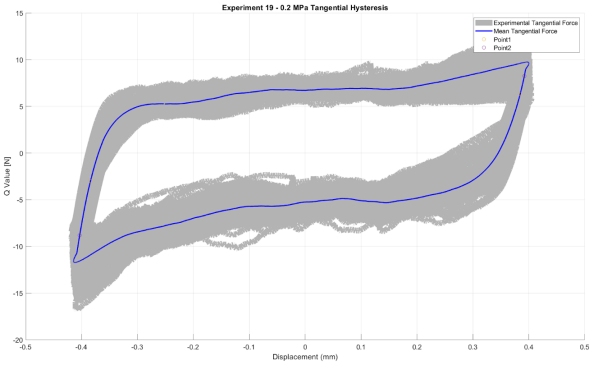

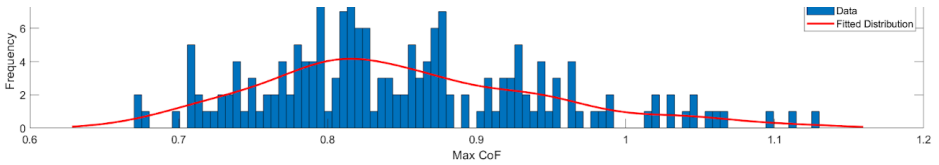

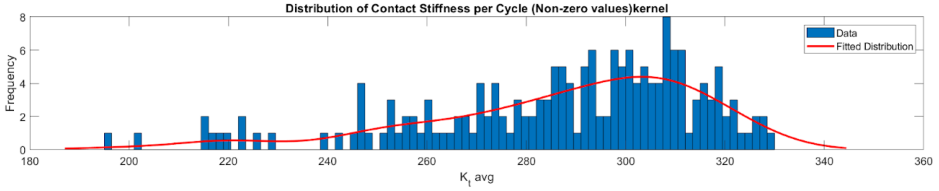

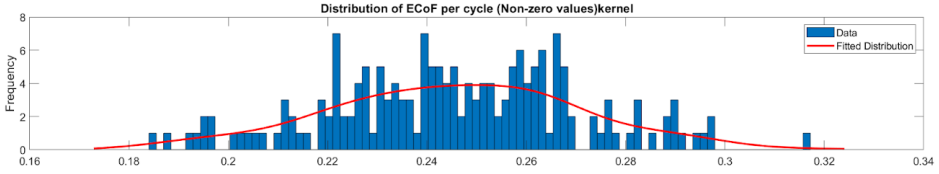

Experiment: 20

Specimen ID:	***C1_12***	***Precompression Stress:***	***0.1 MPa***	***Frequency:***	***0.2 Hz***

Bottom Specimen: C1_12_B

Top Specimen: C1_12_T

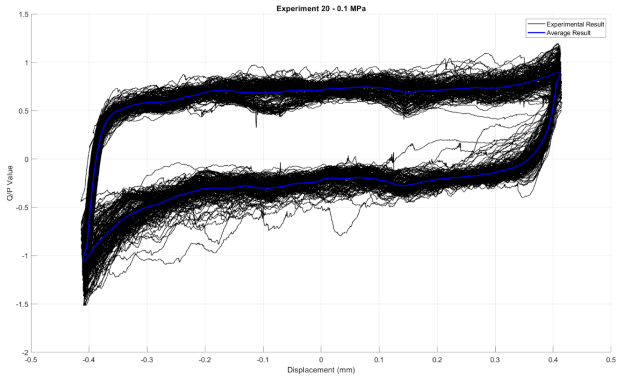

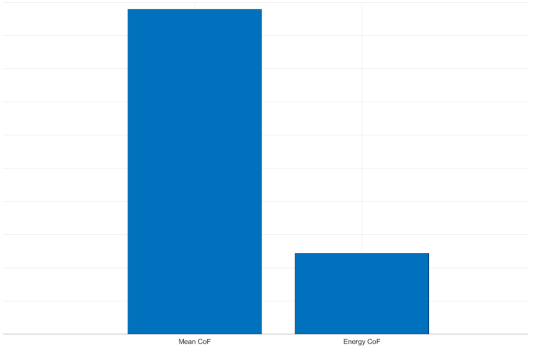

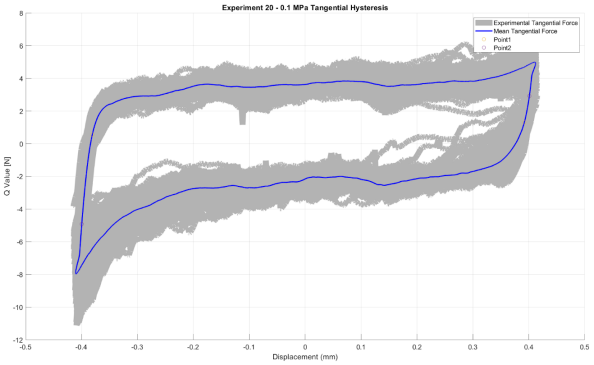

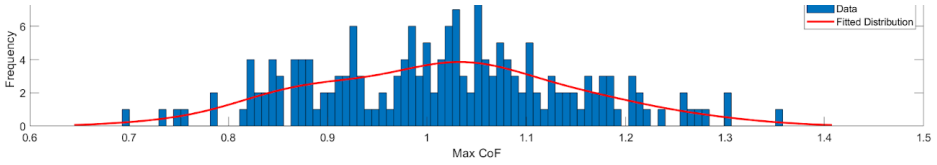

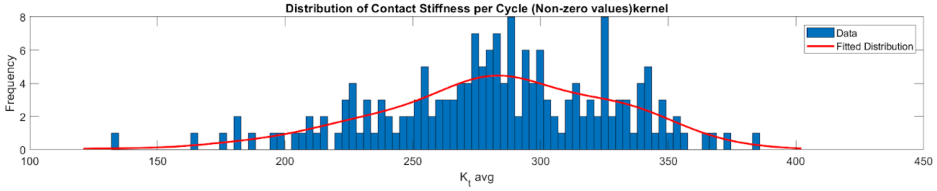

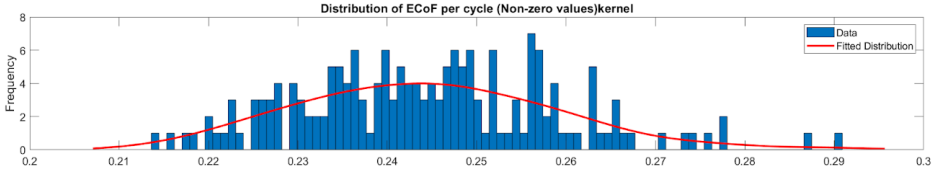

Experiment: 21

Specimen ID:	***C2_1***	***Precompression Stress:***	***0.1 MPa***	***Frequency:***	***0.2 Hz***
Bottom Specimen: C2_1_B			***Top Specimen: C2_1_T***		

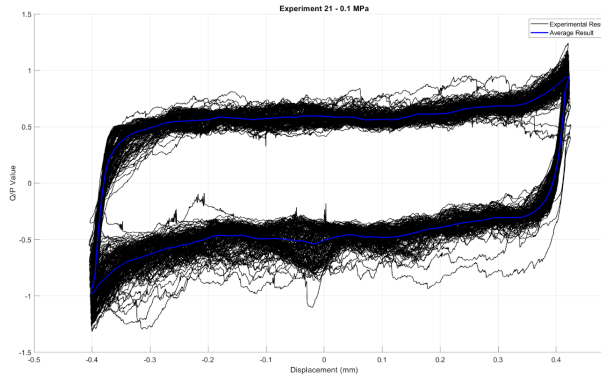

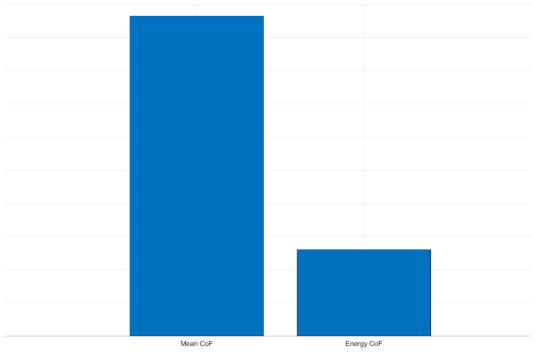

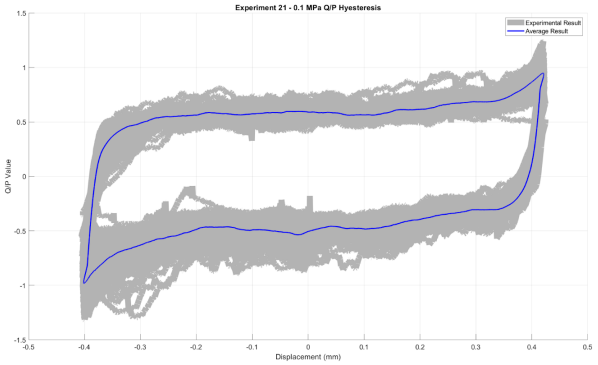

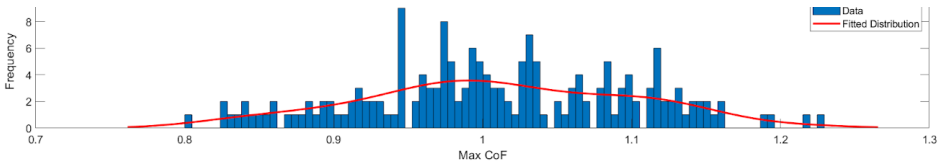

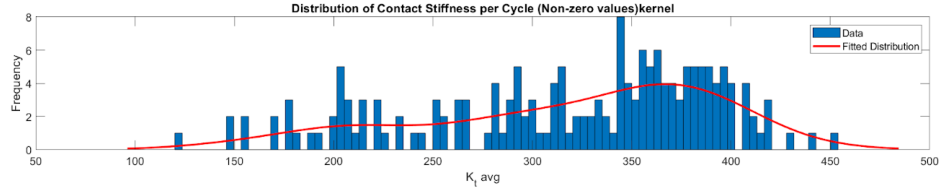

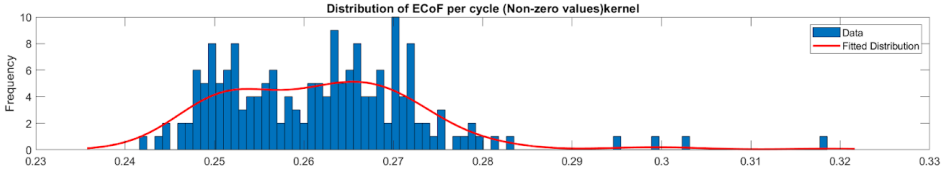

Experiment: 22

Specimen ID:	***C2_4***	***Precompression Stress:***	***0.1 MPa***	***Frequency:***	***0.2 Hz***

Bottom Specimen: C2_4_B

Top Specimen: C2_4_T

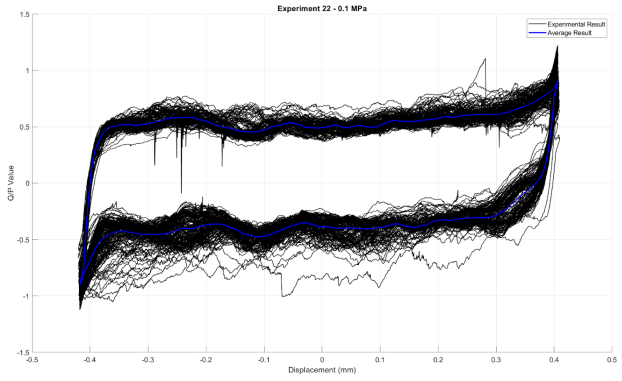

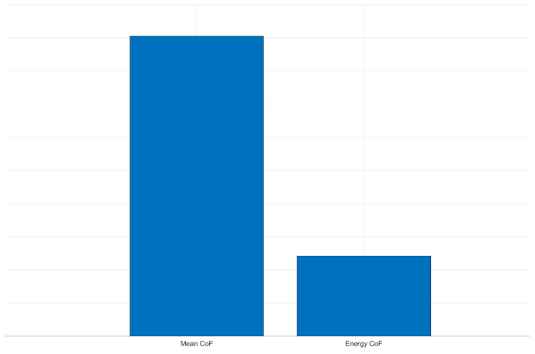

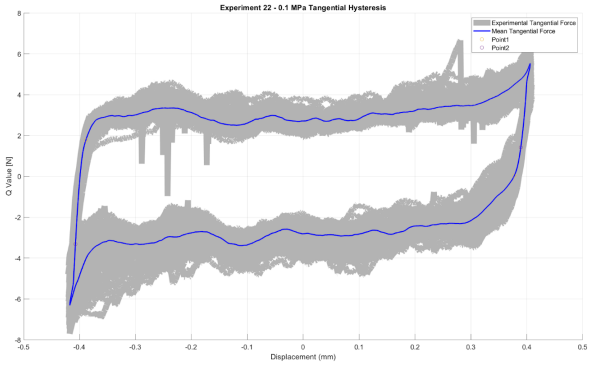

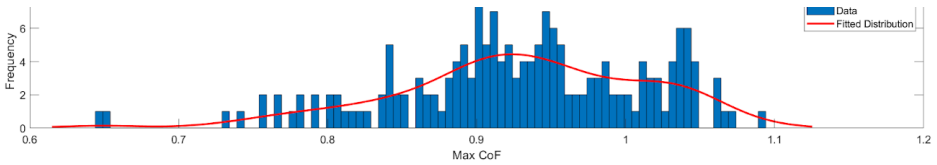

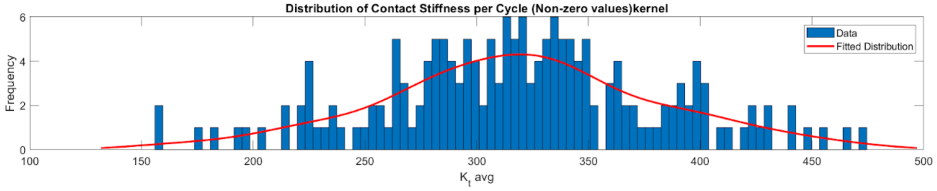

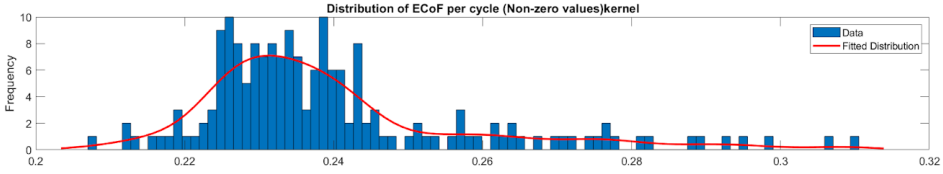

Experiment: 23

Specimen ID:	***C1_12***	***Precompression Stress:***	***0.05 MPa***	***Frequency:***	***0.2 Hz***
Bottom Specimen: C1_12_B			***Top Specimen: C1_12_T***		

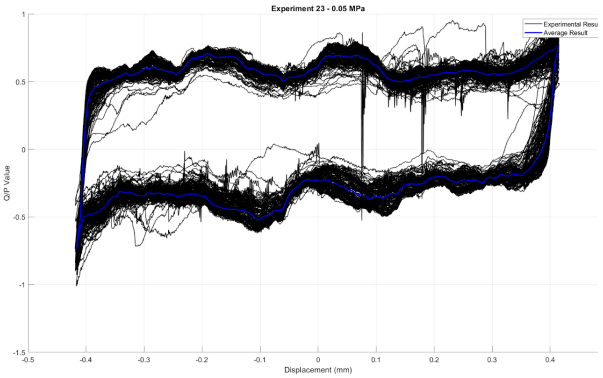

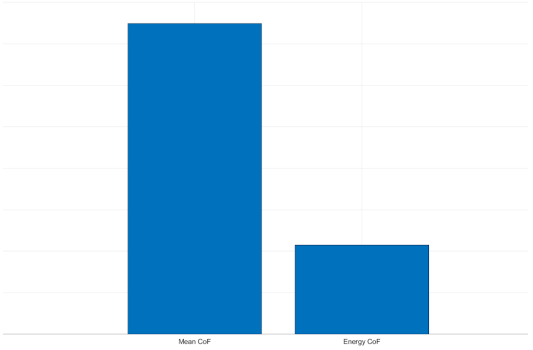

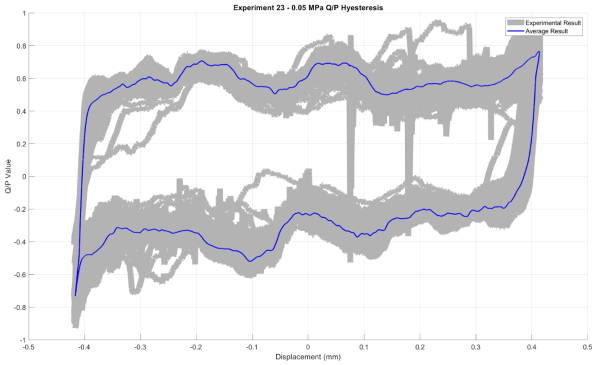

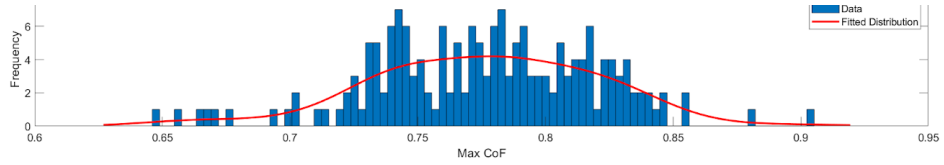

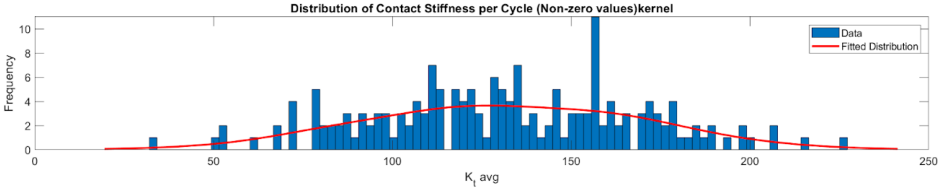

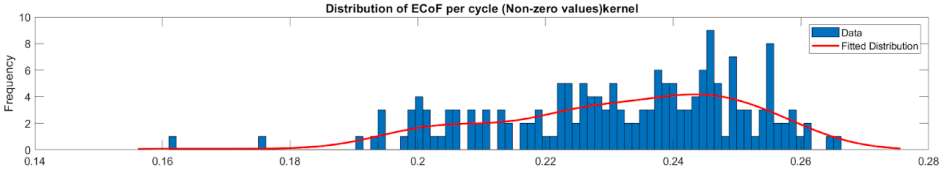

Experiment: 24

Specimen ID:	***C2_1***	***Precompression Stress:***	***0.05 MPa***	***Frequency:***	***0.2 Hz***
Bottom Specimen: C2_1_B			***Top Specimen: C2_1_T***		

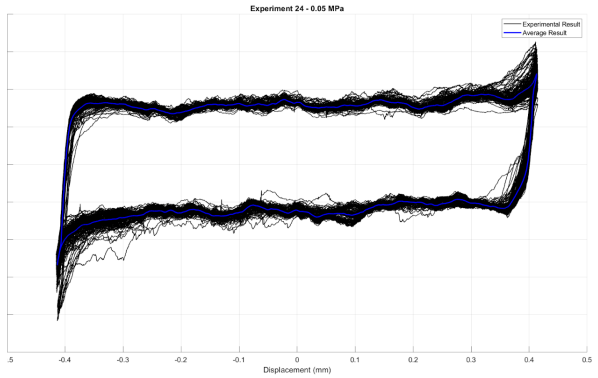

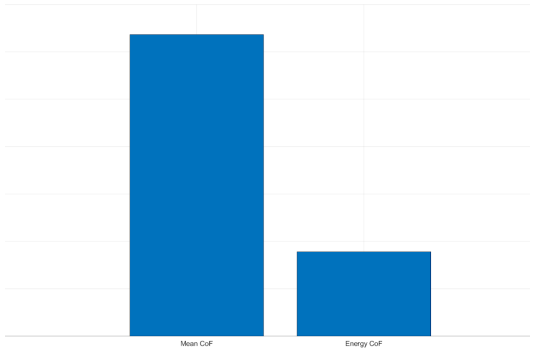

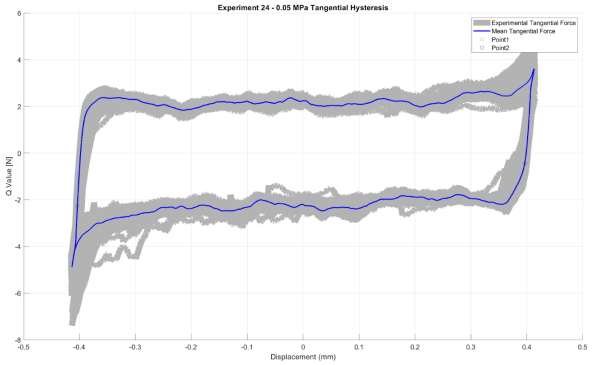

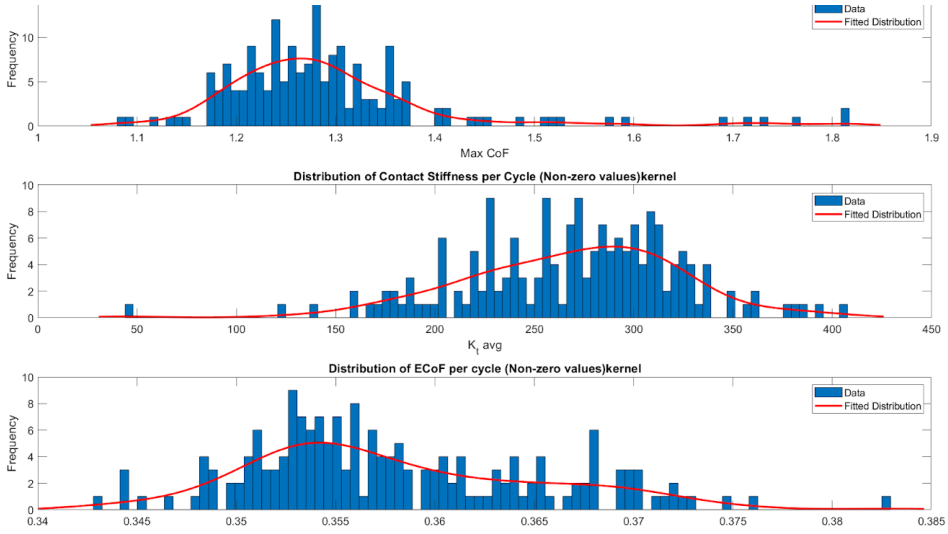

Experiment: 25

Specimen ID:	*C2_4*	*Precompression Stress:*	*0.05 MPa*	*Frequency:*	*0.2 Hz*

Bottom Specimen: C2_4_B	*Top Specimen: C2_4_T*

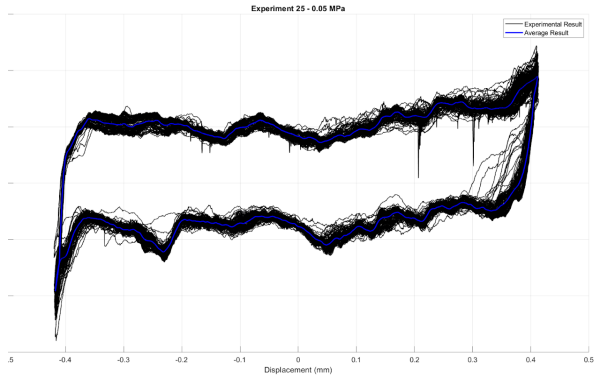

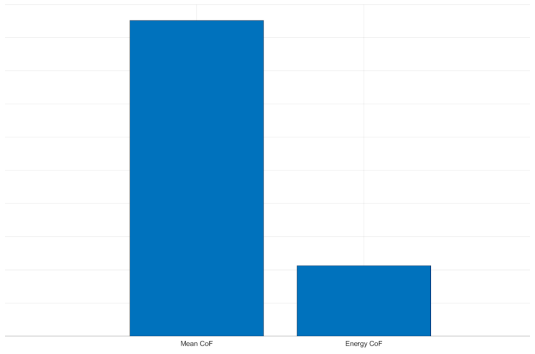

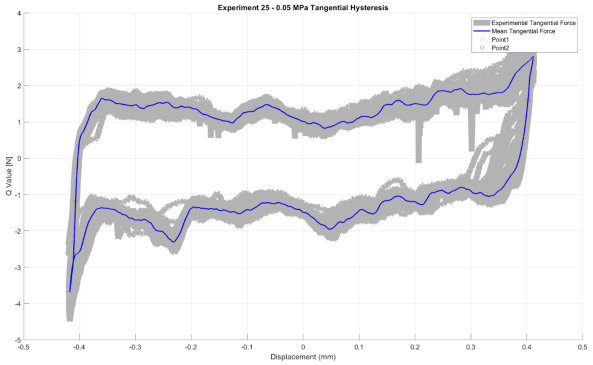

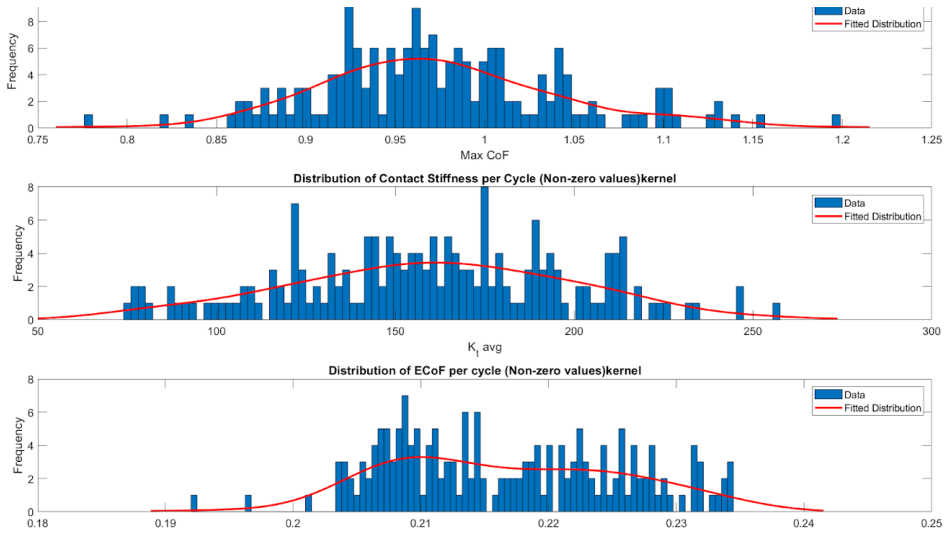

APPENDIX D -

DATA ANALYSIS SUMMARY

Experiments- Sliding Frequency: 3 Hz

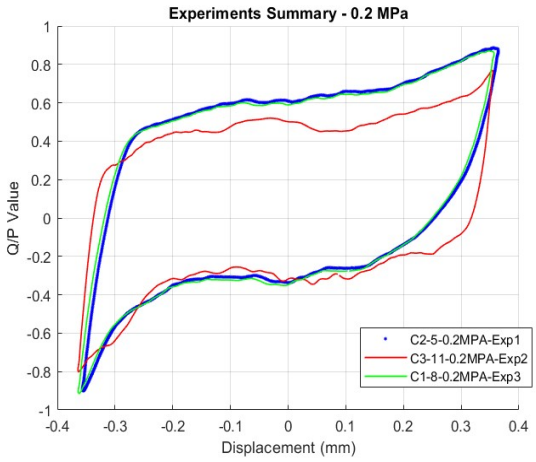

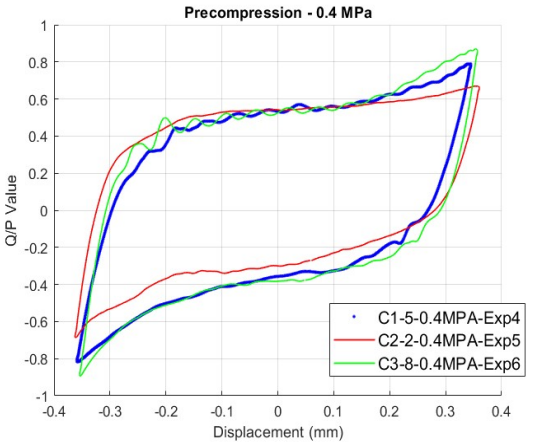

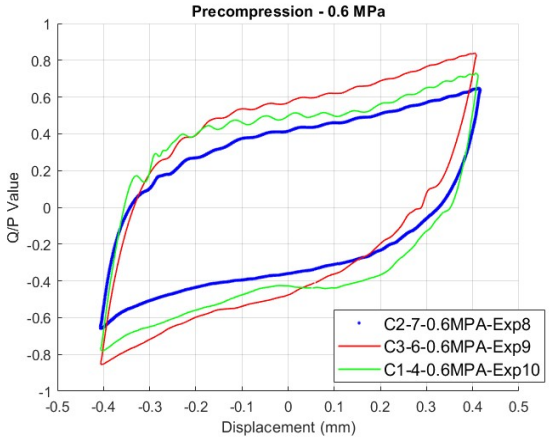

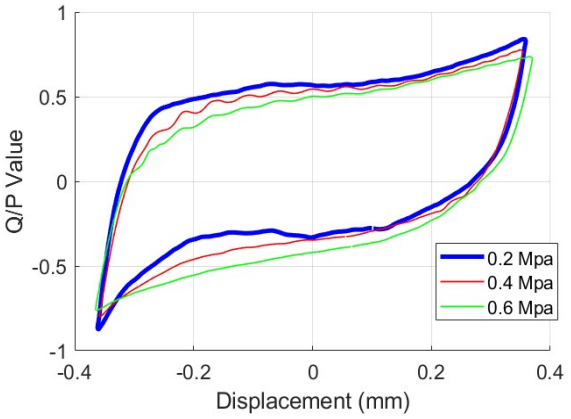

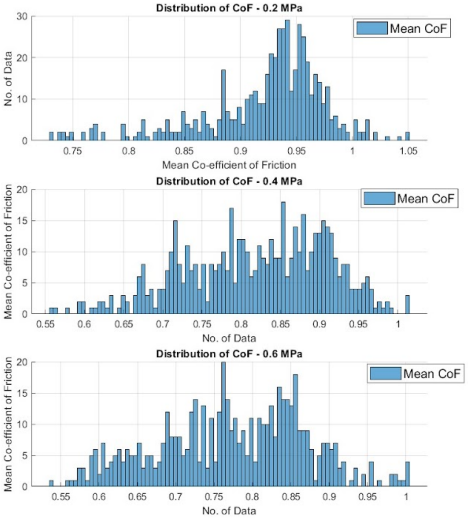

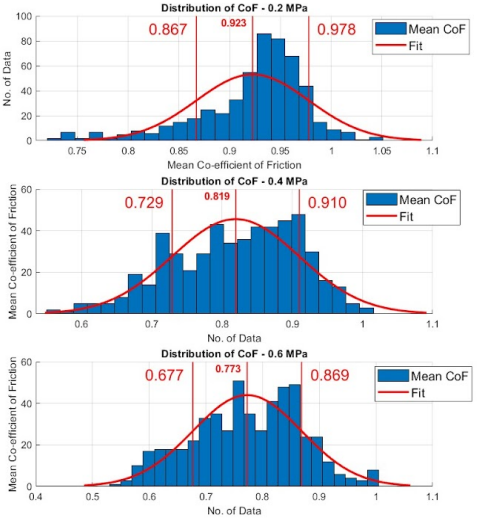

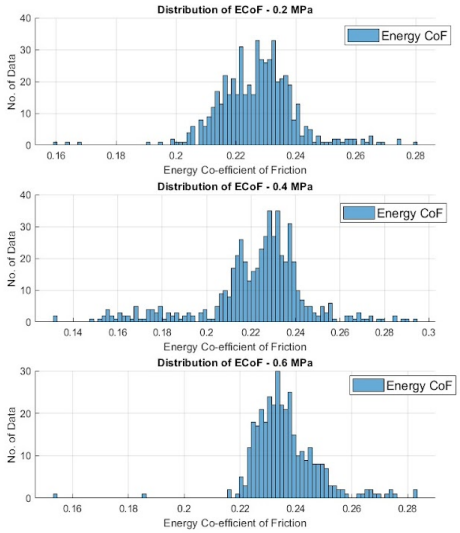
Distribution of ECoF - 0.2 MPa
Energy CoF
No. of Data
Energy Co-efficient of Friction
Distribution of ECoF - 0.4 MPa
Energy CoF
No. of Data
Energy Co-efficient of Friction
Distribution of ECoF - 0.6 MPa
Energy CoF
No. of Data
Energy Co-efficient of Friction

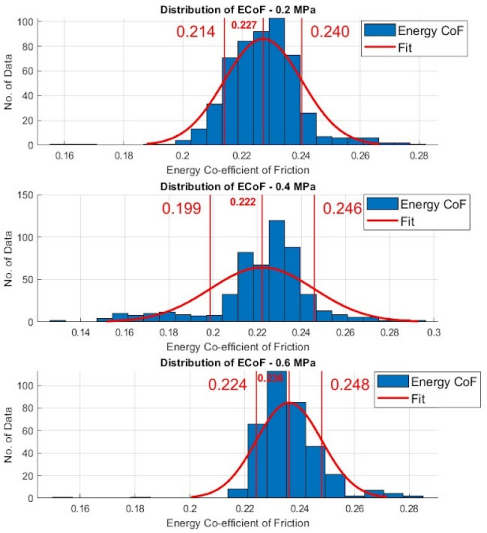
Distribution of ECoF - 0.2 MPa
0.214
0.227
0.240
Energy CoF
Fit
No. of Data
Energy Co-efficient of Friction
Distribution of ECoF - 0.4 MPa
0.199
0.222
0.246
Energy CoF
Fit
No. of Data
Energy Co-efficient of Friction
Distribution of ECoF - 0.6 MPa
0.224
0.248
Energy CoF
Fit
No. of Data
Energy Co-efficient of Friction

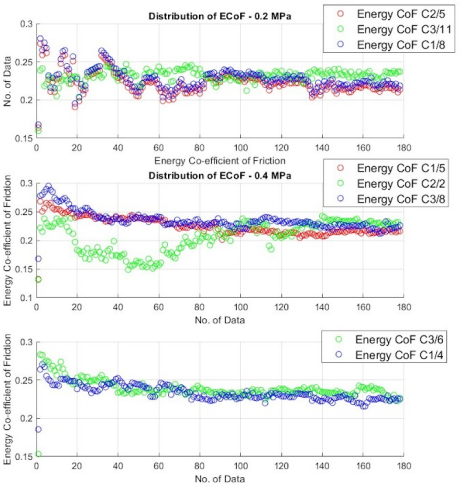
Distribution of ECoF - 0.2 MPa
Energy CoF C2/5
Energy CoF C3/11
Energy CoF C1/8
No. of Data
Energy Co-efficient of Friction
Distribution of ECoF - 0.4 MPa
Energy CoF C1/5
Energy CoF C2/2
Energy CoF C3/8
Energy Co-efficient of Friction
No. of Data
Energy CoF C3/6
Energy CoF C1/4
Energy Co-efficient of Friction
No. of Data

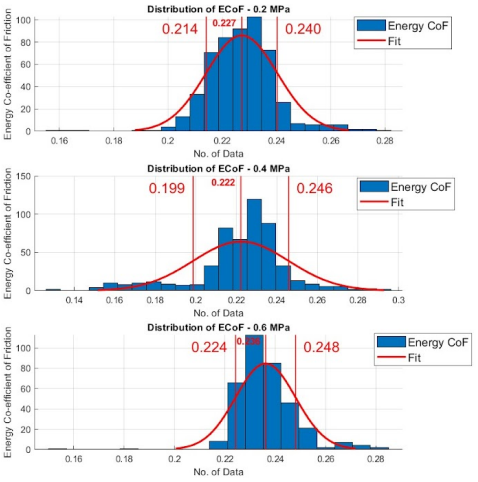
Distribution of ECoF - 0.2 MPa
0.214
0.227
0.240
Energy CoF
Fit
Energy Co-efficient of Friction
No. of Data
Distribution of ECoF - 0.4 MPa
0.199
0.222
0.246
Energy CoF
Fit
Energy Co-efficient of Friction
No. of Data
Distribution of ECoF - 0.6 MPa
0.224
0.248
Energy CoF
Fit
Energy Co-efficient of Friction
No. of Data

Experiments- Sliding Frequency: 0.2 Hz

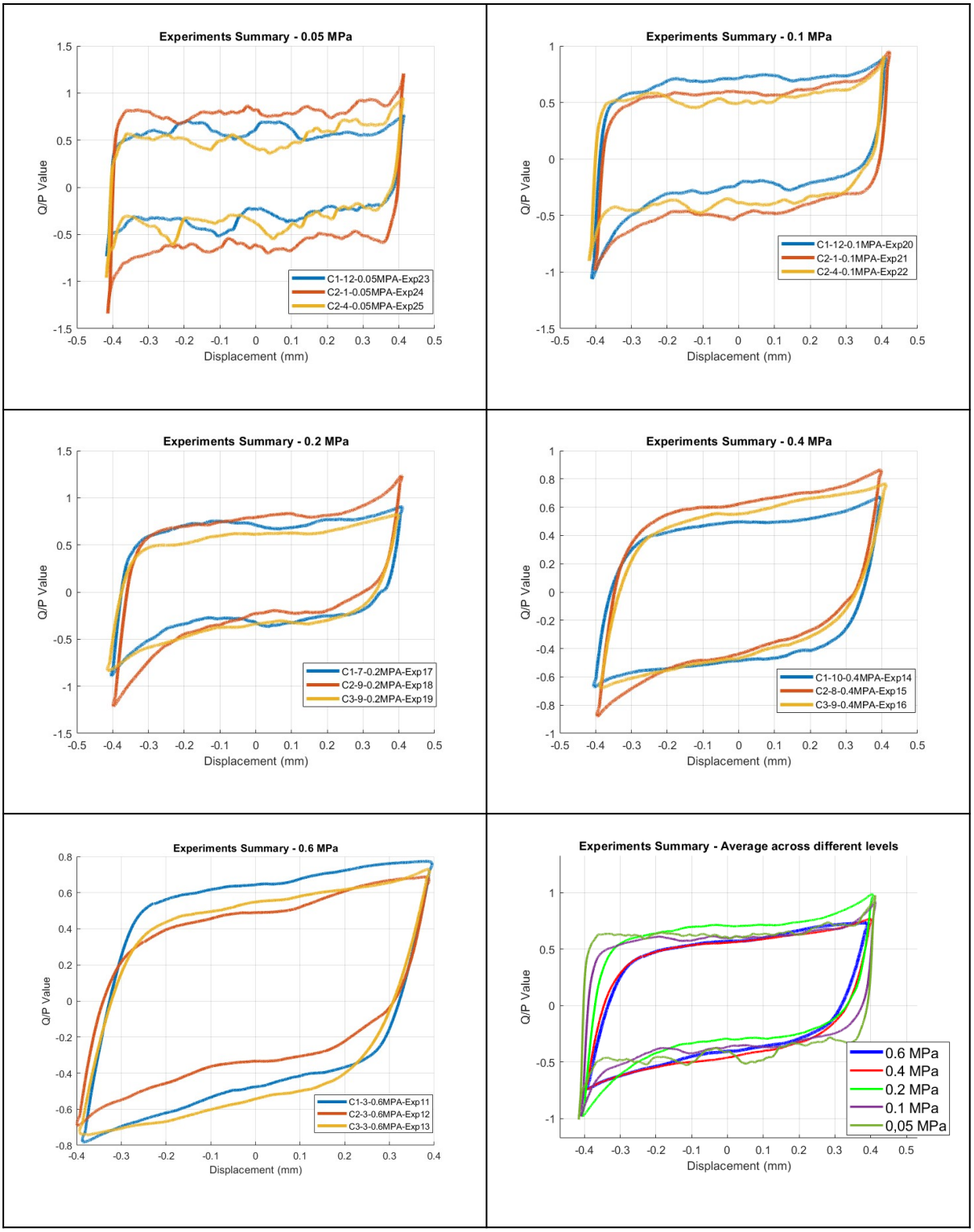

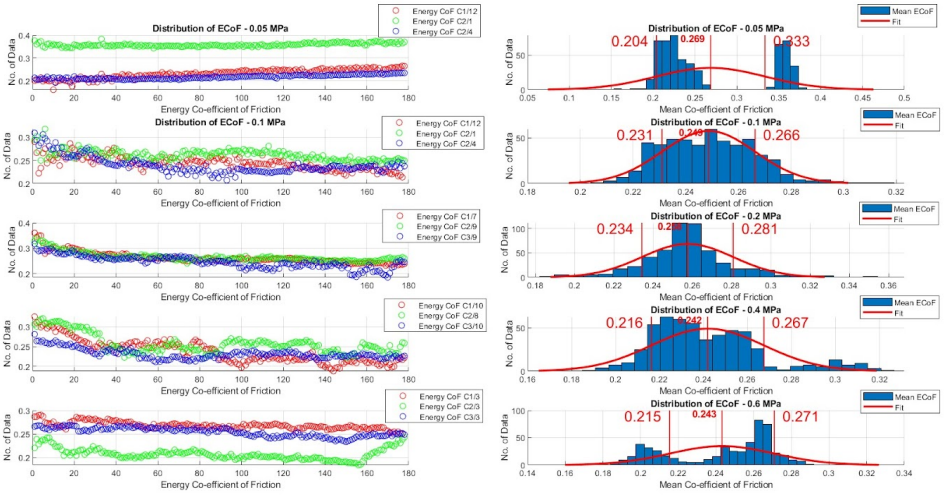
Distribution of ECoF - 0.05 MPa
Energy CoF C1/12
Energy CoF C2/1
Energy CoF C2/4
No. of Data
Energy Co-efficient of Friction
Distribution of ECoF - 0.1 MPa
Energy CoF C1/12
Energy CoF C2/1
Energy CoF C2/4
Distribution of ECoF - 0.2 MPa
Energy CoF C1/7
Energy CoF C2/9
Energy CoF C3/9
Distribution of ECoF - 0.4 MPa
Energy CoF C1/10
Energy CoF C2/8
Energy CoF C3/10
Distribution of ECoF - 0.6 MPa
Energy CoF C1/3
Energy CoF C2/3
Energy CoF C3/3
Distribution of ECoF - 0.05 MPa
Mean ECoF
Fit
0.204
0.269
0.333
Mean Co-efficient of Friction
Distribution of ECoF - 0.1 MPa
0.231
0.249
0.266
Distribution of ECoF - 0.2 MPa
0.234
0.281
Distribution of ECoF - 0.4 MPa
0.216
0.267
Distribution of ECoF - 0.6 MPa
0.215
0.243
0.271

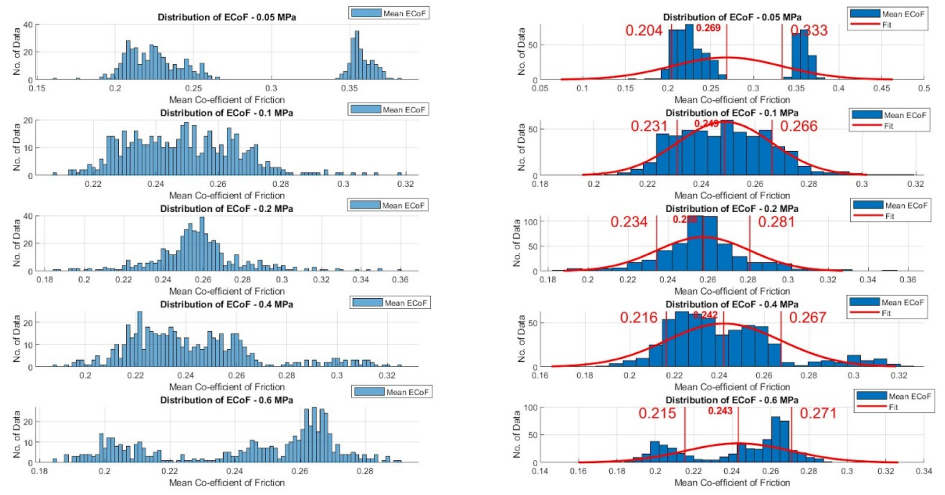
Distribution of ECoF - 0.05 MPa
Mean ECoF
No. of Data
Mean Co-efficient of Friction
Distribution of ECoF - 0.1 MPa
Distribution of ECoF - 0.2 MPa
Distribution of ECoF - 0.4 MPa
Distribution of ECoF - 0.6 MPa
Fit
0.204
0.269
0.333
0.231
0.249
0.266
0.234
0.281
0.216
0.267
0.215
0.243
0.271

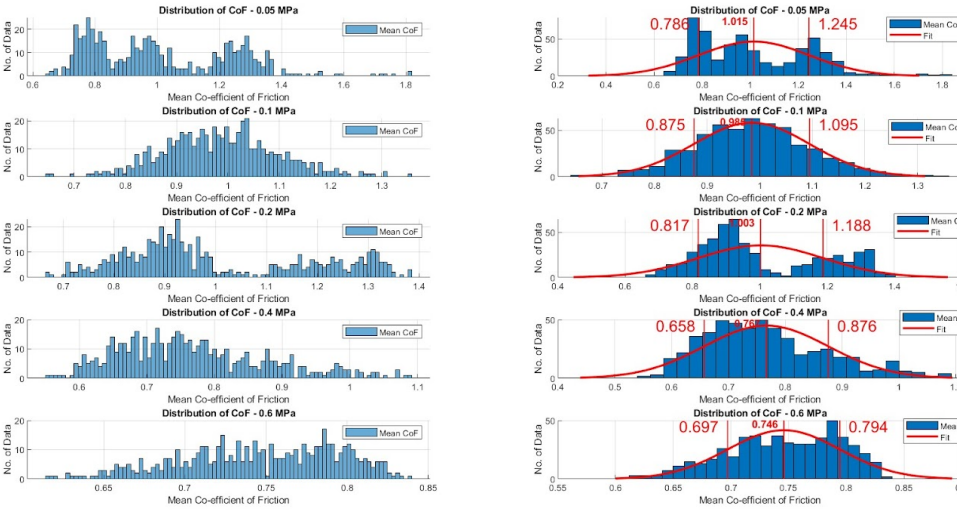
Distribution of CoF - 0.05 MPa
Mean CoF
No. of Data
Mean Co-efficient of Friction
Distribution of CoF - 0.1 MPa
Distribution of CoF - 0.2 MPa
Distribution of CoF - 0.4 MPa
Distribution of CoF - 0.6 MPa
Fit
0.786
1.015
1.245
0.875
1.095
0.817
1.188
0.658
0.876
0.697
0.746
0.794